Rheo-optical Investigation of the Dynamics of Miscible Polymers: Blends and Diblock Copolymers

Thesis by

Barbara Helen Wang

In Partial Fulfillment of the Requirements

for the Degree of

Doctor of Philosophy

California Institute of Technology

Pasadena, California

1996

(Submitted December 20, 1995)

To my husband Michael,

with all my heart,

for his unending love, encouragement and support.

Acknowledgements

I would like to thank my advisor, Julie A. Kornfield, for the many things I have learned from her, including perseverance and the pursuit of excellence. I have gained a deep appreciation for critical reasoning and evaluation of my work because of her.

I am also grateful to Caltech for allowing me to work in both the Division of Physics, Mathematics and Astronomy and the Division of Chemistry and Chemical Engineering. This made it possible for me to pursue the interdisciplinary projects that interested me. I also owe a great deal to the National Physical Science Consortium for its generous support during my entire graduate career. I hope it continues to help students for many years to come.

There are also many of my fellow students that I wish to thank. The members of my group helped make life in the lab much more enjoyable. I also appreciate all my friends who struggled with me through classes and "dorm life" for the first couple of years. I am glad that many of us continue to share our lives, even as we joined our separate research groups and now leave Caltech for our corners of the world.

I want to thank my family for helping me get to where I am today. Both they and

my husband's family have given my the support and perseverance to finish my work here. Finally, I am most grateful to my husband, who has helped me acheive more than I thought possible and given me all his love and encouragement. I look forward to a lifetime of happiness with him.

Abstract

The dynamics of each component in miscible blends of polyisoprene / polyvinylethylene (PIP/PVE) are studied using dynamic stress-optical measurements. We first examine blends in which the two components are nearly equally entangled in order to avoid the effects of polydispersity on the dynamic moduli of each species. While the homopolymers are thermorheologically simple and obey the stress-optic rule, the blends show failure of time-temperature superposition and complex stress-optic behavior. The way in which the stress-optic rule fails reveals the relaxation dynamics of each species. The blend dynamic modulus and complex birefringence coefficient are analyzed to infer the dynamics of each component. Orientational coupling, which affects the birefringence but not the stress, is incorporated based on the value of the coupling coefficient determined from rheo-optical studies of unequally entangled blends. While we cannot rule out contributions of compositional heterogeneity to thermorheological complexity in the PIP/PVE system, it is intrinsic differences between the temperature dependencies of the two species' dynamics which dominate the observed failure of time-temperature superposition.

The entanglement molecular weight, $M_{e,i}(\phi)$, and monomeric friction coefficient, $\zeta_{o,i}(\phi, T)$, of each species are determined from the component dynamic moduli, as functions of blend composition, ϕ and temperature, T. The effect of blending on $M_{e,i}$ of each component is small, with the values varying by only $\sim 30\%$ from those of the pure components over the range of composition. Blending has a much more dramatic effect on $\zeta_{o,i}$ of each species: it strongly speeds the rate of relaxation of the component with the higher glass transition temperature, T_g, (PVE), while more modestly slowing the relaxation of the low-T_g component (PIP). The dynamics of each species have different temperature dependencies in the blend, which leads to the failure of the superposition principle. Furthermore, both the difference between the friction coefficients of the two species and the difference in their temperature dependencies is greater in blends rich in the high-T_g material (PVE).

We then look at blends in which the two species are unequally entangled and the effect of orientational coupling can be characterized. Since orientational coupling contributes to the birefringence but not the stress, simultaneous analysis of these observables allows us to extract the coupling coefficient, ϵ. For blends in which PIP is the faster-relaxing species and couples to a slower-relaxing PVE matrix, $\epsilon_{PIP,PVE}$ $\approx 0.35 \pm 0.04$. Analogous blends are also studied, where PVE is the faster-relaxing species coupling to a PIP matrix, for which $\epsilon_{PVE,PIP} \approx 0.27 \pm 0.08$. Thus, within experimental uncertainty, it appears appropriate to use a single, average value of ϵ. No dependence of ϵ on composition or temperature were detected. Once ϵ was determined we extracted the component dynamic moduli in each blend over a range of

temperatures and blend compositions. The trends observed for the equally entangled blends remain valid and the values determined for $M_{e,i}$ and $\zeta_{o,i}(\phi, T)$ are reproduced. Although failure of time-temperature superposition in these blends is again due to the distinct temperature dependencies of the species' monomeric friction coefficients, both the contrast in friction coefficient and the relative molecular weights of the components determine the degree to which complex thermorheological behavior is observed.

Finally, the dynamics of nearly ideal, disordered PIP-PVE diblock copolymer melts are characterized using the same rheo-optical techniques, for two block compositions ($\phi_{PIP} = 0.25$ and 0.75). Unlike miscible blends of PIP and PVE, for which time-temperature superposition fails, the dynamic moduli of the block copolymers suggest that they are thermorheologically simple. Here we show that this apparent paradox can be resolved by examining the relaxation of the constituent blocks, which can be determined from stress-optic measurements. In block copolymers rich in the low-T_g component (high ϕ_{PIP}), thermorheologically simple behavior is observed because both blocks have similar friction coefficients, in accord with our results on PIP/PVE blends. In copolymers rich in the high-T_g component (low ϕ_{PIP}), the individual blocks show distinct temperature dependencies, again in accord with the blend results. The reason that departure from time-temperature superposition was not previously observed in these diblocks is that the change in $\zeta_{o,PVE}/\zeta_{o,PIP}$ produces subtle changes in the overall relaxation spectrum relative to a linear chain of uniform friction.

Contents

List of Figures

List of Tables

Chapter 1

Introduction

1.1 Motivation

Polymers are of great scientific and technological interest. They are nearly ubiquitous because of the enormous range of properties that can be achieved, often through relatively inexpensive synthesis and processing steps. However, one problem that still plagues the development of new polymers is a lack of understanding of the fundamental physical laws governing their microscopic dynamics, which are in turn manifested by macroscopic physical properties, such as the glass transition temperature, diffusive properties, toughness, and elasticity. The microscopic dynamics are greatly affected by factors such as temperature, composition and sample history, which are important variables in processing schemes. Furthermore, much of the development of new polymers for applications involves significant trial-and-error effort in synthesis and processing. There is as yet no way to reliably predict the macroscopic properties

before actually measuring them.

Given that synthesis of new materials is difficult and costly, it is useful to develop polymer blends from pre-existing homopolymers. The practical significance of blends derives from the fact that a wide range of materials, often exhibiting a desirable and superior combination of the properties of the individual constituents, can be produced economically. Often, the work of tailoring and optimizing the properties of the pure components has already been done. One important caveat to using this technique is that most polymer pairs tend to be immiscible, at least over some range of volume fractions of the two components. The limits of miscibility depend on temperature and molecular weight, since the entropic factors favoring mixing decrease with molecular weight and usually with temperature, thus driving segregation. In order to achieve better control over blend properties, it is desirable that the blend either be miscible or stabilized by the addition of a third component, such as a block or graft copolymer, as a compatibilizer. Commercial blends are typically phase separated, multicomponent systems which consist of at least two chemically distinct homopolymers, of different molecular weights. They frequently contain a third agent as a compatibilizer, thus creating a very complex system.

In phase-separated blends it is necessary to understand the morphology and composition of the immiscible phases and the properties of the interface between them, in order to successfully predict the processing behavior and formulate useful "blending rules." The properties of multiphase blends are greatly affected by temperature, composition, and sample history, which are important variables in processing schemes.

Specific interactions between the components can further complicate the blend dynamics by altering the chain conformations and interactions, as well as the phase diagram of the system. When the components have different molecular weights, polydispersity plays a role, and additional modes of relaxation, such as constraint release, affect the component dynamics.

In immiscible blends, in fact, each phase is itself a miscible blend, so probing the viscoelastic character of miscible blends is a first step in understanding the behavior of immiscible ones. Recently, an increasing number of miscible blends have been discovered and exhibit interesting behavior in their own right. It is important, therefore, to relate the properties of the blend to those of the pure components. Fundamentally, one must examine the homopolymers and understand how their physical properties are modified in a blend. In order to do so, an understanding of the intra- and intermolecular forces and their contributions to polymer dynamics is required. Miscible blends provide systems in which these effects can be examined in a single phase. The relaxation dynamics of miscible blends involve not only the issues present in homopolymers, such as the effects of polydispersity, but also distinctive issues such as the effect of blending on the entanglement molecular weight, $M_{e,i}$, and monomeric friction coefficient, $\zeta_{o,i}$, of each species i in the blend. The complex thermorheological behavior seen for miscible blends, evidenced by failure of time-temperature superposition and a broad glass transition, is quite different from that observed for the pure components and is not well-understood. Thus, miscible blends provide a model system while still exhibiting many of the same complex and interesting features present

in multiphase blends.

1.2 Previous Work

Experimentally it has not been clear why miscible blends show the complex time and temperature dependencies evidenced by failure of time-temperature superposition [1, 2] and the unpredictably broad glass transition temperature [3, 4, 5]. Macroscopic measurements of the stress tensor do not explain on a microscopic level the molecular response of the polymer, since they characterize the bulk response but do not yield much insight into the underlying mechanisms. Differential scanning calorimetry, used to observe the broad glass transistion, also does not distinguish between the two species in a blend. In a blend each species contributes to the bulk properties via intra- and intermolecular interactions, which need to be distinguished.

Several experiments have observed intrinsic differences between the dynamics of the two species in miscible blends, which may be responsible for the distinct temperature dependencies of macroscopic blend properties. For example, on a molecular level it has been found that the activation energies for motions of each type of chain can be dramatically different [6], which would cause the breakdown of time-temperature superposition and produce a broad glass transition. ^{13}C NMR experiments [6, 7] show that the two species can have widely different molecular mobilities in the blend, attributed to their individual characteristics. Recently, two-dimensional ^{2}H-exchange NMR studies of segmental dynamics in miscible blends near their glass transition tem-

peratures show that both local variations in composition and intrinsic differences in chain mobility contribute to the dynamical heterogeneity of local segmental motions [8, 9]. It is not clear, however, how the local dynamics probed by these experiments propagate out to the scale of the entanglement molecular weight, i.e., the length scale that controls the flow behavior of the melt.

Looking on a macroscopic level, mutual diffusion studies [10, 11] demonstrate that each species has a distinct, composition-dependent tracer diffusion coefficient in the blend, and hence distinct friction coefficients. Rheological studies on miscible blends in which the terminal relaxations of the two components remained separated allowed the component dynamics to be tracked over a range of temperatures [2]. However, it is in general difficult to obtain quantitative results using this method. For arbitrary molecular weights and components with similar glass transition temperatures, the relaxations for the two species overlap, making it difficult to determine the characteristic relaxation times of each component from the mechanical data alone. Experiments using infrared dichroism, combined with visible birefringence and stress relaxation measurements, show distinct characteristic relaxation times for each species, which have different dependencies on temperature and blend composition [12, 13, 14, 15]. However, some of these studies have required relatively large strains and have been so limited in their dynamic range that the shape of the relaxation modulus could not be determined [12, 15]. There is still a lack of quantitative information on the dynamics of each species, as well as an understanding of the connection between the differences in local segmental mobility and that manifested in macroscopic viscoelastic and

transport properties.

Based on the limited observations above, attempts have been made to explain microscopically what is physically manifested on a macroscopic level. Two basic concepts have been used to explain the thermorheologically complex behavior observed for miscible blends. The first picture [3, 1, 16] assumes that both species in the blend have the same "blend-average" properties which are determined by the local composition. Local variations in composition which impose various external environments cause local variations in the blend-average properties, thus leading to dynamical heterogeneity. The observed failure of time-temperature superposition is then attributed to the different temperature dependencies for the dynamics of species in different local environments. In the second picture [2, 6] each species is allowed to retain properties intrinsic to its chemical identity. The species' dynamics are then modified by the surrounding chains. Dynamical heterogeneity is then due to the existence of two distinct species in a uniform environment, and failure of time-temperature superposition arises because the relaxation dynamics of two species have different temperature dependencies. Experimentally, it has been difficult to monitor the contribution of the individual components to the bulk properties of the blends and to distinguish between the validity of these two explanations for thermorheological complexity.

Furthermore, the components of a blend system generally have different molecular weights, and polydispersity plays a role in modifying the blend properties. Additional modes of relaxation, such as constraint release, affect the component dynamics, making them more complex. Failure of time-temperature superposition can be much more

dramatic when the blends are bidisperse [2, 13, 14, 17]. It is thus desirable to understand how each component contributes to the blend properties regardless of the relative molecular weights of the two species. To provide "blending rules" we need to determine which properties of the pure components are useful in characterizing the behavior of the species in the blend, and how they are modified by blend composition and temperature.

Finally, we expand our focus to consider block copolymer melts of the same species as the miscible blends. In phase separated, multicomponent systems the compatibilizing agent often consists of a block copolymer. Toward the goal of predicting the processing behavior of blends and understanding the behavior of the stabilizer in a blend environment, we examine the effect of the composition and temperature on the dynamics of disordered, entangled diblock copolymer melts. We investigate the effect of composition and temperature on the dynamics of block copolymers when they are homogeneously mixed. This serves to investigate the dynamic behavior of block copolymer chains which are diffusing through a given blend phase, as they would to reach the interfacial regions between blend phases, to act as compatibilizers.

In addition, there are fundamental questions regarding the properties of disordered diblock copolymer melts which remain unanswered. While bidisperse miscible blends show dramatic failure of time-temperature superposition [2, 13, 14, 17], rheological studies of diblock copolymers of the same components paradoxically show no such thermorheological complexity [18]. In miscible blends the failure of time-temperature superposition has been attributed to the different temperature dependences of the

relaxation of each component. The largest departures from thermorheological simplicity are observed in blends where an anomolously broad glass transition is observed in thermal measurements. Furthermore, diblock copolymers and blends of the same overall composition *both* have anomalously broad glass transitions compared to the homopolymers [18, 5], suggesting a similarity between the distribution of local mobilities in the block copolymer and blend. Thus, it is not understood why time-temperature superposition fails for miscible blends, yet it applies to disordered diblock copolymers of the same components.

1.3 Project Objectives

At present there are relatively few experimental or theoretical studies of miscible blends and from the studies that exist there are persistent questions regarding the molecular origins of the complex behavior demonstrated by these systems. More practically, one cannot yet predict the viscoelastic properties of miscible blends from a knowledge of the constituent homopolymer properties. One reason these previous experiments have not been able to distinguish among the various explanations for dynamical heterogeneity is because they cannot quantitatively and selectively observe the dynamics of each species in a miscible blend.

In order to clarify the existing experimental data and help ascertain which model is appropriate, as well as elucidate the microscopic factors controlling dynamical heterogeneity, we will use a spectroscopic method capable of distinguishing between the

two species in the blend, over a wide dynamic and temperature range. These measurements will be used to determine the entanglement molecular weight and monomeric friction coefficient of each species as a function of blend composition and temperature, rather than treat them as blend-averaged parameters. We want to probe the nature of the intra- and intermolecular forces controlling blend dynamics, i.e., those due to the intrinsic chemical nature of a given chain and those due to the blend environment consisting of the surrounding chains.

Using the technique described in Chapter 2, we simultaneously analyze the behavior of the stress and the birefringence, using mechanical measurements and polarimetry techniques, respectively. By taking advantage of the inherent optical contrast between the components of the blend, we are able to determine the contribution of each species to the overall relaxation dynamics of the blend, over a range of compositions and temperatures. The two species contribute differently to the stress and birefringence; consequently, these two observables provide sufficient information to extract the individual dynamic moduli of the two components. This allows us to compare *quantitatively* mechanical and optical results obtained simultaneously, under identical sample conditions.

In order to test the concepts above regarding miscible blends, it is necessary to observe the relaxation dynamics of each species. Compositional heterogeneity leads to thermorheological complexity because the temperature dependence of the dynamics of a given species varies with its local environment. Thus, chains of a *given* species lying in different regions will shift differently with temperature, and the shape of the

corresponding relaxation spectrum may change as well. If, however, the failure of the superposition principle is due to species-specific temperature dependencies, then the relaxation spectrum of each species will not change shape with temperature. To determine the relative importance of these two effects, it is advantageous to examine blends in which the shape of the relaxation spectra of each species is not greatly altered by other effects, particularly polydispersity. While this requires that the components' relaxations overlap completely in the blend, making it impossible to distinguish them using rheometry alone [2], our rheo-optical methods are particularly useful, and are capable of distinguishing the dynamics of the distinct species in a multi-component system [19, 20, 21].

Using the same technique, we then focus on miscible blends of components with very different molecular weights. In these unequally entangled blends the effects of polydispersity, such as constraint release, and orientational coupling make the determination of the components' dynamics more complex than in the equally entangled case, with additional modes of relaxation possible. We want to determine whether the trends observed in the entanglement molecular weights and friction coefficients of the equally entangled blends are sufficient to describe the behavior of the components in these unequally entangled blends. We also seek to determine the amount of orientational coupling induced in the faster-relaxing component due to the remaining orientation of the slower-relaxing matrix, which is represented by a coupling parameter, ϵ. Finally, we investigate the possible dependence of ϵ on temperature, composition and species. Where possible we will compare our results to the work of

Zawada et al. [13, 14].

Finally, we turn to the dynamics of PIP/PVE diblock copolymers. We seek to understand why the thermorheological complexity seen for miscible polymer blends is not observed for diblock copolymers of the same constituent species. To do so, we apply the same methods as used in the blend studies. The stress-optic behavior is observed in order to infer the contribution of each block to the relaxation dynamics of the whole chain. We want to determine whether there is a relationship between the dynamics of each block of the disordered diblock copolymers and those of each species in the miscible blends. This will allow us to provide a more complete picture of the effects of blending two chemically different species, whether they are on the same chain or on distinct chains.

1.4 Summary of Results

The dynamics of each component in miscible blends of polyisoprene / polyvinylethylene (PIP/PVE) were studied using dynamic stress-optical measurements. By using a blend of components that are nearly equally entangled, we avoided the effects of polydispersity on the dynamic moduli of each species. We used both dynamic stress and birefringence measurements to determine the contributions of each species to the blend dynamic modulus. Orientational coupling, which affects the birefringence but not the stress, was incorporated, based on the value of the coupling coefficient determined from rheo-optical studies of unequally entangled blends [13, 14, 17]. This

combination of model blend and rheo-optical method allowed us to examine the effect of the chemical composition of the blend on the dynamics of each species. While we cannot rule out contributions of compositional heterogeneity to thermorheological complexity in the PIP/PVE system, we found that it is the intrinsic differences between the temperature dependencies of the dynamics of two species which dominate the overall failure of the superposition principle.

Blending produces minor changes in the entanglement molecular weights of PIP and PVE from those of the pure components (only $\approx 30\%$ over the full range of composition), but dramatically alters their monomeric friction coefficients. The dynamics of the component with the higher glass transition temperature in the pure state (PVE) are more sensitive to blend ratio and temperature. The observation that the dynamics of both species retain distinct temperature dependencies is in accord with previous experimental studies of PIP/PVE blends [2, 8, 9]. The present approach can be contrasted to earlier rheological approaches in which the relative position of two, often overlapping, loss peaks are monitored to determine the temperature shift of each species in a bidisperse miscible blend [2]. Stress-optical measurements facilitate quantitative determination of the monomeric friction coefficients of each component by revealing the contributions of each species to the blend dynamic modulus. Our results are consistent with prior studies and better establish the precise values of the species' friction coefficients in PIP/PVE blends.

We then studied PIP/PVE blends in which the components have contrasting molecular weights and the effects of polydispersity become important. Again, si-

multaneous analysis of the shear stress and birefringence was used to extract the relaxation of each component. The analysis of the stress-optic data incorporated the effects of orientational coupling, from which we were able to estimate the average coupling coefficient, ϵ, for the PIP/PVE system. When the species' relaxations in the blend remain well-separated over the range of temperature and composition probed, the value of ϵ can be determined, leading to $\epsilon_{PIP,PVE} \approx 0.35 \pm 0.04$ and $\epsilon_{PVE,PIP} \approx 0.27 \pm 0.08$. To within experimental uncertainty it appears appropriate to use a single average value of ϵ. No perceptible dependence of ϵ on temperature or composition was observed and the values lie within the range established for other systems [13, 14, 22].

The component moduli in the blends were then extracted as functions of temperature and blend composition, from which we determine the component entanglement molecular weights and monomeric friction coefficients. The main trends observed are the same as those determined for the equally entangled system [23]. Thus, for all three blend systems, blending does not greatly affect the values of the component entanglement molecular weights. It is the species' monomeric friction coefficients which are the most sensitive to blending, and the values obtained for the unequally entangled blends quantitatively agree with those for the equally entangled system. While failure of time-temperature superposition is again due to the distinct temperature dependencies of the monomeric friction coefficients of the two species, it is both the contrast in friction coefficient and the relative weights of the components which determine the degree to which complex thermorheological behavior is observed.

Finally, coordinated analysis of the shear stress and birefringence is used to monitor the relaxation of each block in disordered diblock copolymer melts. Qualitatively, the main features observed in the frequency dependence of the complex stress-optic behavior can be explained in terms of the relaxation of chains with blocks having distinct stress-optic coeffficients. The center portion of the block copolymer dominates the behavior at low frequencies. Quantitative comparison to predictions of the reptation model reveals that for a diblock in which the distinct blocks have similar friction coefficients ($\phi_{PIP} = 0.75$), the chain relaxes like a chain having uniform friction. However, if there is a significant contrast between the friction coefficients of the two blocks, combined with a change in this contrast with temperature, then significant departures from the uniform-friction relaxation dynamics can occur. This is observed when the diblock is rich in the component with the higher glass transition temperature (PVE) ($\phi_{PIP} = 0.25$).

Failure of time-temperature superposition for the mechanical moduli is not noticable for these block copolymer melts because the relaxation spectrum is always nearly that of a monodisperse homopolymer. However, the lack of superposition achieved for the stress-optic data when using the shift factors determined from superposition of the mechanical data shows that complex thermorheological behavior is in fact present. It is more noticeable in the block copolymer rich in the component with the higher glass transition temperature (PVE), as it was in the corresponding miscible blend. Thus, the apparent time-temperature superposition paradox has been resolved.

1.5 Outline of Thesis

Chapter 2 details the principles behind the mechanical measurements and how they yield information regarding the relaxation behavior of polymer chains. The basis for the optical measurements is also described, and the instrumentation used in all the studies discussed here is presented. A formulation of the measured quantities in terms of physical properties of interest is also given.

In Chapter 3 we discuss experiments on equally entangled PIP/PVE blends. We begin with a review of the previous results which leads us to study these blends. A brief description of the model polymer system and review of the relevant measurements obtained using the rheo-optical instrument is given. Then we present the results of dynamic stress and birefringence measurements, followed by interpretation in terms of the relaxation dynamics of each species in the blend. We discuss the relative importance of compositional heterogeneity and intrinsic differences in mobility of the components for these blends. Finally, we present our conclusions regarding the effect of blending on the entanglement molecular weight and monomeric friction coefficient of each species.

Chapter 4 contains results on unequally entangled PIP/PVE blends, for which we are able to determine the effects of orientational coupling and extract the coupling coefficient, ϵ. We first describe the polymers used in these experiments and briefly mention the variables of interest, based on the rheo-optical technique described in Chapter 2. Next, we present the results of our dynamic stress and birefringence mea-

surements for unequally entangled blends: ones in which PVE is the slower-relaxing species and ones in which PIP is slower-relaxing. We describe how the contribution of each component to the blend dynamic moduli and the values of the coupling coefficient, ϵ, were determined. The dependence of ϵ on temperature, composition and species is examined. This is followed by a discussion of the results in terms of the component dynamics in the blends, from which we again extract component entanglement molecular weights and monomeric friction coefficients. We look at the effect of orientational coupling on the component parameters. Finally, comparisons are made between the different blends.

In Chapter 5 we present our studies of the dynamics of disordered diblock copolymers of PIP and PVE for two compositions ($\phi_{PIP} = 0.25$ and 0.75), over a range of temperatures. We describe the properties of the model diblock system and the rheo-optical instrument used. Next, we present the results of our dynamic stress and birefringence measurements. This is followed by a preliminary interpretation based on the reptation model for mechanically uniform, entangled, linear polymers. We examine the relationship between the dynamics of the species of each block of the disordered diblock copolymers and those of each species in the corresponding miscible blends. We resolve the recently reported paradox where time-temperature superposition fails for PIP/PVE blends, yet applies to these disordered PIP-PVE diblock copolymers.

Bibliography

[1] Colby, R. H. *Polymer* **1989**, *30*, 1275.

[2] Roovers, J.; Toporowski, P. M. *Macromolecules* **1992**, *25*, 3454.

[3] Lau, S.; Pathak, J.; Wunderlich, B. *Macromolecules* **1982**, *15*, 1278.

[4] Zetsche, A.; Kremer, F.; Jung, W.; Schulze, H. *Polymer* **1990**, *31*, 1883.

[5] Trask, C. A.; Roland, C. M. *Macromolecules* **1989**, *22*, 256.

[6] Miller, J. B.; McGrath, K. J.; Roland, C. M.; Trask, C. A.; Garroway, A. N. *Macromolecules* **1990**, *23*, 4543.

[7] LeMenestrel, C.; Kenwright, A. M.; Sergot, P.; Lauprêtre, F.; Monnerie, L. *Macromolecules* **1992**, *25*, 3020.

[8] Chung, G. C.; Kornfield, J. A.; Smith, S. D. *Marcromolecules* **1994**, *27*, 964.

[9] Chung, G. C.; Kornfield, J. A.; Smith, S. D. *Marcromolecules* **1994**, *27*, 5729.

[10] Composto, R. J.; Kramer, E. J.; White, D. M. *Macromolecules* **1988**, *21*, 2580.

[11] Composto, R. J.; Kramer, E. J.; White, D. M. *Polymer* **1990**, *31*, 2320.

[12] Zawada, J. A.; Ylitalo, C. M.; Fuller, G. G.; Colby, R. H.; Long, T. E. *Macromolecules* **1992**, *25*, 2896.

[13] Zawada, J. A.; Fuller, G. G.; Colby, R. H.; Fetters, L. J.; Roovers, J.; *Macromolecules* **1994**, *27*, 6851.

[14] Zawada, J. A.; Fuller, G. G.; Colby, R. H.; Fetters, L. J.; Roovers, J.; *Macromolecules* **1994**, *27*, 6861.

[15] Zhao, Y.; Jasse, B.; Monnerie, L. *Polymer* **1989**, *30*, 1643.

[16] Fischer, E. W.; Zetsche, A. *ACS Polymer Preprints: Spring, San Francisco* **1992**, *78*.

[17] Arendt, B. H.; Krishnamoorti, R.; Kornfield, J. A.; Smith, S. D. *Manuscript in preparation.*

[18] Roovers, J.; Wang, F. *J. Non-Cryst. Solids*, **1994**, *172-4*, 698.

[19] Kannan, R. M. *Ph.D. Thesis*; California Institute of Technology: Pasadena, 1994.

[20] Kannan, R. M.; Kornfield, J. A. *Rheologica Acta* **1992**, *31*, 535.

[21] Kannan, R. M.; Kornfield, J. A. *Journal of Rheology* **1994**, *38*, 1127.

[22] Ylitalo, C. M.; Zawada, J. A.; Fuller, G. G.; Abetz, V.; Stadler, R. *Polymer*, **1992**, *33*, 2949.

[23] Arendt, B. H.; Kannan, R. M.; Zewail, M.; Kornfield, J. A.; Smith, S. *Rheologica Acta*, **1994**, *33*, 322.

Chapter 2

Instrumentation

A powerful and selective technique will be utilized in our experiments to determine the contributions of each component to the dynamics of the blends and the block copolymer (BCP) melts. It combines measurement of optical anisotropies with mechanical rheometry. Measurement of the bulk stress in a miscible blend or disordered BCP melt only yields information regarding the backbone orientation of the components. Since the two species in each system contribute additively to the stress, there is no means to distinguish the contribution of one component from another. Simultaneous use of polarized light to measure the birefringence also provides information about the segmental orientation of both species, but the components now contribute in proportion to their anisotropic polarizabilities which can be of opposite signs and quite different in magnitude. By using the technique of optical rheometry and making use of the optical contrast between the two species in our systems, we will be uniquely able to quantitatively study the individual contribution of each component

to the overall behavior of the system, while simultaneously monitoring the properties of the system as a whole.

2.1 Rheology and Viscoelastic Properties

To quantify the mechanical properties of polymers it is useful to probe their viscoelastic behavior. The viscoelastic nature of a material characterizes how it behaves under deformation, and elucidates the relaxation spectra corresponding to changes in the molecular conformation. For a perfectly elastic, Hookean solid the stress, $\sigma(t)$, which is a measure of the distribution of forces in a deformed body, is proportional to the applied strain, $\gamma(t)$. In the case of oscillatory shear, the material responds perfectly in phase with the strain applied to it. The work of deformation is stored elastically and is totally recoverable, because the relaxation time of an ideal solid is infinite. For a perfectly viscous Newtonian fluid, the stress is proportional to the rate of strain, $\dot{\gamma}(t)$. In the case of oscillatory shear the material responds perfectly out of phase with the strain applied to it. The work of deformation is dissipated viscously and is totally lost because an ideal fluid is able to relax infinitely quickly.

Polymers are neither perfect solids nor perfect liquids. In fact, the nature of their mechanical response depends on the time scale over which the deformation and measurement occur, as well as the intrinsic relaxation spectrum of the material. Polymers exhibit a behavior which is both elastic and viscous, i.e., they are *viscoelastic.* For slow deformations there is sufficient time for molecular relaxation to occur and the re-

sponse is that of a viscous liquid. Similarly, for rapid deformations relaxation cannot occur quickly enough, and the material behaves like an elastic solid.

One can measure the characteristic relaxation times of a material via mechanical experiments. In a step shearing experiment a constant strain of amplitude γ_o is applied to a slab of material between parallel plates (see Figure 2.1a). The force required to maintain this constant deformation as a function of time yields the relaxation modulus, $G(t)$. The form of $\log(G(t))$ vs. $\log(t)$ for a linear, well-entangled homopolymer melt is shown in Figure 2.1b. At sufficiently short times the polymer behaves as a glassy solid and is unable to relax, thus the modulus remains essentially constant. At slightly longer times the polymer undergoes a transition where local relaxation of the polymer backbone via Brownian motion occurs, manifested by a reduction in the modulus. At still longer times there is a rubbery plateau region in which the polymer melt acts as a transitory elastic network. The value of the modulus in the plateau, G_N^o, is associated with the molecular weight between chain entanglements, M_e, and is characteristic of the polymer. At sufficiently long times, the polymer chains can relax completely and the modulus decays to zero. There is a characteristic time, τ_d, at which the decay from the plateau modulus occurs. The existence of the rubbery plateau with modulus independent of molecular weight and terminal relaxation time that varies as a high power of molecular weight are all captured by reptation theory [1], presented in more detail in Chapters 3-5.

The information contained in the relaxation modulus as a function of time can also be obtained in dynamic experiments as a function of frequency. Here we perform

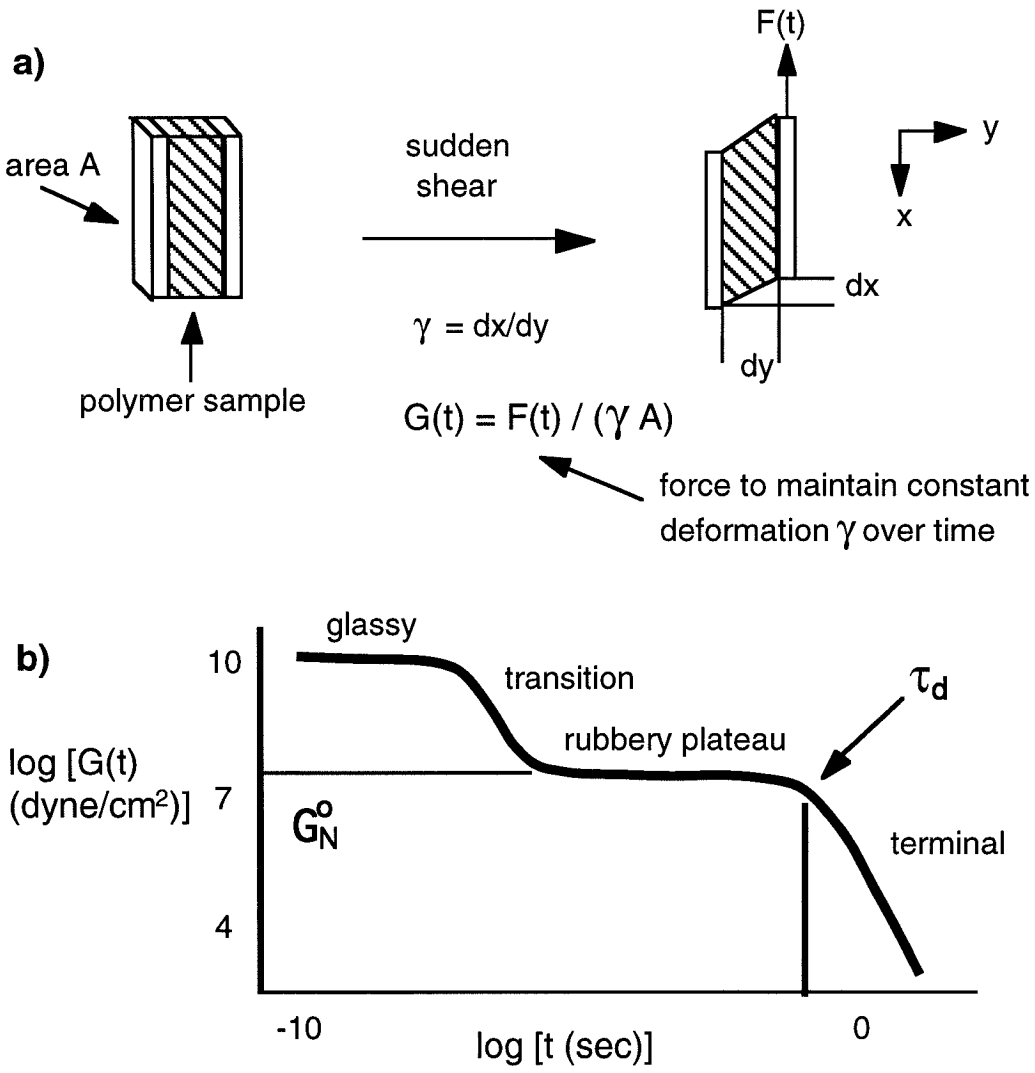

Figure 2.1: **a)** Schematic setup for a sudden step shear experiment. The force required to maintain a constant deformation is measured over time. **b)** The relaxation modulus as a function of time for sudden step shear experiment. Note the rubbery plateau and terminal relaxation regions.

dynamical tests in which a range of four decades (0.01 - 100 rad/sec) in shearing frequency is probed at each chosen temperature. In this case the applied shear strain is sinusoidal with frequency ω: $\gamma(t) = \gamma_o \sin(\omega t)$. The observed shear stress is also oscillatory, but out of phase by an amount $\delta(\omega)$ from the shear, as seen in Figure 2.2a. The modulus can then be written as $G^*(\omega) = G'(\omega) + iG''(\omega)$, for which the stress becomes

$$\sigma = \gamma_o[G'(\omega)\sin\omega t + G''(\omega)\cos\omega t] \tag{2.1}$$

where $G'(\omega)$ and $G''(\omega)$ are termed the dynamic moduli. The storage modulus, $G'(\omega)$, represents the energy stored elastically and recovered per cycle. $G''(\omega)$, the loss modulus, represents the energy dissipated viscously and lost as heat per cycle. The phase lag between the stress and strain is given by $\delta(\omega) = \tan^{-1}[G''(\omega)/G'(\omega)]$.

At long times, or in the limit that $\omega \to 0$ the dynamic moduli take on characteristic shapes where $G'(\omega) \approx \omega^2$ and $G''(\omega) \approx \omega$. These dependencies can be understood by considering the motion of a chain on the longest time scales, for which relaxation occurs by motion of the chain as a whole. In this limit the dynamics are dominated by a single, longest relaxation time, τ_d, characteristic of this relaxation mode, and $G(t) \sim e^{-t/\tau_d}$. The components of the Fourier transform of $G(t)$, in the limit $\omega \to 0$, yield the characteristic exponential dependence on frequency with slopes of 2 and 1 for the storage and loss moduli, respectively. Experiments on entangled homopolymer melts confirm these results as seen in Figure 2.2b, which shows the dynamic moduli of a 190 kg/mol sample of polyisoprene ($T_{g,PIP} \approx -65°$C) [2]. The parameters of interest

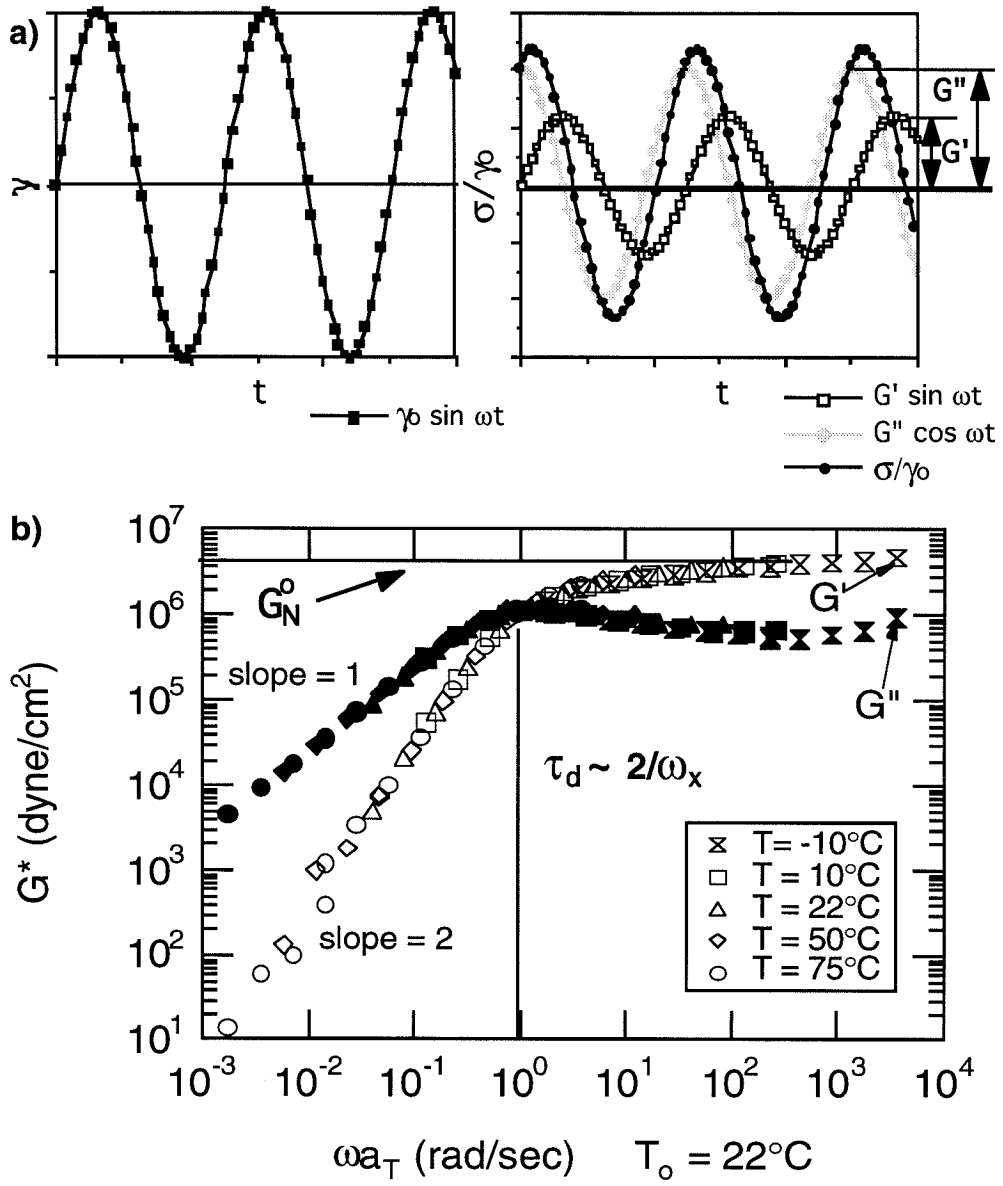

Figure 2.2: **a)** Shear, stress and dynamic moduli as a function of time for an oscillatory shear experiment, with a sample setup similar to that used in the sudden step shear experiment. **b)** The dynamic moduli versus reduced freqeuncy, where the data at several temperatures have been superimposed by shifting horizontally. Notice the terminal regime behavior where the moduli take on slopes of 1 and 2. Also note the rubbery plateau and terminal relaxation.

from these measurements are the plateau modulus, G_N^o, in $G'(\omega)$ which characterizes the degreee of chain entanglement, and the cross-over frequency $\omega \approx 2/\tau_d$ for which $G'(\omega_x) = G''(\omega_x)$, which gives a measure of the longest relaxation time of the chain. Interpretation of these features within the context of a particuar model for polymer melt dynamics, the reptation model [1], is discussed in more detail in Chapters 3 and 4.

Experimentally, it is often desirable to extend measurements over a wide range of frequencies in order to probe a large window of time, and hence length scales. Practically, however, limitations are imposed by the speed of data acquisition, the dynamic range of the apparatus and the patience of the observer. When dealing with homopolymers, the principle of time-temperature superposition [2, 3] can be used to extend the effective range of shearing frequency. By increasing the temperature, slower motions can be sped up, moving them into the experimental window. Similarly, decreasing the temperature causes faster motions to be slowed down. Thus, measurements over a large range of frequencies can be reproduced by making measurements over a limited range of frequencies but at many temperatures, as seen in Figure 2.2b. The dynamic moduli at various temperatures are related to those at an arbitrary reference temperature, T_{ref}, by scaling the shearing frequency by a_T, the horizontal shift factor needed to overlay the data on a reduced frequency axis, and the moduli by b_T, a vertical shift factor.

$$G'(\omega, T_{ref}) = b_T G'(\omega a_T, T) \tag{2.2}$$

$$G''(\omega, T_{ref}) = b_T G''(\omega a_T, T) \tag{2.3}$$

Values of the shift factors are less than 1 for $T > T_{ref}$, and *vice versa.* In general, a_T, which can vary by orders of magnitude, is much more temperature dependent than b_T, which is often taken to be unity. It is important to note that in order to use time-temperature superposition effectively, it is necessary that the steps in temperature be small enough so that there is sufficient overlap and features present in the data sets to accurately determine the shift factors.

Physically, we can qualitatively understand why time-temperature superposition holds for a homopolymer melt. Relaxation of the polymer chain requires motion and rearrangement of the backbone segments. For glassy motions on the shortest time scales, this corresponds to motions involving only a few backbone bonds. Motions with longer time scales require more coordinated reorganization of larger portions of the chain. Fundamentally, however, each relaxation mode is based on the fastest, most local mode, with slower, larger-scale relaxations merely requiring more of these local rearrangements to occur. Thus, as the rate of local motions increases with temperature, so do those of all other modes, each being based on the fastest mode. This is true for each chain in the melt. Thus, the frequency dependence of the dynamic moduli, which reflects the underlying relaxation spectra of the polymer, scales with the temperature and the moduli shift together on the frequency axis. The magnitude of the moduli themselves also scale with temperature, but since they are also proportional to the melt density, which decreases with increases in temperature,

the effects partially cancel. Thus, the vertical shift is often neglected [2, 3].

Relaxation processes are thermally activated, thus the horizontal shift factors, a_T, roughly follow an exponential dependence on inverse temperature. Near the glass transition temperature, where the onset of the most local motions occurs, a_T depends even more strongly on temperature, and time-temperature superposition has been known to fail [2]. In our work, however, we focus on temperatures above the glass transition regime. Empirically, the temperature dependence of the horizontal shift factors, i.e., the polymer dynamics, can be described by the WLF relation (proposed by Williams, Landel and Ferry) [2, 3]

$$\log\left(\frac{a_T}{a_{T_{ref}}}\right) = \log(a_T) = \frac{-C_1^{ref}(T - T_{ref})}{C_2^{ref} + (T - T_{ref})} \tag{2.4}$$

since $a_{T_{ref}}$ is taken to be unity. C_1^{ref} and C_2^{ref} are material constants and T_{ref} is the reference temperature. Often, the reference temperature is taken to be the glass transition temperature, T_g, of the polymer. The values of C_1^g and C_2^g can then be related to the fractional free volume of the polymer at T_g and the coefficient of thermal expansion of the fractional free volume [2].

While time-temperature superposition holds for homopolymers, one might expect it to fail for blends, particularly if the dynamics of the two components have different temperature dependencies. If the dynamics of each species still maintain, to some degree, their own temperature dependencies in the blend, due to the distinct, intrinsic chemical nature of the two components, then the blend moduli would depend on the underlying shift factors of both species. Thus we would expect to see the fail-

ure of the superposition principle if the temperature dependence of the two species' dynamics in the blend were sufficiently different. By extracting the component moduli, we will be able to investigate this for the miscible blends of our study, which have fairly widely separated pure-component T_g's. Such potential disparities between the temperature dependence of the relaxation dynamics of each species could have consequences for the relaxation of the BCP melts. If the relative relaxation rates of the species comprising the two blocks changes sufficiently with temperture, then one would also expect to see evidence of the failure of time-temperature superposition for the disordered block copolymers as well. We will be able to observe selectively the contribution of each component by using our unique apparatus, which combines the mechanical measurements described so far with polarimetric experiments detailed in the next sections.

2.2 Optical Rheometry

A polymer sample with an otherwise isotropic segment orientation can be made anisotropic via application of mechanical shearing. Optically, this is manifested by an anisotropy in the index of refraction, which affects the retardation and absorption of polarized light passing through the sample. The rheo-optic measurements we perform utilize this anisotropy. By passing light with a well-defined state of polarization through a polymer under shear and analyzing changes in the state of polarization, we gain additional, often selective information about the system's response to flow.

The anisotropic part of the index of refraction tensor can be written as

$$\tilde{\mathbf{n}} = \mathbf{n}' - i\mathbf{n}'' \tag{2.5}$$

where the real part, $\mathbf{n}'$, describes the anisotropic retardation of polarized light and the imaginary component, $\mathbf{n}''$, the anisotropic absorption.

The birefringence, $\Delta n'_{ij}$, is defined as the difference between the principal values of $\mathbf{n}'$. Similarly, the dichroism, $\Delta n''_{ij}$, is the difference between the principal values of $\mathbf{n}''$. Physically, the birefringence describes the anisotropic retardation of polarized light passing through the sample. Light polarized in one principal direction travels faster than if polarized in an orthogonal one, and this is manifested by a phase shift between these two components of a polarized beam. Similarly, the dichroism describes the anisotropic absorption. Light is absorbed preferentially depending on the dipole moment orientation of the segments capable of absorbing light of the wavelength of interest.

Birefringence can have two sources. *Form* birefringence is observed when a sample contains microscopic structures of anisotropic shape or arrangement and whose refractive index differs from the material surrounding or suspending them. *Intrinsic* birefringence is the result of anisotropic polarizability which is inherent to the molecules or particles themselves. In miscible blends or disordered block copolymer melts with one homogeneous phase, only intrinsic birefringence is assumed to be observed.

Dichroism can also have two sources. *Conservative* dichroism is due to scattering

of light by anisotropically-distributed structures or domains whose size is on the order of the wavelength used. *Consumptive* dichroism arises from isotropic absorption by the medium, which is related to the microscopic orientation of its molecules. For our systems no dichroism is observed, hence we focus on measurements of the intrinsic birefringence.

2.3 Two-Axis Optical Rheometry

The apparatus and tool cell are shown schematically in Figures 2.3 and 2.4, respectively. Details of its construction and setup are described elsewhere [4, 5, 6, 7, 8, 9]. Mechanical measurements are performed entirely within a commercially available rheometer, a Rhometrics Solids Analyzer (RSA II), which can apply a controlled deformation to a sample and measure the resulting force. To perform optical measurements, the tool cell was constructed with non-birefringent, transparent CaF_2 windows. The sample can be probed in either the 1,2- or 1,3-geometry, with light passing through or across the sample gap, as shown by the axes defined in Figure 2.4.

In this work, a sample thickness of 0.5 mm was used, for which strains of 0.2 - 100% could be applied. The frequency of oscillatory shear covers four decades of response, from 0.01 to 100 rad/sec, and forces from 1 to 10^3 gm can be detected. The environmental chamber is capable of maintaining uniform and stable temperatures from -100 to 400°C (±0.1°C). In order to allow for optical measurements, apertures were cut in the environmental chamber walls and replaced with non-birefringent,

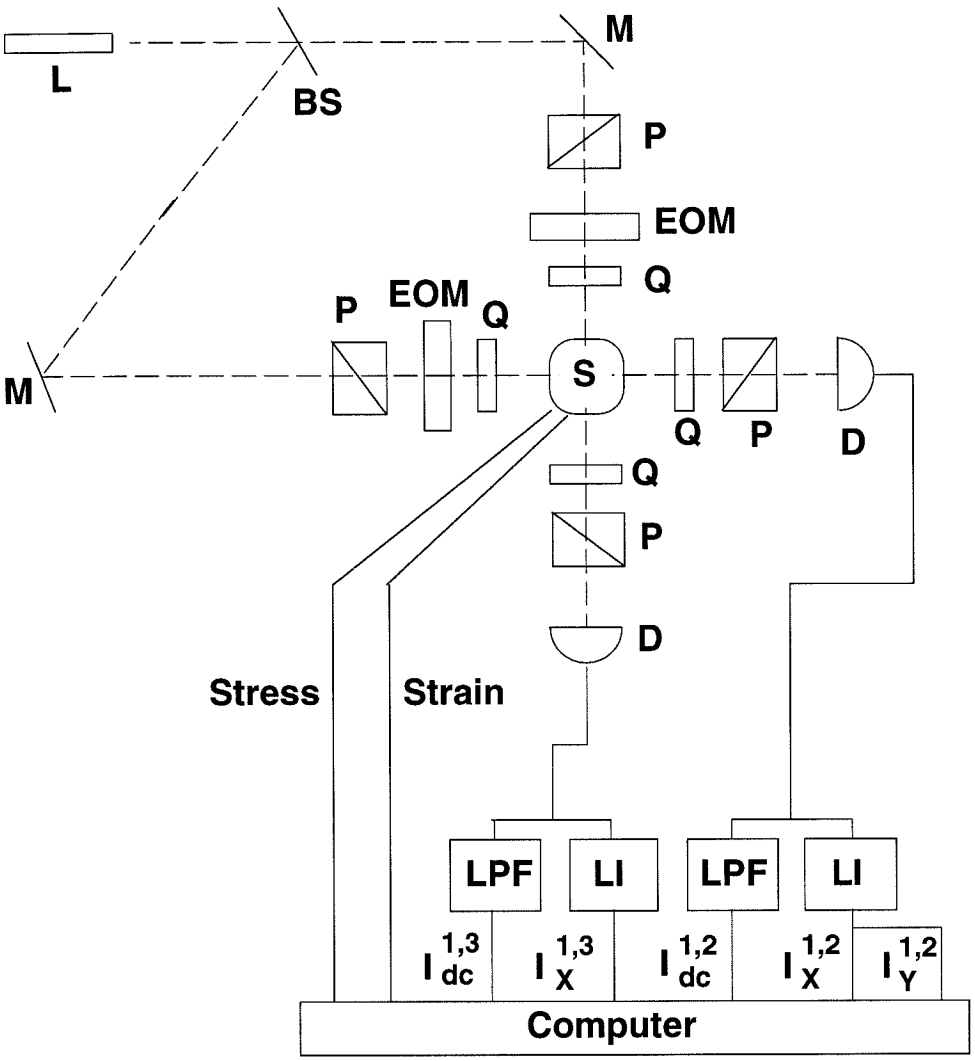

Figure 2.3: Two-axis rheometer setup. **L** denotes the HeNe laser, **M**, mirrors, **BS**, a beamsplitter and **S**, the sample inside the RSA II. The optical elements consist of polarizers **P**, electro-optic modulators **EOM**, quarter waveplates **Q** and detectors **D**. The stress and strain signals from the RSA II are fed to a computer, as are the *dc* signals from the low-pass filters **LPF** and the components from the lock-in amplifiers **LI**. See the text for discussion.

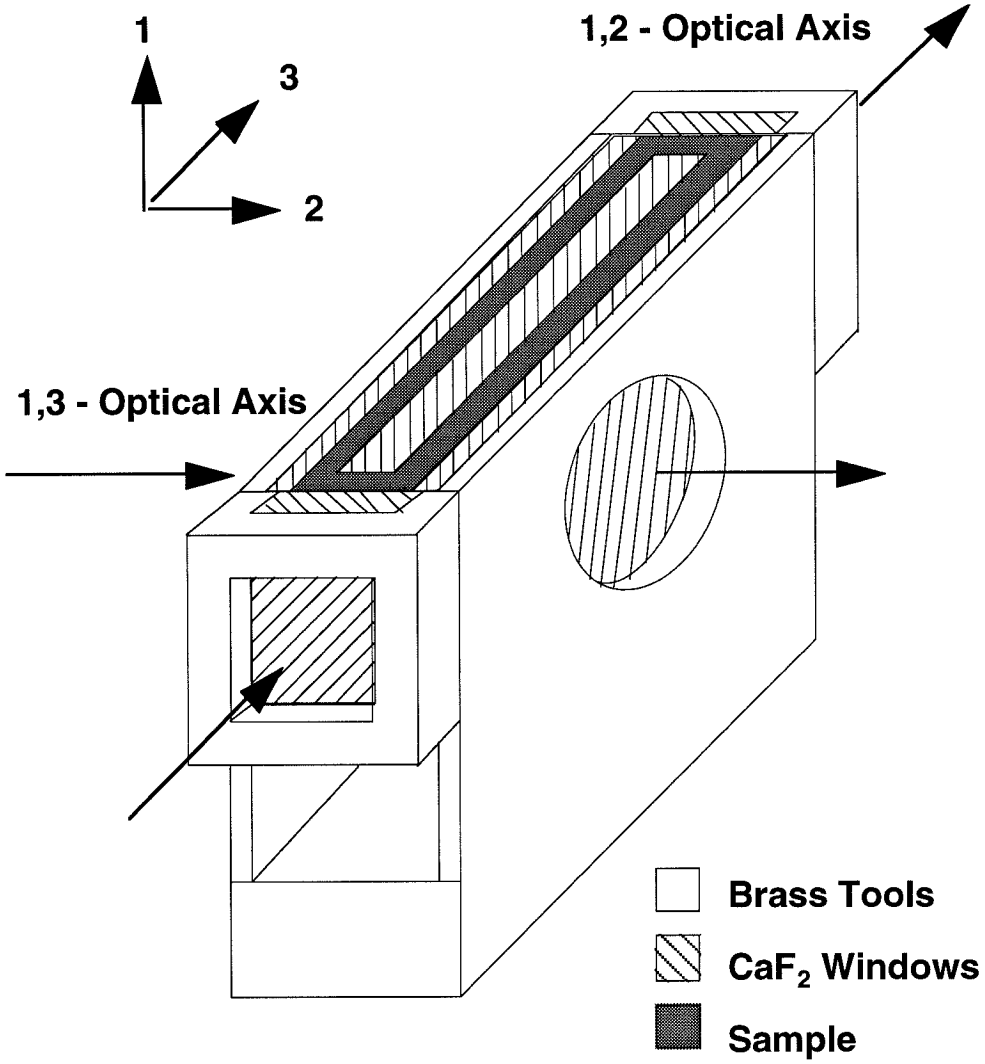

Figure 2.4: Tool cell used in the two-axis rheometer. The tool cell is brass with CaF_2 windows on four sides. The center window is also made out of CaF_2, and the sample forms an annulus around it. Apertures cut in the tool cell allow the laser beam to pass through the sample in two orthogonal directions, thus probing the 1,2- and 1,3-planes, as defined by the axes in the figure.

transparent NaCl windows.

Outside of the rheometer are added the optical elements that form the polarization state generator and analyzer, before and after the sample, respectively. The optical train prepares the light to a known polarization state before it passes through the sample, and then analyzes it afterward to determine how the sample has affected it, thus probing the sample anisotropies. In the following description, the angles given for the orientation of the optical elements are with respect to the vertical, which is the direction of shearing.

The arrangement of optical elements is given in Figure 2.3. The laser light, from a visible HeNe ($\lambda \approx 0.63\ \mu$m) source, first passes through a polarization state generator consisting of a linear polarizer at 0°, an electro-optic modulator with its axes at 45° and a quarter waveplate at 0°. The modulator imposes a relative phase shift between the components of light along its principal axes. In our instrument the retardation continuously ramps from Ωt to $\Omega t \times 2\pi$, and then drop to Ωt instantaneously, in a saw-tooth pattern, which is equivalent to a retardation that increases linearly with time. Physically, the polarization state before entering the sample is a linearly polarized beam whose direction of polarization sweeps continuously clockwise over an angle of 360°, at a modulation frequency, Ω. The light then passes through the sample, which is in a flow cell contained in the RSA II, and then through analyzing optics consisting of a quarter waveplate at 45° and a linear polarizer at 90°, which is equivalent to a circular polarizer. This signal is then measured at an intensity detector and passed to a lock-in amplifier tuned to the modulation frequency, to determine the magnitude

of the birefringence and its orientation.

For a birefringent sample the total intensity of the transmitted light remains constant. However, if we consider orthogonal components of a polarized beam, a relative phase shift will be introduced between them by the sample, causing the light to become elliptically polarized. For a linearly polarized beam sweeping in polarization direction, passage through the sample causes the degree of ellipticity to be modulated as the relative phase shift changes. This can be analyzed by passing the emerging beam through a circular polarizer, which will yield a birefringence signal modulated in intensity to be analyzed at the detector.

Briefly, one can determine the intensity of the signal received at the detector by using the mathematical formalism of the Jones or Stokes matricies for the action of each optical element on the state of polarization of the beam [8, 10]. Here we state the resulting modulated intensity observed at the detectors in our apparatus for a sample that is purely birefringent,

$$I(t) = I_{dc}[1 + b(\cos[\Omega t]\sin[\mu]\sin[2\chi] - \sin[\Omega t]\sin[\mu]\cos[2\chi])], \tag{2.6}$$

where I_{dc} is the dc-component of the intensity, b is a calibration factor and Ω is the modulation frequency. Information about the magnitude of the birefringence is contained in the retardation of the sample $\mu = (\frac{2\pi d}{\lambda})\Delta n'$, where $\Delta n'$ is the birefringence, d, the optical path length and λ, the wavelength of light used in the measurement. The orientation of the principal axes of the birefringence is given by χ with respect to the direction of shear.

In the 1,2-geometry $\chi_{1,2}$ is non-zero, hence both the $\sin[\Omega t]$ and $\cos[\Omega t]$ components of the intensity must be analyzed. These are captured by the lock-in amplifier as orthogonal signals relative to the reference sawtooth driver function of the electro-optic modulator. The calibration constant, b, can be determined by inserting a quarter wave-plate as an ideal sample for which the orientation axis, χ, and the retardation, $(\mu = \pi/2)$, are known. Normalizing the signals by I_{dc} and b yields the component intensities

$$X_{1,2} = \sin[\mu]\cos[2\chi_{1,2}] \tag{2.7}$$

$$Y_{1,2} = \sin[\mu]\sin[2\chi_{1,2}]. \tag{2.8}$$

In the 1,3-plane the principal axes of the birefringence are coaxial with the flow direction ($\chi_{1,3} = 0$) and the magnitude of the birefringence is determined from the normalized signal

$$X_{1,3} = \sin[\mu_{1,3}] \tag{2.9}$$

under the geometry of shear flow.

As discussed in the next section, this analysis completely describes the part of the anisotropic index of refraction tensor due to birefringence, as long as the retardation remains first order ($-\pi/2 < \mu < \pi/2$). In our instrument, the modulation frequency Ω (20 kHz) and the shearing frequency ω (10^{-3} - 10^{1} Hz) are well separated, thus giving rapid response and high sensitivity for quantitative measurement of the birefringence simultaneously with the shear stress. The commercial sources for the components and process for setting up the apparatus, as well as a more detailed description of the

data analysis, are presented in the work of Kannan et al. [4, 5].

2.4 Stress-Optic Material Functions

For a sample under shear flow as in the coordinates of Figure 2.4, the stress tensor has the form [2, 3]

$$\sigma = \begin{bmatrix} \sigma_{11} & \sigma_{12} & 0 \\ \sigma_{21} & \sigma_{22} & 0 \\ 0 & 0 & \sigma_{33} \end{bmatrix}. \tag{2.10}$$

The symmetry of the system dictates that the shear stress, σ_{12}, is an odd function of the strain. The normal stress differences, $N_1 = \sigma_{11} - \sigma_{22}$ and $N_2 = \sigma_{22} - \sigma_{33}$, are even functions. We directly measure the shear stress. For small deformations the shear stress is linear in the strain and, for the case of sinusoidal shear, has the form

$$\sigma_{12} = \gamma_o[G'(\omega)\sin\omega t + G''(\omega)\cos\omega t] \tag{2.11}$$

as described by equation 2.1. The anisotropic index of refraction tensor for a material in shear flow has a form analogous to the stress tensor [8, 3]

$$\tilde{\mathbf{n}} = \begin{bmatrix} \tilde{n_{11}} & \tilde{n_{12}} & 0 \\ \tilde{n_{12}} & \tilde{n_{22}} & 0 \\ 0 & 0 & \tilde{n_{33}} \end{bmatrix}. \tag{2.12}$$

Using the dual-axis instrument we are able to probe the projections of the birefrin-

gence in the 1,2- and 1,3- planes,

$$\mathbf{n'}_{1,2} = \begin{bmatrix} n'_{11} & n'_{12} \\ n'_{12} & n'_{22} \end{bmatrix} \tag{2.13}$$

and

$$\mathbf{n'}_{1,3} = \begin{bmatrix} n'_{11} & 0 \\ 0 & n'_{13} \end{bmatrix}. \tag{2.14}$$

In the 1,2-plane the optical axis is along the vorticity direction and the magnitude of the birefringence in this plane, $\Delta n'_{1,2}$, equals the difference between the principal eigenvalues of the tensor $\mathbf{n'}_{1,2}$ (see equation 2.5). Relative to the laboratory flow direction, the principal axes of $\mathbf{n'}_{1,2}$ form an angle of χ. In terms of the experimentally measured $\Delta n'_{1,2}$ and χ, the components of $\mathbf{n'}_{1,2}$ are [11]

$$n'_{12} = \frac{1}{2}\Delta n'_{1,2}\sin(2\chi) \tag{2.15}$$

$$n'_{11} - n'_{12} = \Delta n'_{1,2}\cos(2\chi). \tag{2.16}$$

Under small amplitude oscillatory shear, the behavior of n'_{12} is similar to that of σ_{12} in equation 2.11. The complex birefringence coefficient, $B^* = B' + iB''$, can be defined for n'_{12} where

$$n'_{12} = \gamma_o[B'(\omega)\sin\omega t + B''(\omega)\cos\omega t] \tag{2.17}$$

analogous to the expression for the shear stress.

In the 1,3 plane, where the optical axis is along the velocity gradient direction, symmetry implies that the laboratory axis and axis 3 are coaxial with the principal

axes of $\mathbf{n'}_{1,3}$ ($\chi = 0$). Thus, the magnitude of the birefringence $\Delta n'_{1,3} = n'_{11} - n'_{33}$ completely describes the anisotropy in the index of refraction in this plane.

In this work we focus on the birefringence in the 1,2-plane. In particular, we look at the relative magnitudes of and the phase between the birefringence and shear stress. We define the stress-optic ratio and phase difference between σ_{12} and n'_{12} as

$$SOR \equiv \frac{|B^*|}{|G^*|} = \frac{\sqrt{B'^2 + B''^2}}{\sqrt{G'^2 + G''^2}} \tag{2.18}$$

and

$$\delta_B - \delta_B \equiv \tan^{-1}(\frac{B''}{B'}) - \tan^{-1}(\frac{G''}{G'}). \tag{2.19}$$

For simple fluids and homopolymer melts under small deformations, these are both independent of frequency, with SOR being the stress-optic coefficient, C, and $\delta_B - \delta_G \approx 0$ rad. This means that the stress and birefringence remain in phase and in constant proportion to each other, and is called the stress-optic rule. The stress-optic coefficient [11] is a function of the average index of refraction of the material and the difference between the principal polarizabilities of the polymer segments. In general, the stress-optic coefficient depends on the chemical nature of the polymer and varies weakly with temperature. Ideally, it is independent of the polymer molecular weight and a weak function of the wavelength of light used for the birefringence measurements. For polymers which exhibit a strongly polarizable group that orients perpendicular to the flow direction, the stress-optic coefficient can be negative. This is the case for the phenyl side-group of polystyrene and the vinyl pendent group of 1,2-polybutadiene (polyvinylethylene). Typical absolute values range from 10^{-10} to

10^{-11} cm^2/dyne.

The relation of mechanical measurements of stress to optical anisotropies such as birefringence relies upon a microscopic statistical treatment of chain orientation, which is discussed in more detail in Chapters 3 and 4. Qualitatively, the familiar stress-optic rule, embodied in equation 2.18, states that the stress and birefringence are linearly proportional via the stress-optic coefficient. For a homopolymer one can physically understand this proportionality by considering that the anisotropy in chain segment orientation, which contributes to the stress on the scale of entanglements, also leads birefringence due to differences in the principal polarizabilities of the polymer segments on a molecular level.

While the stress and the birefringence of a homopolymer are due to the anisotropic orientation of chemically-identical segmental units, the situation is more complex for miscible blends and disordered diblock copolymers. Though the stress-optical rule holds for homopolymers, it is **not** generally valid for blends or block copolymers, where the stress and birefringence are differently weighted averages of the two species' or blocks' orientation, i.e., the second moment of their segmental orientation distributions. The failure of the stress-optic rule is particularly obvious, for example, if one component has a negative stress-optic coefficient. Then the two species contribute additively to the stress but oppositely to the birefringence. Furthermore, the optical behavior may be dominated by one species if its stress-optic coefficient is much larger than that of the other species.

Thus, there is no method to predict the birefringence of a blend or block copoly-

mer melt from the bulk stress measurements alone. This is of concern because the birefringence is a commercially useful (or troublesome) property of polymers which are used in optical applications. Since the optical properties are affected by flow, which occurs during processing, it is of interest to simultaneously characterize both the mechanical and optical behaviors of such systems. Futhermore, we will take advantage of the failure of the stress-optic rule for both miscible blends and disordered block copolymer melts. By observing the way in which it fails, we will be able to infer the underlying contribution of each component's dynamics to the bulk properties, over a range of compositions and temperatures.

Bibliography

[1] Doi, M.; Edwards, S. F. *The Theory of Polymer Dynamics*; Oxford University Press: Oxford, 1986.

[2] Ferry, J. D. *Viscoelastic Properties of Polymers*; Wiley: New York, 1980.

[3] Larson, R. G. *Constitutive Equations for Polymer Melts and Solutions*; Butterworths: Boston, 1988.

[4] Kannan, R. M. *Ph.D. Thesis*; California Institute of Technology: Pasadena, 1994.

[5] Kannan, R. M.; Kornfield, J. A. *Journal of Rheology* **1994**, *38*, 1127.

[6] Kornfield, J. A.; Fuller, G. G.; Pearson D.S. *Macromolecules* **1991**, *24*, 5429.

[7] Kornfield, J. A.; Fuller, G. G.; Pearson D.S. *Macromolecules* **1992**, *22*, 1334.

[8] Fuller, G. G. *Optical Rheometry of Complex Fluids*; Oxford University Press: New York, 1995.

[9] Johnson, S. J.; Frattini, P. L.; Fuller, G. G. *J. of Colloid and Interface Science* **1985**, *104*, 440.

[10] Azzam, R. M. A.; Bashara, N. M. *Ellipsometry and Polarized Light*; North-Holland Physics Publishing: Amsterdam, 1987.

[11] Janeschitz-Kriegl, H. *Polymer Melt Rheology and Flow Birefringence*; Springer-Verlag: Berlin, 1983.

Chapter 3

Component Dynamics in Equally Entangled Blends of Polyisoprene and Polyvinylethylene

3.1 Introduction

Polymer blends are becoming increasingly important from both a scientific and technological viewpoint. Many polymers are immiscible and form complex, phase-separated systems, however, making prediction of the blend properties difficult. Miscible blends, which are interesting in their own right, also provide a model system with which we can probe the thermorheological properties of individual phases in immiscible blends. Using miscible blends we can study the temperature and composition dependence of the dynamics of each component in the system and how each

species contributes to the overall properties of the blend. In particular, we want to understand the effects of blending on properties characteristic of each species, such as the entanglement molecular weight, M_e, and monomeric friction coefficient, ζ_o.

Previous work on miscible blends has demonstrated complex thermorheological behavior as evidenced by unpredictably broad glass transitions and the failure of time-temperature superposition [1, 2]. Intrinsic differences in the dynamics of the two species in miscible blends have been observed in various experiments, and may be responsible for the distinctive temperature dependence of the macroscopic properties of blends. On a segmental level, ^{13}C NMR experiments show that the two types of chains in a miscible blend can have widely different molecular mobilities [3, 4]. Recent two-dimensional ^{2}H-exchange NMR studies by Chung et al. [5, 6] of segmental dynamics in a miscible blend near the glass transition indicate that both local composition variations and intrinsic differences in chain mobility play a role in the dynamical heterogeneity of local segmental motions. However, it is not clear how these local dynamics propagate out to scales comparable to the entanglement molecular weight, M_e, and beyond, i.e., the scales that control the flow behavior of the melt and the diffusivity of each species in it.

On a macroscopic level, Composto et al. [7, 8] have shown that each species in the blend has a distinct, composition-dependent tracer diffusion coefficient, and hence a distinct friction coefficient. Infrared dichroism measurements combined with birefringence and stress relaxation experiments have shown distinct characteristic relaxation times for each species, which depend differently on blend composition and

temperature [9, 10, 11, 12]. However, there is still a lack of quantitative information on the dynamics of each species, as well as an understanding of the connection between heterogeneity in local segmental mobility and that manifested in macroscopic viscoelastic and transport properties.

Early studies by Roland [13] of miscible-blend viscoelasticity asserted that both components should share the same blend-average friction coefficient. In a more sophisticated model based on free volume arguments [14], each species is allowed to have its own friction coefficient, but both are predicted to shift in the same way with temperature. Therefore, both models predict the applicability of time-temperature superposition for miscible blends.

In order to explain the observed thermorheologically complex behavior of miscible blends, two basic concepts have arisen. The first picture assumes that both species in the mixture have the same "blend average" properties that vary with local composition [15, 1, 16, 17]. Dynamical heterogeneity is viewed as arising from composition variations, and failure of time-temperature superposition is attributed to different temperature dependencies of dynamics in different local environments [1]. The second scheme allows each species to retain individual properties due to its distinct chemical identity. Their dynamics, however, are modified by the mean-field environment of the surrounding chains. Failure of time-temperature superposition can then be attributed to the presence of two species whose relaxation dynamics have distinct temperature dependencies [2]. A scheme that incorporates both types of dynamic heterogeneity has been put forth by Ngai and Plazek [18], in which the failure

of time-temperature superposition in the terminal regime is explained via the Ngai coupling model.

To test these concepts it is necessary to observe the dynamics of each species. The notion that compositional heterogeneity leads to failure of the superposition principle is based on the idea that the dynamics of different local environments have different temperature dependencies. Chains of a given species lying in different regions, then, will shift differently with temperature. Therefore, the shape of the relaxation spectrum of each species may change with temperature. On the other hand, if the failure of the superposition principle is due to species-specific temperature dependencies, then the shape of the relaxation spectrum of each species will not change with temperature. In order to examine the extent to which each of these effects occurs, it is desirable to examine blends in which the shape of the relaxation spectra of each species is not changed by other effects, particularly polydispersity. This requires blends in which the components' relaxation spectra overlap completely, making it impossible to distinguish the two using rheometry alone [2]. Here, rheo-optical methods are particularly useful, since they are capable of distinguishing the dynamics of distinct species in a multi-component system [19, 20, 21].

Therefore, the present stress-optical experiments are designed to provide information on the relaxation spectra of the individual components in blends that minimize the effects of polydispersity. In miscible blends each species contributes differently to the stress and birefringence. Consequently, these two observables provide sufficient information to extract the individual dynamic moduli of the two components. We

perform dynamic rheo-optical experiments using the instrument described in Chapter 2 to simultaneously measure stress and visible birefringence [22, 23], allowing us to compare quantitatively mechanical and optical results obtained under identical sample conditions. We begin with a description of the polymers chosen as the model system and briefly review the relevant measurements obtained using the rheo-optical instrument. Then we present the results of dynamic stress and birefringence measurements, followed by interpretation in terms of the relaxation dynamics of each species in the blend. Finally, we present our conclusions regarding the effect of blending on the entanglement molecular weight and monomeric friction coefficient of each species.

3.2 Experimental

3.2.1 Materials

We choose as a model system blends of 1,4-polyisoprene (PIP) and polyvinylethylene (PVE). The homopolymer glass transition temperatures are widely separated, with $T_{g,PIP} \approx$ - 60°C and $T_{g,PVE} \approx$ 0°C. Their miscibility is well-established [24, 25]; however, since these polymers interact only weakly, the chain statistics and conformations are very close to those of the pure components [13, 26]. Thus, any changes in the dynamics of each species can be attributed to the effect of changing the composition of the neighboring chains. Indeed, previous studies indicate that the dynamics of the two species in PIP/PVE blends are sensitive to composition and are quite different from each another [5, 6, 3, 27, 2].

Table 3.1: Characterization of Polyisoprene (PIP) and Polyvinylethylene (PVE) Homopolymers

Sample	M_w*(kg/mol)	M_w/M_n*	$\omega_{x,i}$ (rad/s) @ 25°C	T_g(°C)**
E-PIP	190	1.09	1.7	-65.8
E-PVE	80	1.09	0.022	-2.1

* From gel-permeation chromatography in tetrahydrofuran at 25°C, using PIP standards.

** From differential scanning calorimetry (DSC) heating at 10°C/min.

The molecular weights, polydispersity, and microstructure of the homopolymers synthesized by Dr. S. D. Smith at Procter and Gamble are given in Table 3.1. Details of their synthesis are given elsewhere [5, 6, 28, 29]. Based on ^{13}C NMR characterization, the microstructure of $E-PIP$ is 78% $cis-$1,4-, 16% $trans-$1,4-, and 6% 3,4- units. $E-PVE$ consists of 94% 1,2- units and 6% 1,4- units [5, 6].

Three blends of compositions 75/25, 50/50 and 25/75 w/w% PIP/PVE were prepared by dissolving $E-PIP$ and $E-PVE$ in reagent grade cyclohexane to form 1% solutions, which are then mixed. The solutions are then cast into thin films in Pyrex petri dishes, and the solvent is allowed to evaporate under a fume hood for approximately 1 hour. The remainder of the solvent is removed by drying under vacuum. Typically, the samples are dried for two weeks under vacuum at 25°C. During the final 72 hours of drying, the temperature is raised to approximately 60°C.

Typical weight loss during the second week of drying is less than 0.5%.

3.2.2 Methods

Dynamic mechanical and birefringence measurements were made using a rheo-optical instrument recently developed in our laboratory [23], described in Chapter 2. As described in the previous chapter, we can infer the relaxation behavior of each component in the blend by characterizing the departure from the stress-optic rule. The quantities we will focus on are the stress-optic ratio SOR

$$SOR \equiv \frac{|B^*|}{|G^*|} \tag{3.1}$$

and the relative phase difference between stress and birefringence coefficient

$$\delta_B - \delta_G \equiv \tan^{-1}(\frac{B''}{B'}) - \tan^{-1}(\frac{G''}{G'}). \tag{3.2}$$

In the experiments described here, frequencies from 0.01 to 100 rad/sec were employed, at temperatures ranging from -25°C to 110°C. At high frequencies, oscillatory strains on the order of 1% were applied. With decreasing frequency, when the force signal decreased to the limit of the transducer, the strain was increased. At the highest temperatures and the lowest frequencies, strains on the order of 50-100% were used. In all cases, it was verified that the viscoelastic response was in the linear regime. Experiments at the lowest and highest temperatures were performed under nitrogen atmosphere to prevent sample degradation. In addition to using an inert atmosphere, the exposed surfaces of the samples were coated with an antioxidant, 2,6-Di-tert-butyl-4-methyl-phenol (BHT).

Table 3.2: Shift Factors, a_T, of Homopolymers and E-PIP/E-PVE Blends

	Homopolymers			Blends (PIP/PVE w/w %)		
T(°C)	$b_{T,PIP}$	PIP	PVE	75/25	50/50	25/75
-10	1.09	46	-	90	500	-
5	1.02	6.9	1900	11	23	70
15	-	-	-	-	-	7.5
25	1	1	1	1	1	1
40	0.97	0.35	0.055	0.32	0.24	0.14
60	0.92	0.118	0.00355	0.086	0.048	0.0175
80	0.89	0.051	0.000495	0.032	0.014	0.0038
110	0.87	0.020	0.000064	0.0106	0.00375	0.00073

3.3 Results

3.3.1 Stress-Optic Characterization of the Homopolymers

The homopolymers have dynamic moduli characteristic of narrow molecular weight distribution, entangled linear polymers. The dynamic moduli versus reduced frequency (Figure 3.1), show that time-temperature superposition holds for both PIP and PVE, as expected for homopolymers [30]. The values of the homopolymer horizontal shift coefficients, a_T, are listed in Table 3.2 and agree well with the previously established WLF behavior [2, 28, 29]. For $E - PIP$ vertical shift coefficients, b_T,

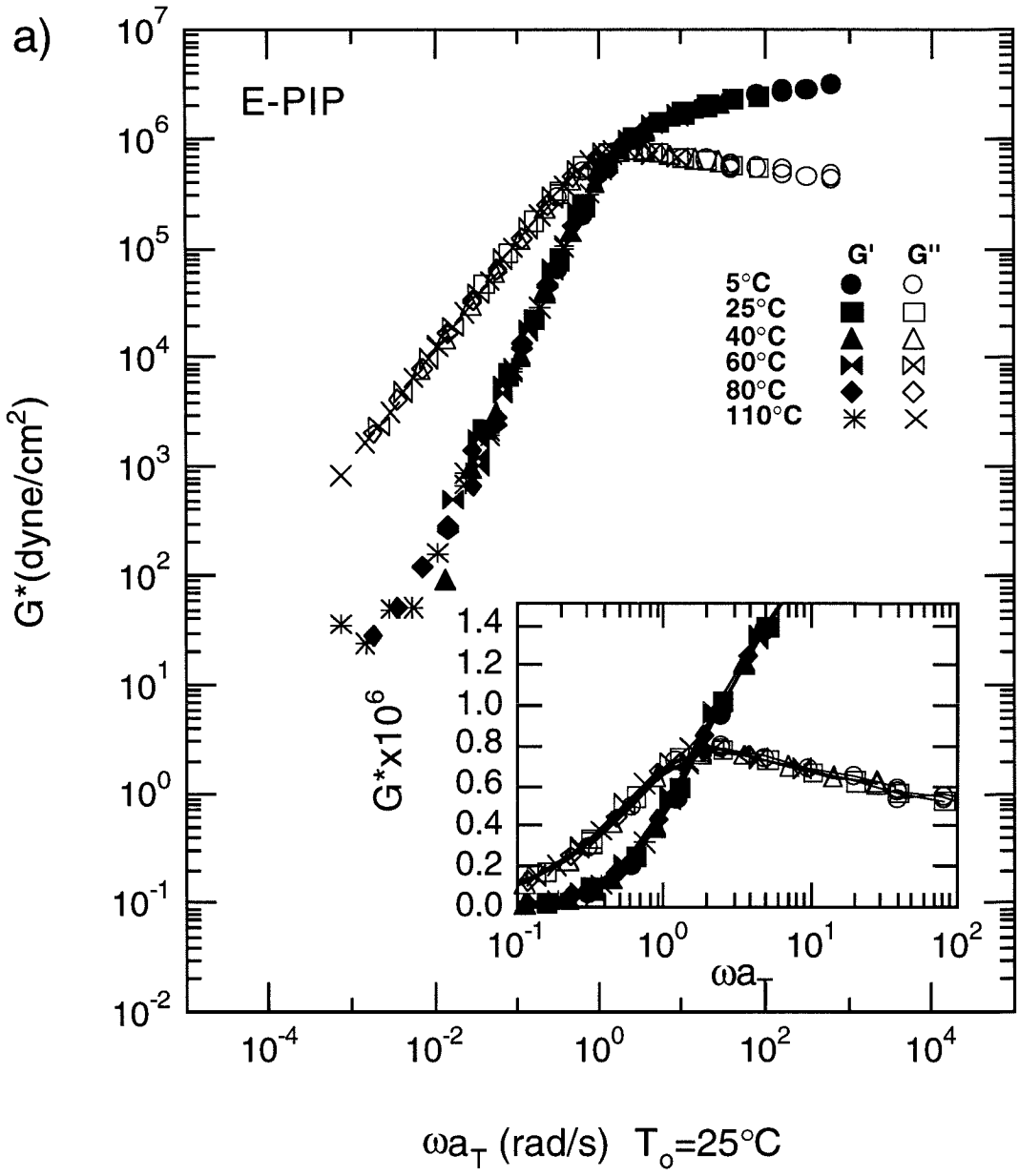

Figure 3.1: **a)** Dynamic moduli of $E-PIP$. Master curves were obtained by shifting the results at different temperatures along the frequency axis until the data at the low frequency extreme of the experimental range were superposed. For $E-PIP$ a small vertical shift was required (see text). The inset shows an expanded view of the loss peak, using a linear modulus scale.

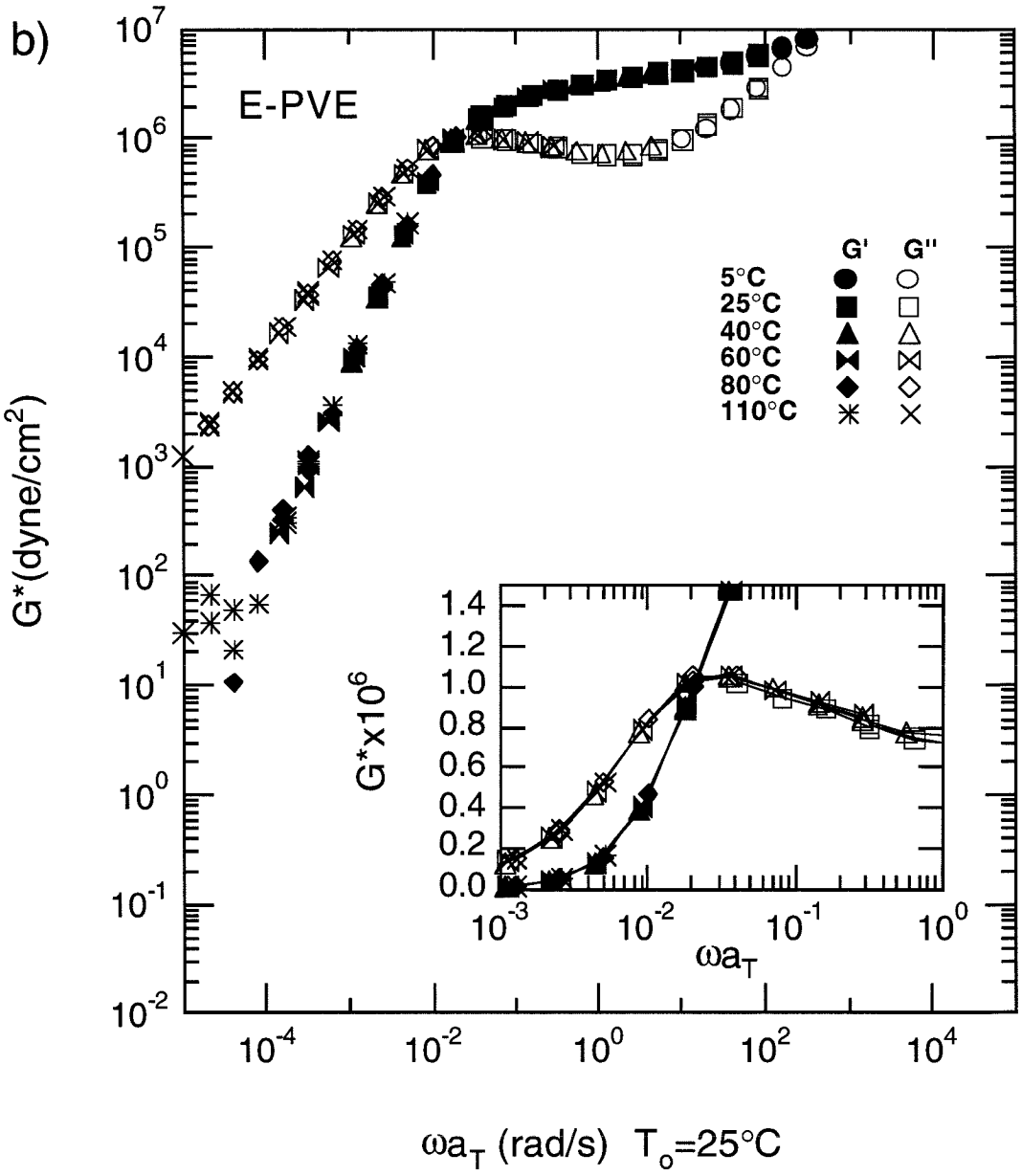

Figure 3.1: **b)** Dynamic moduli of $E-PVE$. Master curves were obtained by shifting the results at different temperatures along the frequency axis until the data at the low frequency extreme of the experimental range were superposed. The inset shows an expanded view of the loss peak, using a linear modulus scale.

Table 3.3: Stress-Optic Coefficients of Polyisoprene (E-PIP) and Polyvinylethylene (E-PVE) Homopolymers

	$C \times 10^{10}$ (cm^2/dyne)	
T (°C)	PIP	PVE
-10	1.82	-0.36
5	1.73	-0.30
15	1.70	-0.27
25	1.66	-0.23
40	1.63	-0.18
60	1.59	-0.105
80	1.51	-0.047
110	1.42	+0.015

were also required to superimpose the moduli. The values of b_T are close to unity, in accord with the literature [29]. For $E - PVE$ no vertical shifting was required. The reference temperature is taken as $T_o = 25°\text{C}$ in all cases.

By comparing the dynamic birefringence $G_{so}(\omega)^* \equiv \frac{B^*(\omega)}{C_i(T)}$ to the dynamic modulus (Figure 3.2), one sees that for both homopolymers the stress-optic rule holds away from the dynamic glass transition [31]. The values of C_{PVE} are an order of magnitude smaller than C_{PIP}, and of opposite sign (Table 3.3). Thus, if the two species maintain the same relative C_i's upon blending, PIP will tend to dominate

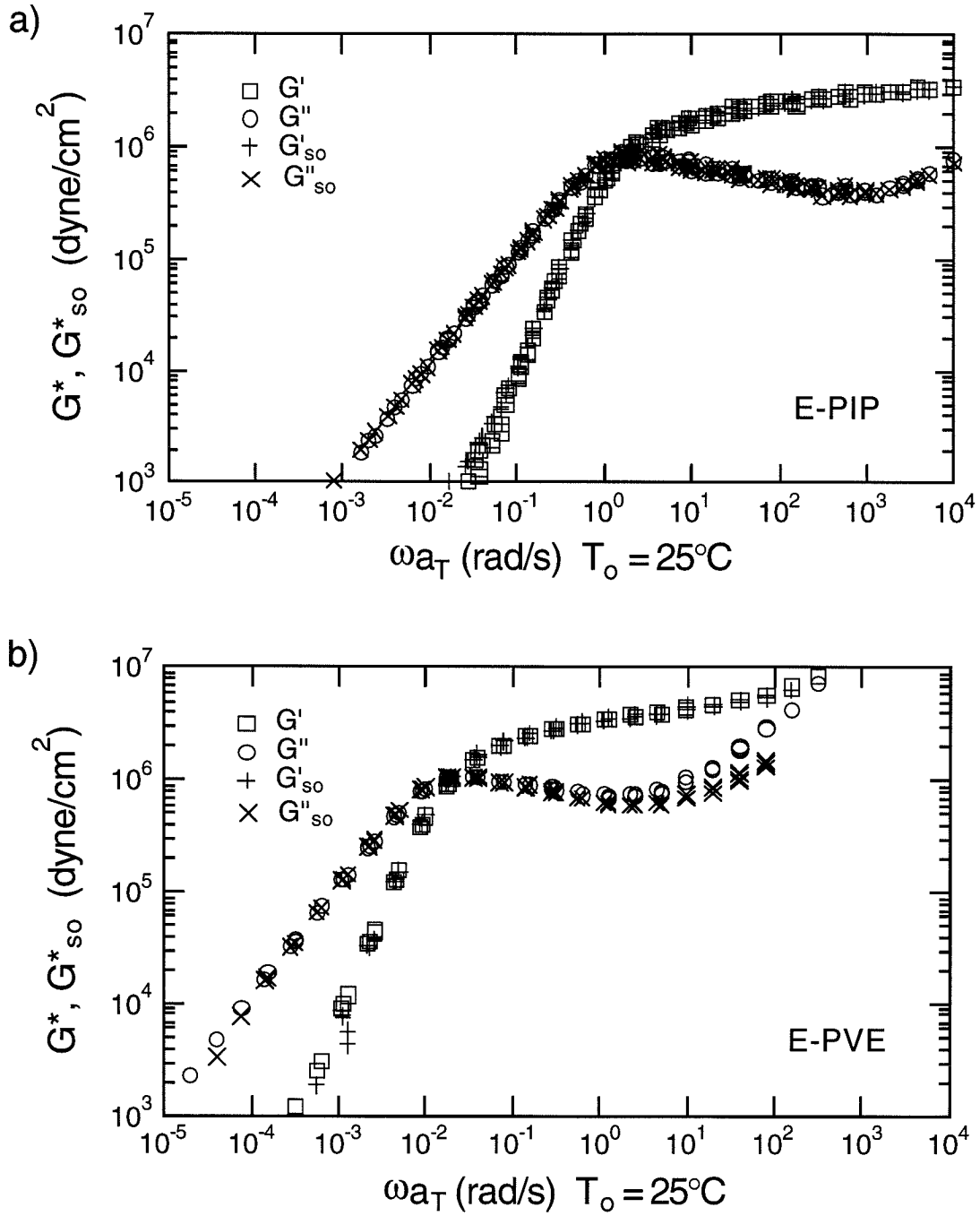

Figure 3.2: Stress-optic behavior of **a)** $E-PIP$ and **b)** $E-PVE$. G^*_{so} is the ratio of the complex birefringence coefficient to the stress-optic coefficient (given in Table 3.3) and G^* is the dynamic modulus.

the dynamic birefringence of the blend. Also, $C_{PVE}(T)$ depends unusually strongly on temperature, varying by over an order of magnitude and even changing sign over the modest temperature range spanned by these experiments; this is quite different from the behavior of other homopolymers, including PIP, for which $C_{PIP}(T)$ varies only ~21% over the same range of T [22]. The values of $C_{PIP}(T)$ are slightly lower than those reported previously by Kannan and Kornfield [22], but have a similar temperature dependence.

3.3.2 Blends: Dynamic Moduli

For the blend dynamic moduli no combination of a_T and b_T yield superposition. Thus, we shift the data acquired at different temperatures along the frequency axis only, until the values at the lowest experimental frequencies superpose [2]. The blend horizontal shift factors are listed in Table 3.2. The dynamic moduli of the 75/25, 50/50, and 25/75 w/w % PIP/PVE blends are shown versus reduced frequency in Figure 3.3. All three blends have dynamic moduli that resemble those of the homopolymers and nearly obey time-temperature superposition. However, upon expanding the frequency scale in the crossover regime and using a linear scale for the moduli (insets, Figure 3.3), we see that time-temperature superposition fails, in agreement with previous studies of this system [2]. With increasing temperature, with respect to a reduced frequency scale that superposes the low-frequency tail, the position of the loss peak shifts to higher frequency. This is most evident in the 50/50 blend (Figure 3.3b). However, we clearly cannot distinguish the characteristic relaxation

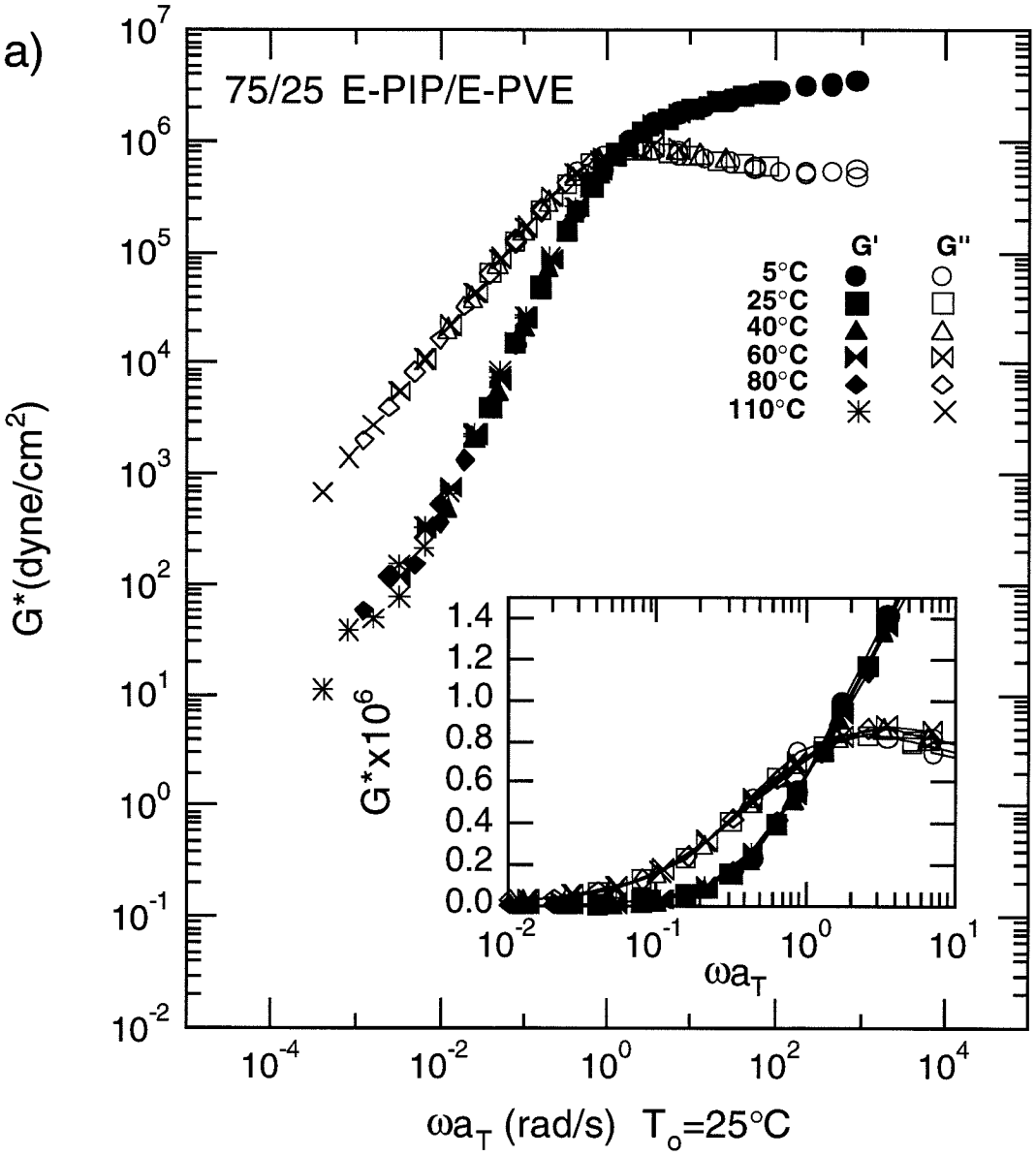

Figure 3.3: **a)** Dynamic moduli of blends of $E-PIP$ and $E-PVE$ with blend ratio of 75/25 w/w PIP/PVE. Only a horizontal shift along the frequency axis was applied to superimpose the results at different temperatures (see text).

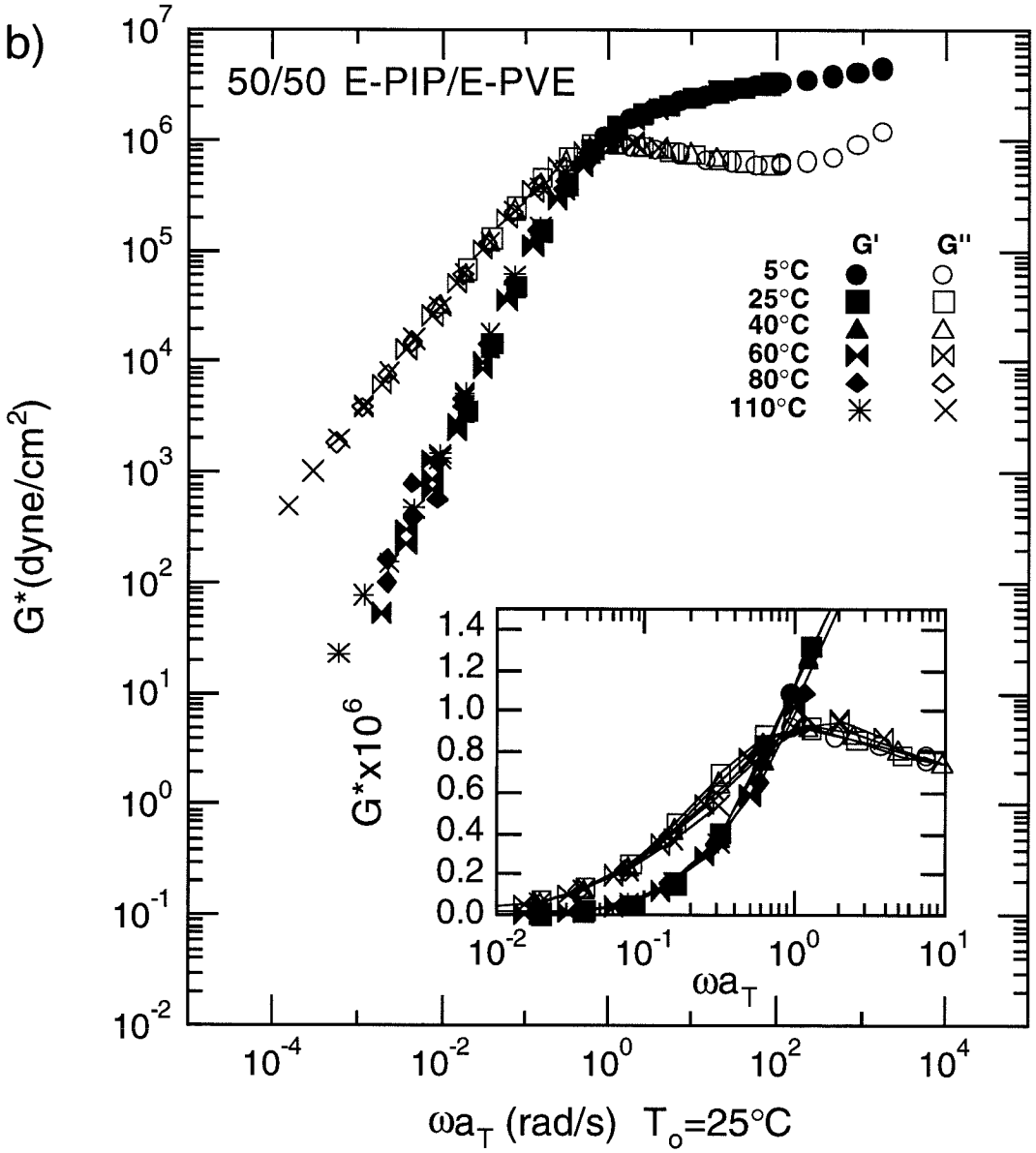

Figure 3.3: b) Dynamic moduli of blends of $E-PIP$ and $E-PVE$ with blend ratio of 50/50 w/w PIP/PVE. Only a horizontal shift along the frequency axis was applied to superimpose the results at different temperatures (see text).

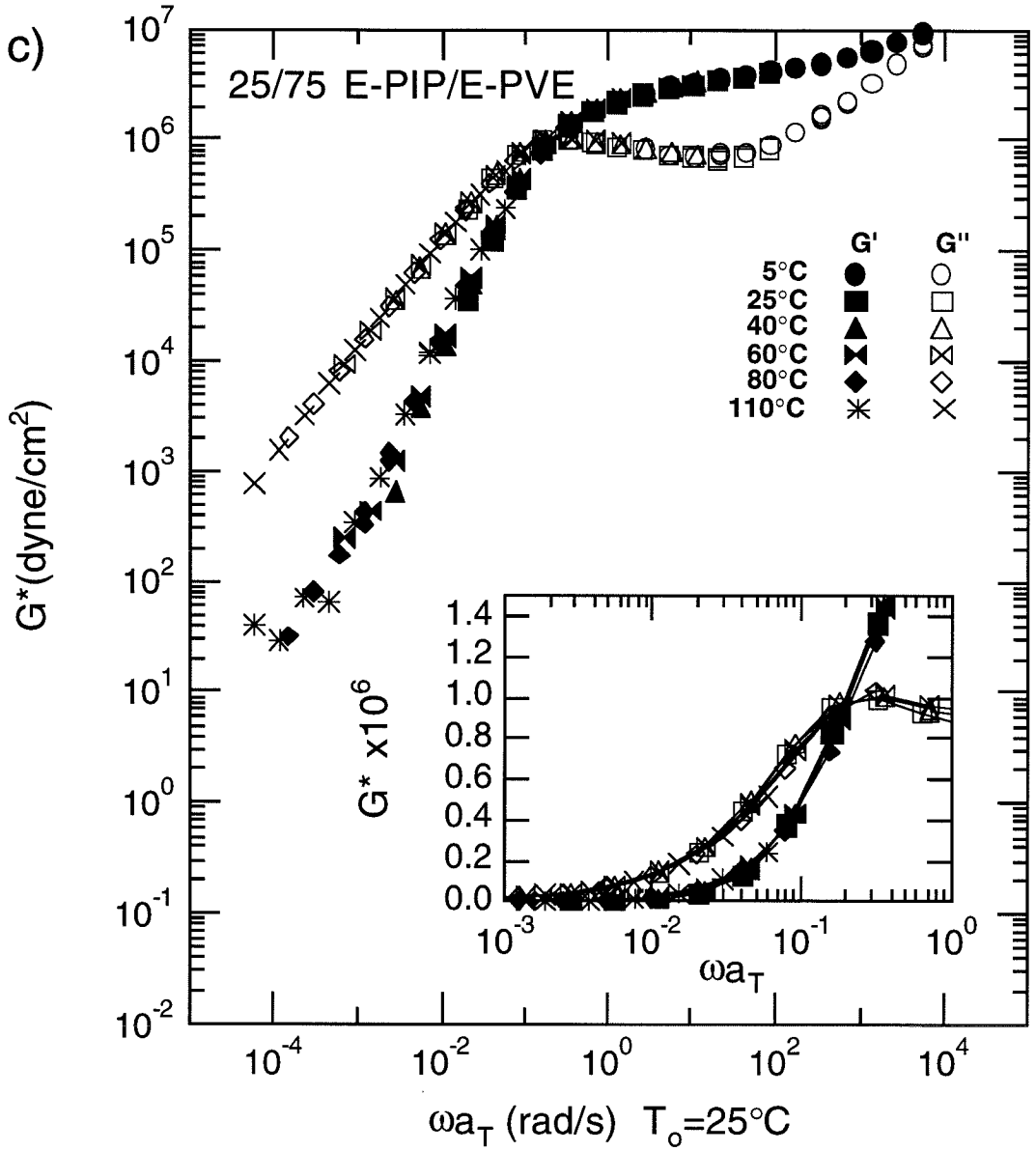

Figure 3.3: **c)** Dynamic moduli of blends of $E-PIP$ and $E-PVE$ with blend ratio of 25/75 w/w PIP/PVE. Only a horizontal shift along the frequency axis was applied to superimpose the results at different temperatures (see text).

dynamics of each species from the dynamic moduli alone because their loss peaks overlap so strongly.

The failure of time-temperature superposition evident in the dynamic moduli is subtle for these blends, due to the similarity in the relaxation times of both species in the blend. In each case there is only one loss peak, the position of which varies from $\omega''_{max} \approx 3.0$ to 1.2 to 0.3 rad/s at T= 25°C as the wt. % of PIP in the blend decreases from 75 to 50 to 25%. These can be compared to the relaxation times of the homopolymers at T= 25°C, with $\omega''_{max} \approx 2.6$ rad/s for $E - PIP$ and $\omega''_{max} \approx 0.04$ rad/s for $E - PVE$. In the blends the loss peaks for both species overlap. For this to be the case, in all the blends the PVE dynamics must be sped up a great deal relative to the homopolymer values. Those of PIP must remain nearly unchanged for the 75/25 PIP/PVE blend and slow down for the 50/50 and 25/75 blends.

To monitor the effect of blending on the plateau modulus, G^o_N, we use two characteristic moduli: the value of the moduli at the crossover frequency, $G'(\omega_x) = G''(\omega_x)$, and the value of the storage modulus at the frequency at which the loss modulus passes through a minimum in the plateau region $G'(\omega''_{min})$. In narrow distribution homopolymers $G^o_N \propto G'(\omega_x)$ [32]. Since the shape of the dynamic moduli of the blends is so similar to those of the constituent narrow distribution homopolymers, this relationship should also be appropriate for the blends. Also, previous studies have shown that $G^o_N \approx G'(\omega''_{min})$ [33]. The effect of blend ratio on both $G'(\omega_x)$ and $G'(\omega''_{min})$ is nearly identical (Figure 3.4). Both show no significant deviation from a linear interpolation between the homopolymer values, suggesting that the entangle-

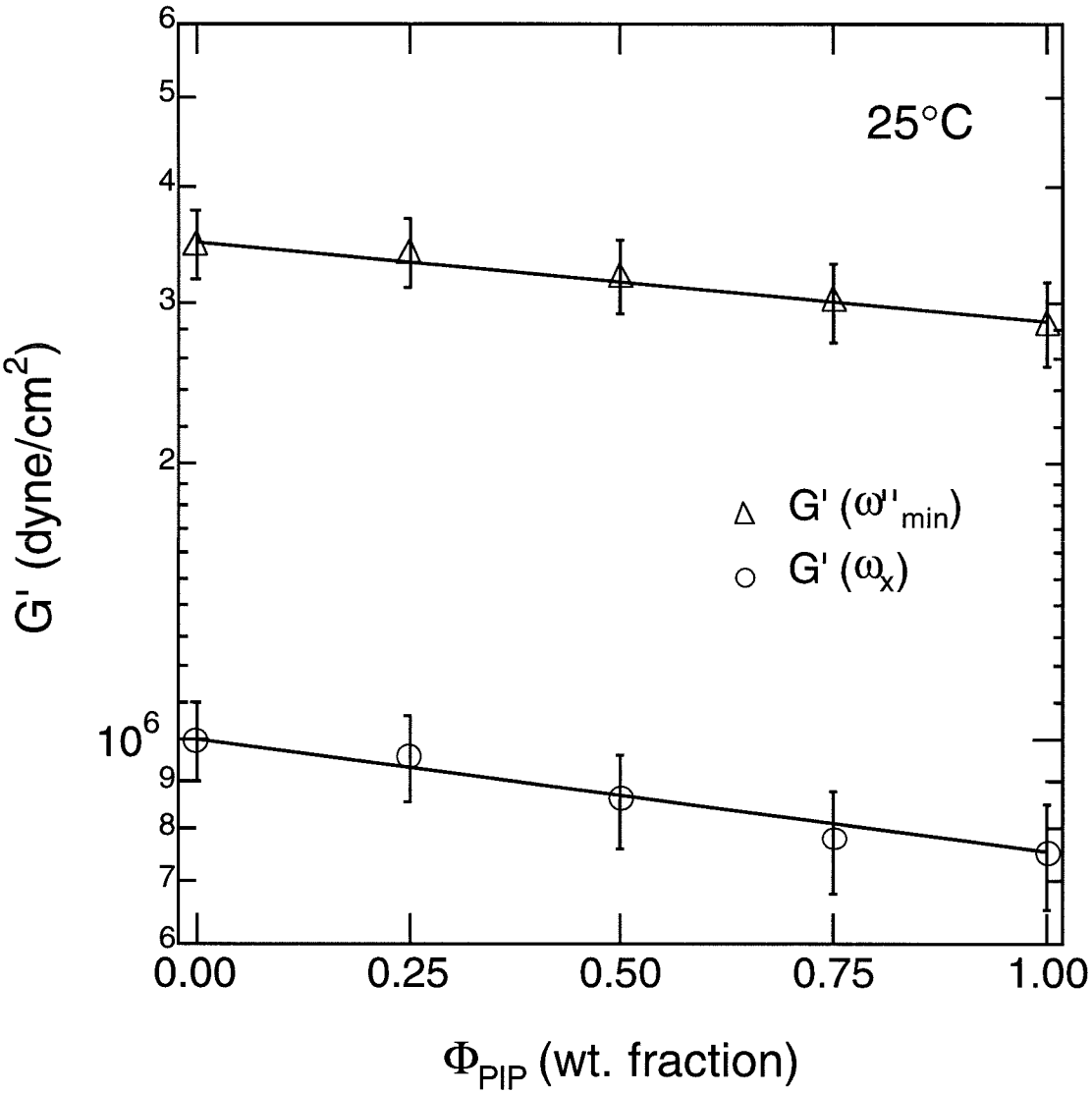

Figure 3.4: Effect of blending on the plateau modulus as indicated both by the value of the storage modulus G' at the frequency of the minimum in G'', denoted ω''_{min}, and by the value of the modulus at the frequency where G' and G'' cross, ω_x.

ment molecular weights of PIP and PVE are insensitive to blending.

3.3.3 Blends: Dynamic Birefringence

The dynamic birefringence was measured simultaneously with the dynamic moduli. In Figures 3.5 and 3.6 the stress-optic data is displayed using the same reduced frequencies as the respective blend dynamic moduli. In contrast to the homopolymers, for which SOR is independent of frequency, SOR of the blends show a distinct frequency dependence (Figure 3.5). At high frequencies the blend SOR reaches a plateau value. Then, as the frequency decreases, SOR increases and appears to reach a second plateau at low frequency. As will be discussed later, the increase in SOR is indicative of relaxation of $E - PVE$, reducing its contribution to both the birefringence and stress. The reduced frequency at which the upturn in SOR occurs increases with wt. % PIP from $\approx$ 0.3 to 1.2 to 5.0 rad/s for 25, 50, and 75% PIP respectively at 25°C (Figure 3.5). While the high frequency plateau of SOR is relatively insensitive to temperature, the magnitude of the rise in SOR at lower frequencies can be sensitive to temperature, as is evident in the results for the 25/75 blend.

The value of the high frequency plateau of SOR reflects contributions from both species, at frequencies ($\omega > \omega_x$), where neither species has relaxed. Its value increases monotonically with increasing weight fraction PIP (Figure 3.7). The increase roughly follows a linear trend between the two homopolymer stress-optic coefficients.

In addition to SOR, we calculate the phase difference between the complex birefringence coefficient and the dynamic modulus, $\delta_B - \delta_G$. For the constituent ho-

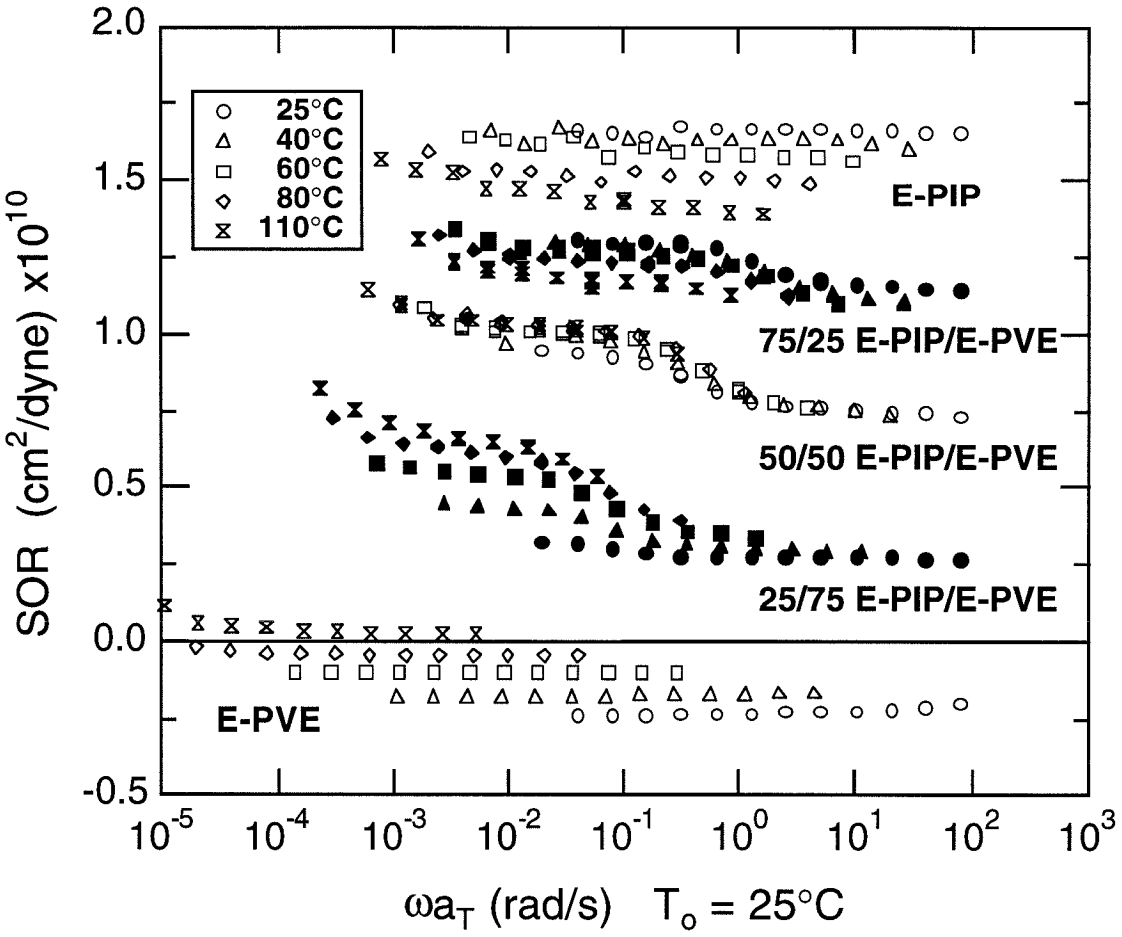

Figure 3.5: SOR of the $E-PIP/E-PVE$ blends versus the same reduced frequencies as the dynamic moduli of the respective samples. Shown for comparison are the stress-optic coefficients of the pure components.

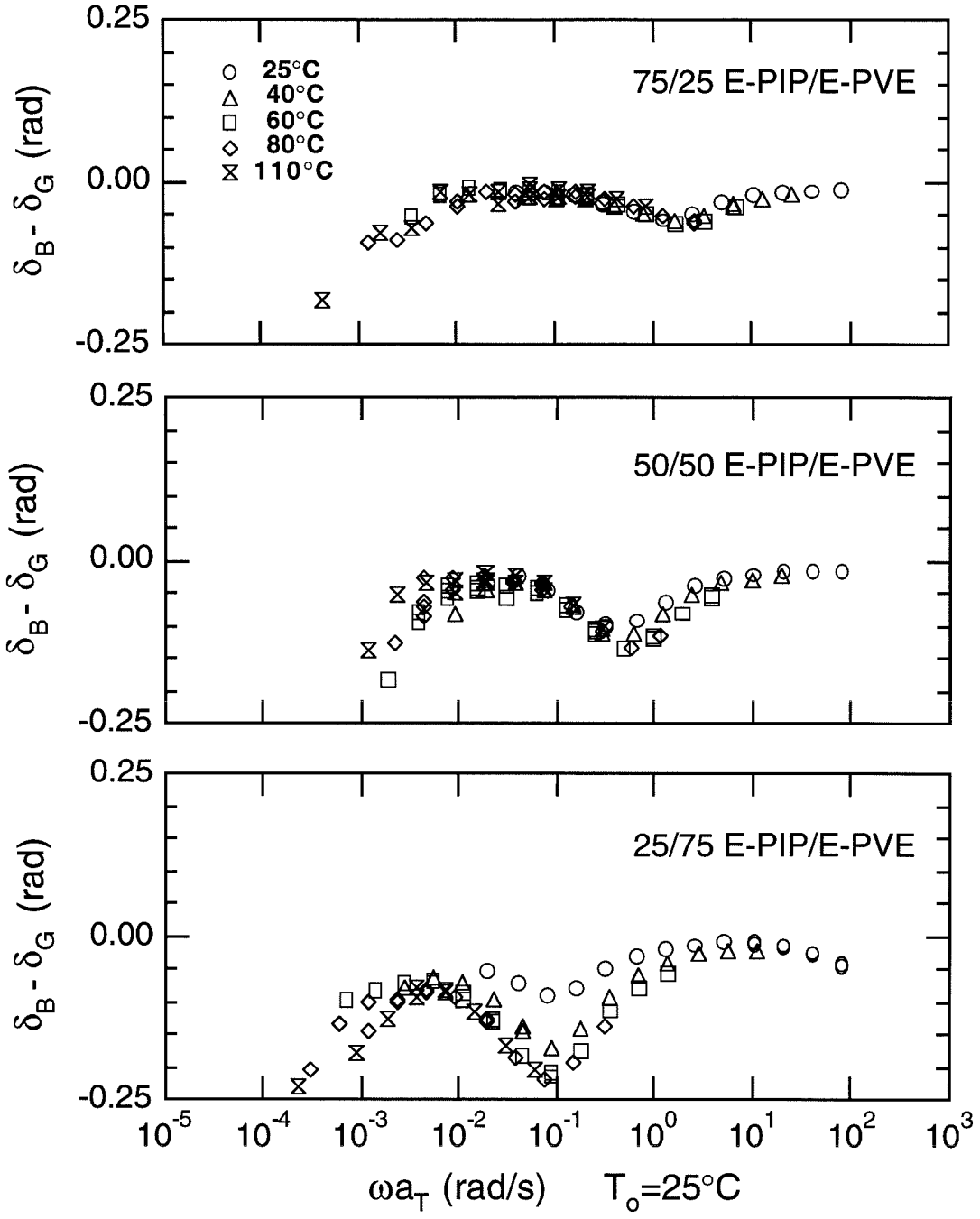

Figure 3.6: Phase difference between the dynamic birefringence and shear stress for the $E-PIP/E-PVE$ blends.

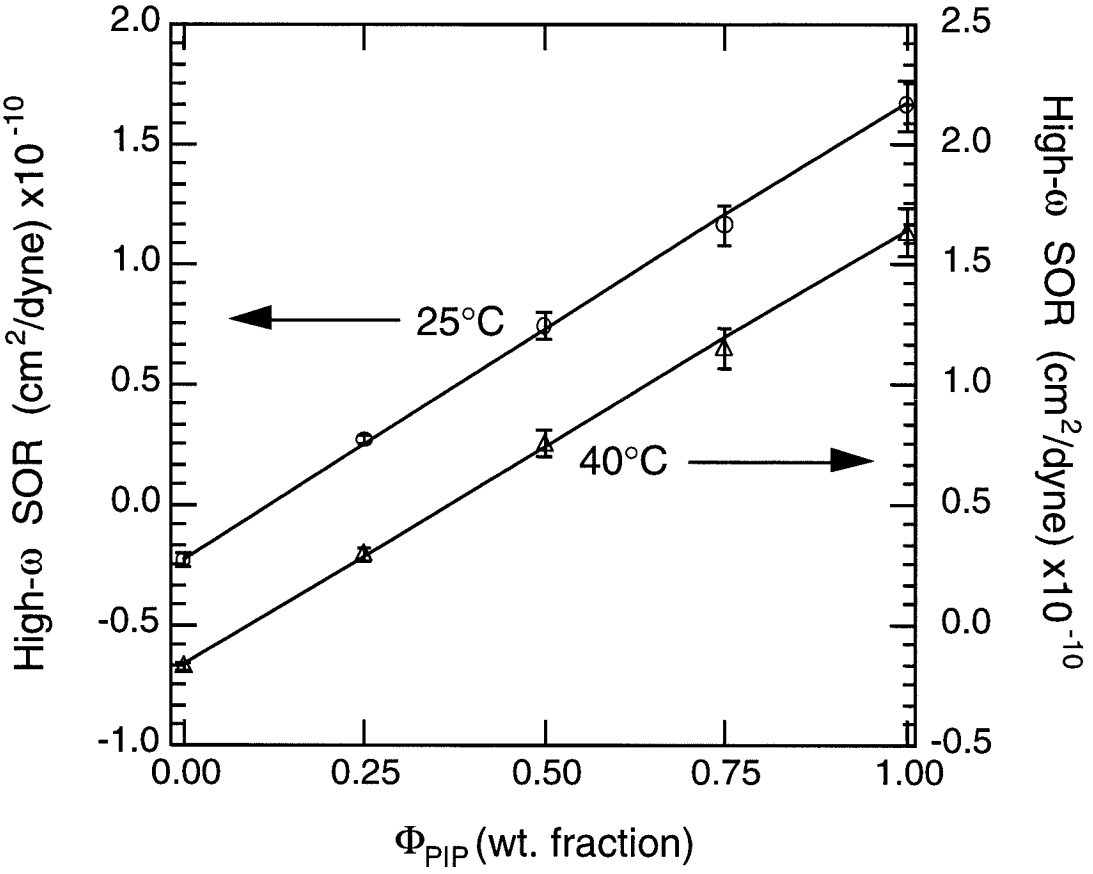

Figure 3.7: High frequency plateau value of the stress-optic ratio of the blends (high-ω *SOR*) at temperatures $T = 25°\mathrm{C}$ (circles, left axis), and $T = 40°\mathrm{C}$ (triangles, right axis). For comparison, lines show a linearly weighted average of the homopolymer stress-optic coefficients C_{PVE} and C_{PIP} at each temperature.

mopolymers, away from the dynamic glass transition, we observe $\delta_B - \delta_G \approx 0$ (± 0.04 rad) for PIP and $\approx \pi$ (3.14 ± 0.04 rad) for PVE, with the birefringence 180° out of phase with the shear stress, indicative of the negative stress-optic coefficient of PVE. This is in accord with the stress-optic rule. In contrast, $\delta_B - \delta_G$ for the blends shows significant deviations from zero, which are largest in magnitude in the vicinity of the upturn in SOR (Figure 3.6). As the wt. % PIP varies from 75 to 50 to 25%, the reduced frequency of the dip shifts from $\approx$ 1.2 to 0.4 to 0.09 rad/sec.

3.4 Discussion

In these experiments, we use blends in which the two species are approximately equally entangled to focus on those effects that are unique to blends of distinct polymers (e.g., the effect of composition on $M_{e,i}(\phi)$ and $\zeta_{o,i}(\phi, T)$), rather than those features that are present even in binary blends of a given polymer (e.g., constraint release). This is achieved by choosing the molecular weights of these homopolymers to be similar multiples of their entanglement molecular weights: $M_i \approx 30\ M^o_{e,i}$ for each species i, where the superscript o denotes the pure state. In the resulting blends, changes in composition shift the component dynamic moduli to higher or lower frequency without introducing changes in their shape due to polydispersity. This makes it relatively easy to determine $\zeta_{o,i}(\phi, T)$. In addition, such a system offers the possibility of observing changes in the shape of the relaxation spectrum that might arise from compositional heterogeneity, which has been hypothesized to explain the failure of time-temperature

superposition [1]. Thus a blend with equally entangled species is also an ideal system to probe whether superposition failure is due to differences in the temperature shifts of the two species or to compositional heterogeneity, or both.

In this section, we first show how the experimental dynamic moduli and complex birefringence coefficient of miscible blends can provide the information required to determine the contributions of each species to the dynamic moduli, which can then be used to determine $M_{e,i}(\phi)$ and $\zeta_{o,i}(\phi, T)$ for each species $i = PIP$ or PVE in the blend. We then discuss how these are affected by temperature and blend composition, comparing the results to existing ideas regarding miscible blends.

3.4.1 Relaxation of Each Species in a Miscible Blend

The experimental values of G^*_{blend} and B^*_{blend} provide two observables that can be used to determine the contribution of each species to the dynamic modulus of the blend, $G^*_i(\omega; \phi_A, T) \equiv G^o_{N,i} F^*_i(\omega; \phi_A, T)$, where ϕ_A is the volume fraction of component A, $G^o_{N,i}(\phi_A, T)$ is the plateau modulus of species i, and $F^*_i(\omega; \phi_A, T)$ is its relaxation function, with $i = A$ or B. The dynamic modulus of each species in the blend may be modified from the homopolymer relaxation dynamics (e.g., by constraint release). This is evident when the components have well separated terminal relaxation times in the blend [2].

Analogous to the approach taken in describing binary blends of polymers of identical chemical structure [32, 34, 35], the bulk stress in a miscible blend is the sum of the individual stresses that each component carries *within the blend.* Thus, the

corresponding dynamic moduli are given by

$$G^*_{blend}(\omega;\phi_A,T) = \phi_A G^*_A(\omega;\phi_A,T) + \phi_B G^*_B(\omega;\phi_A,T). \tag{3.3}$$

If we neglect the effects of orientational coupling, each segment will contribute to the birefringence in the blend in proportion to its contribution to the stress, with the constant of proportionality being the pure-component stress-optic coefficient [36]. The blends we focus on here are miscible, but with very weak interactions, so that changes in local chain statistics due to blending are negligible [25, 26, 24]. Furthermore, the observation that the value of the high-freqeuncy plateau in SOR is a linearly weighted average of the pure-component C_i's suggests that the stress-optic coefficients of the two components are not changed significantly upon blending. Thus, under the approximation that orientational coupling is *neglected*, the blend birefringence is given by

$$B^*_{blend}(\omega;\phi_A,T) = C_A(T)\phi_A G^*_A(\omega;\phi_A,T) + C_B(T)\phi_B G^*_B(\omega;\phi_A,T) \tag{3.4}$$

where $C_i(T)$ is the stress-optic coefficient of species i in the blend [20, 21]. This analysis is restricted to frequencies that exclude the dynamic glass transition, where failure of the stress-optic rule occurs even for homopolymers [37, 38, 39, 31]. Solving for the species dynamic moduli yields

$$G^*_A(\omega;\phi_A,T) = \frac{B^*_{blend}(\omega;\phi_A,T) - C_B(T)G^*_{blend}(\omega;\phi_A,T)}{\phi_A(C_A(T) - C_B(T))}, \tag{3.5}$$

and

$$G^*_B(\omega;\phi_A,T) = \frac{C_A(T)G^*_{blend}(\omega;\phi_A,T) - B^*_{blend}(\omega;\phi_A,T)}{\phi_B(C_A(T) - C_B(T))}. \tag{3.6}$$

To qualitatively illustrate the interpretation of the blend G^*_{blend}, SOR and δ_B- δ_G, we first apply the above analysis to a hypothetical, nearly equally entangled blend. In this hypothetical 50/50 blend of two monodisperse components, designated A and B, the relaxation of each species is similar to that of a monodisperse homopolymer (Figure 3.8a). This is a consequence of the fact that constraint release plays a minor role when the terminal relaxation times of the two species are similar (in this illustration $\tau_{d,B}/\tau_{d,A} = 4$). The overall dynamic modulus calculated using eqn. 3.3 also shows a single loss peak (Figure 3.8b).

If the two species have stress optic coefficients with very different magnitudes, the blend stress-optic ratio calculated from eqn. 3.3 and 3.4 has a high frequency plateau and a low frequency plateau (Figure 3.8c). The high frequency plateau value is a weighted average of the C_i's of the individual species, determined by the blend ratio and the ratio of the species $M_{e,i}$. In the terminal regime, the magnitude of the plateau depends on the separation between the relaxation times of the two species. The greater the disparity in their relaxation times, the smaller the relative contribution of the faster relaxing species compared to the slower relaxing one in the terminal regime.

Here we show the behavior observed when the faster relaxing species, A, has a negative stress-optic coefficient and the slower relaxing species, B, has a positive one. In this case, SOR rises as frequency decreases, toward the positive C_i of the slower relaxing species as the negative contribution of species A relaxes (Figure 3.8c). This is analogous to the behavior observed in Figure 3.5. For the hypothetical system, the phase angle between the birefringence and stress passes through a minimum at

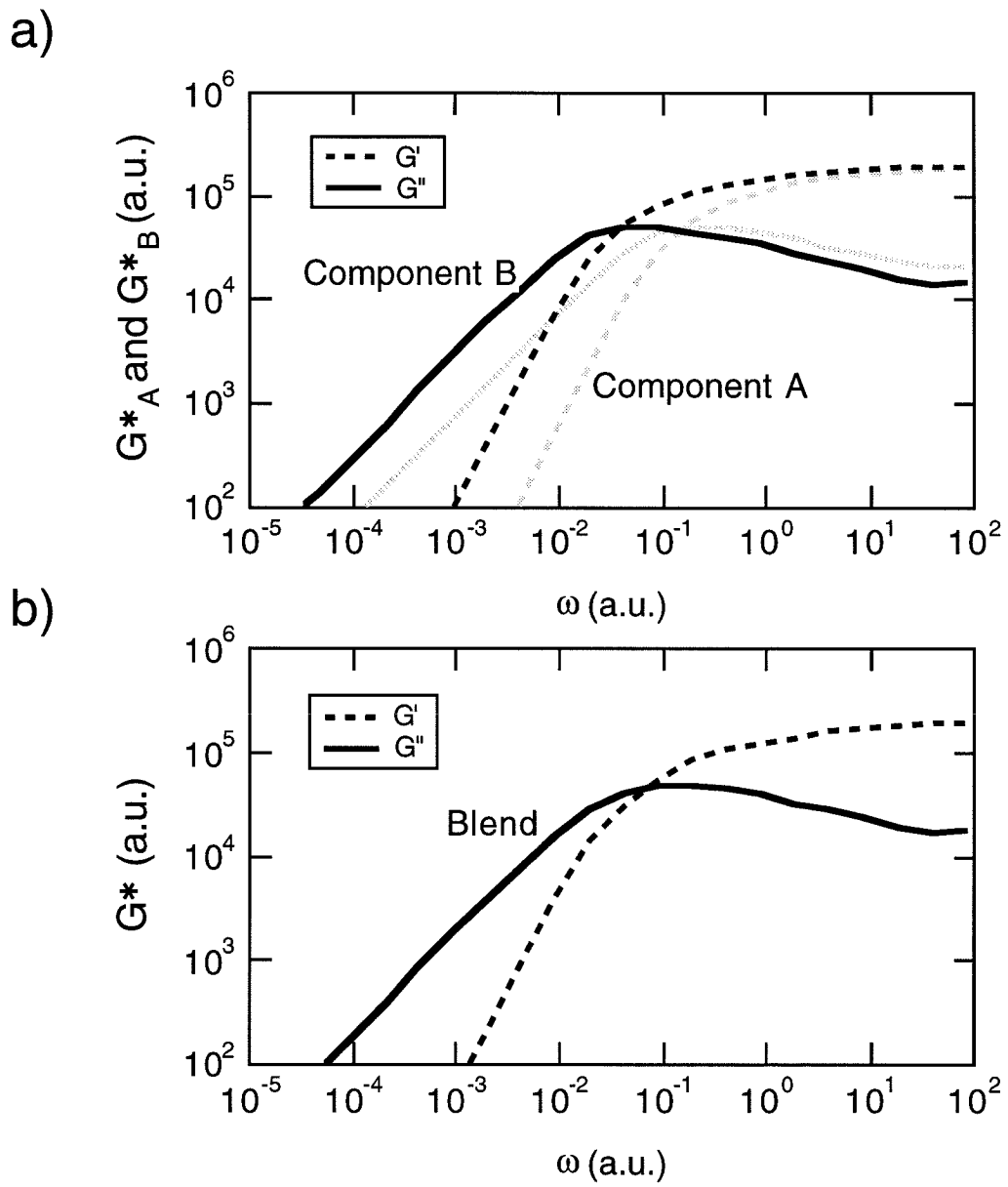

Figure 3.8: Illustration of the failure of the stress-optic rule. **a)** Dynamic moduli of the individual species A and B in a hypothesized blend and **b)** the resulting blend modulus calculated from G_A^* and G_B^* using eqns. 3.5 and 3.6.

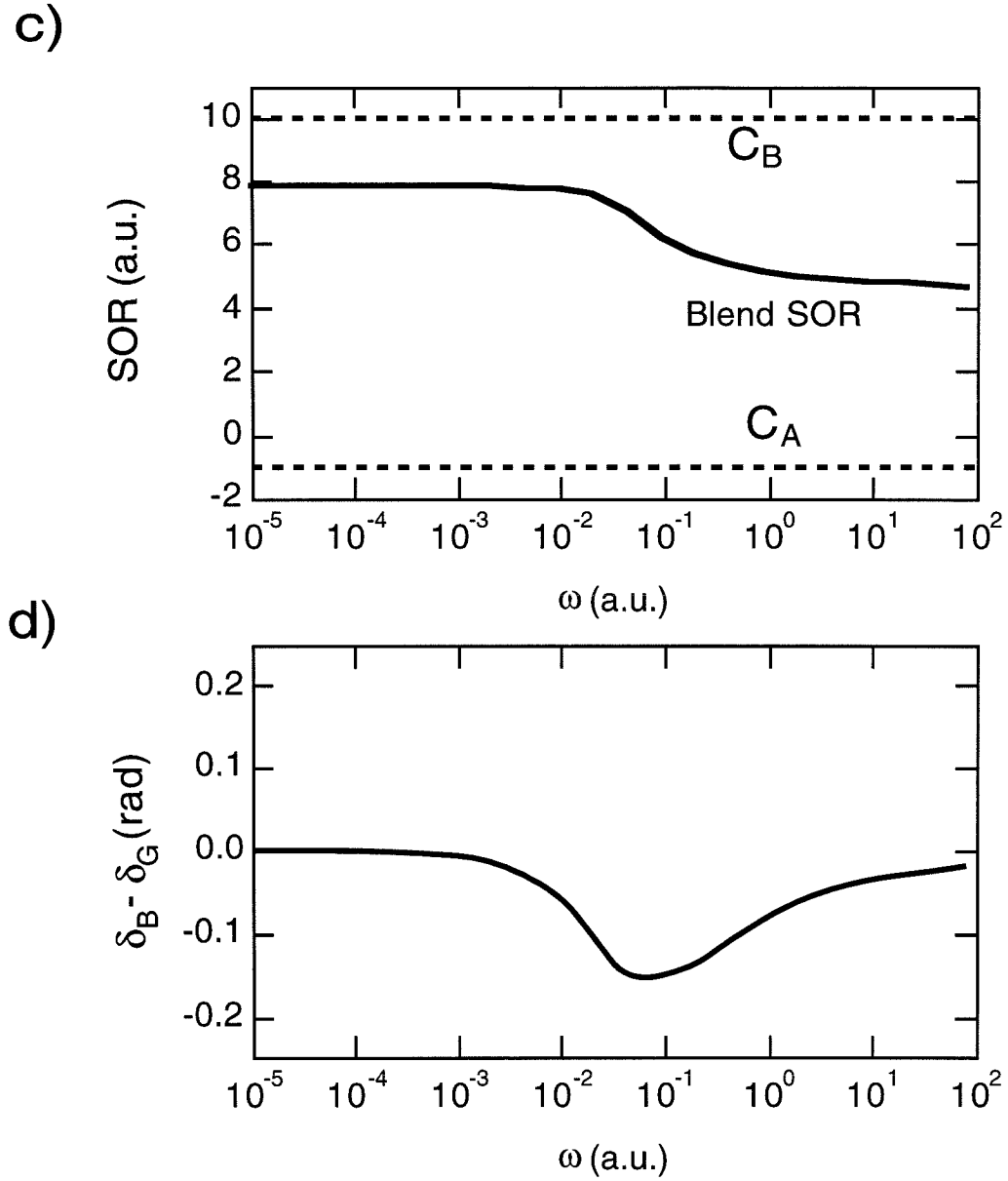

Figure 3.8: **c)** The species C_i's, in arbitrary units, and the resulting blend *SOR* calculated from eqn. 2.18 and **d)** the phase shift calculated from eqn. 2.19.

intermediate frequency (Figure 3.8d), analogous to that observed in Figure 3.6. Thus, the experimental results may be interpreted as showing that, although the terminal relaxation times of the two species are very similar, PVE is the faster relaxing species in each of the blends in this study. If the component with the positive C_i were the faster relaxing species, then the inflection in SOR would be downward with decreasing frequency, and $\delta_B - \delta_G$ would pass through a maximum rather than a minimum. Thus, while it is difficult to distinguish the relaxation of the individual species using the $G^*_{blend}(\omega)$ alone, the behavior of $SOR(\omega)$ and $\delta_B - \delta_G$ shows that PVE is the faster relaxing species. Understanding qualitatively how the stress and birefringence data can be analyzed to yield the component moduli in the blend and how the basic features evidenced by the failure of the stress-optic rule arise, we now look at a more complete analysis of the blend data.

A more accurate interpretation of the stress-optic behavior must incorporate orientation coupling, even in the equally entangled system. In *all* blends the effect of orientational coupling must be included if we are to properly account for the contribution of each species to the blend birefringence. Orientational coupling is currently viewed as a packing effect that couples the orientation of a given chain to the orientation of the surrounding matrix. This coupling has the consequence that a chain that is conformationally relaxed on the scale of entanglement strands can remain anisotropic on the local bond level, if it exists in an oriented matrix of unrelaxed chains. Such relaxed chains, affected only by orientational coupling, bear no stress. Consequently, when the relaxations of the two components in the blend are well-separated in fre-

quency, orientational coupling clearly manifests itself in the stress-optic behavior. Not only does each component contribute to the birefringence in proportion to its own dynamic modulus, it also contributes in proportion to the local orientation imposed by both like and unlike segments via orientational coupling.

This effect is described in more detail in other references [41, 10, 42]. Following the work of Doi et al. and Zawada et al. [41, 10, 11], the complete expression for the blend birefringence is

$$B^*_{blend} = C_A(1-\epsilon)[\frac{\phi_A G^*_A + \frac{\phi_A}{\phi_B}(\frac{\phi_B\epsilon}{1-\phi_B\epsilon})\phi_B G^*_B}{(1-\phi_A\epsilon) - (\frac{\phi_B\epsilon}{1-\phi_B\epsilon})\phi_A\epsilon}] + \\ C_B(1-\epsilon)[\frac{\phi_B G^*_B + \frac{\phi_B}{\phi_A}(\frac{\phi_A\epsilon}{1-\phi_A\epsilon})\phi_A G^*_A}{(1-\phi_B\epsilon) - (\frac{\phi_A\epsilon}{1-\phi_A\epsilon})\phi_B\epsilon}] \quad (3.7)$$

where ϵ denotes the average coupling coefficient, C_i is the stress-optic coefficient of pure component i and ϕ_i is the weight fraction of that component in the blend. Using equations 3.3 and 3.7, the underlying component moduli in the blend, $G^*_A(\omega;\phi_A,T)$ and $G^*_B(\omega;\phi_A,T)$, can be determined from simultaneously measured values for the blend dynamic moduli and birefringence coefficients and the stress-optic coefficients of the pure components. It is important to note that, unlike Zawada et al., we directly and simultaneously measure the *corresponding* components of the stress and anisotropic index of refraction tensors, σ_{12} and n_{12} (eqns. 2.11 and 2.17), on the same instrument and do not rely on constitutive relations to relate the mechanical and optical measurements.

In the above equations, ϵ denotes the average of four distinct coupling coefficients,

$\epsilon_{PIP,PIP}$, $\epsilon_{PVE,PVE}$, $\epsilon_{PIP,PVE}$ and $\epsilon_{PVE,PIP}$, which describe coupling between like species, PIP to PIP and PVE to PVE, and between unlike segments, PIP to PVE and PVE to PIP, respectively. Without sufficient information to determine all four coupling coefficients, we simplify our analysis by assuming that an average value of ϵ will be a good approximation for all couplings. In Chapter 4 we examine two sets of blends, one where PIP is the short component and one where PVE is, to determine how symmetric the degree of coupling is and whether an average value for ϵ is sufficient. The possible values of ϵ lie between 0 (no coupling) and 1 (complete coupling). When $\epsilon = 0$, eqn. 3.7 reduces to eqn. 3.4, used in our simple model analysis and previous work [40].

We examine the equally entangled blends by incorporating the effects of orientational coupling, using the values of $\epsilon \approx 0.35$ determined from studies of unequally entangled blends [10, 11] (see also Chapter 4). At each temperature, we use the blend dynamic moduli and birefringence data to calculate $G^*_A(\omega; T, \phi)$ and $G^*_B(\omega; T, \phi)$ from equations 3.3 and 3.7. For a given blend composition, the dynamic moduli of each species at different temperatures are then shifted along the frequency axis until they best superimpose. Uncertainty in the values of $C_i(\phi, T)$ and ϵ mainly affects the magnitude of the component moduli, thus precluding a meaningful determination of vertical shift. Horizontal shifting alone, however, appears sufficient to superimpose the data at different temperatures. The values of the horizontal shift factors, $a_{T,i}$ (Table 3.4), show that the dynamics of PVE are more sensitive to temperature than those of PIP. The disparity between the species' temperature dependencies

Table 3.4: Shift Factors, $a_{T,i}$, of Each Species in E-PIP/E-PVE Blends

	Blends (PIP/PVE w/w %)					
	75/25		50/50		25/75	
T(°C)	PIP	PVE	PIP	PVE	PIP	PVE
-10	90	160	290	800	-	-
5	11	15	18	30	49	80
15	-	-	-	-	6	7.9
25	1	1	1	1	1	1
40	0.32	0.33	0.25	0.2	0.18	0.131
60	0.088	0.089	0.0505	0.039	0.0275	0.0145
80	0.0325	0.03	0.0159	0.0094	0.007	0.00285
110	0.011	0.01	0.0044	0.0021	0.0015	0.0005

decreases with increasing PIP concentration. This is qualitatively in accord with the observations of Roovers and Toporowski on PIP/PVE blends [2].

The master curves for the dynamic moduli of both components in the blend are very similar in shape to those of the homopolymers (Figure 3.9), indicating the absence of complications due to differences in the component terminal relaxation times in the blends. Changes in the shape and magnitude of the component dynamic moduli are barely perceptible when variations of $\pm$ 10% in the C_i's are assumed. The results obtained when the effects of orientational coupling are properly taken into

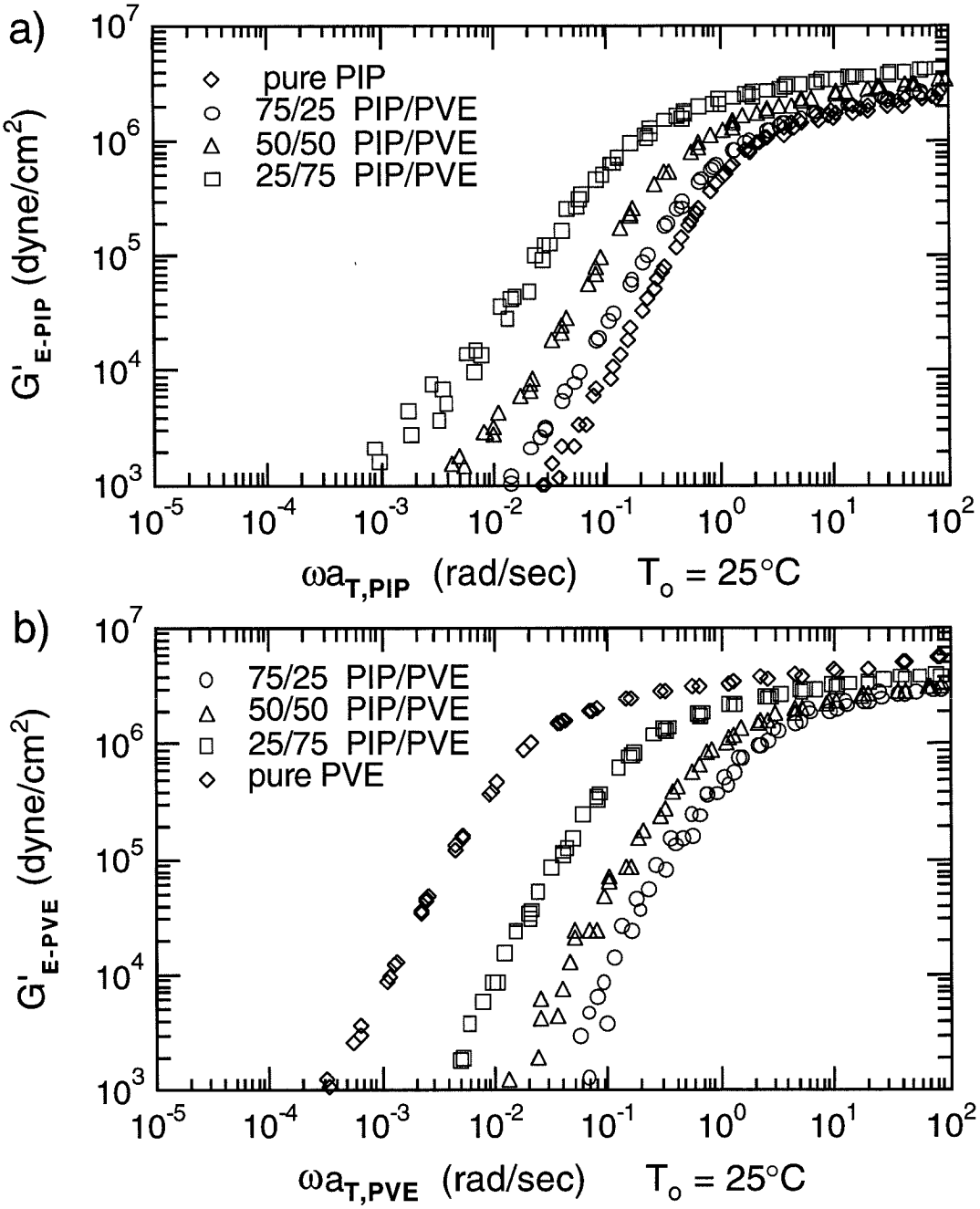

Figure 3.9: Contributions of $E-PIP$ and $E-PVE$ to the storage modulus of the blends: **a)** $E-PIP$ and **b)** $E-PVE$, with the storage modulus of pure $E-PIP$ and $E-PVE$ shown for reference.

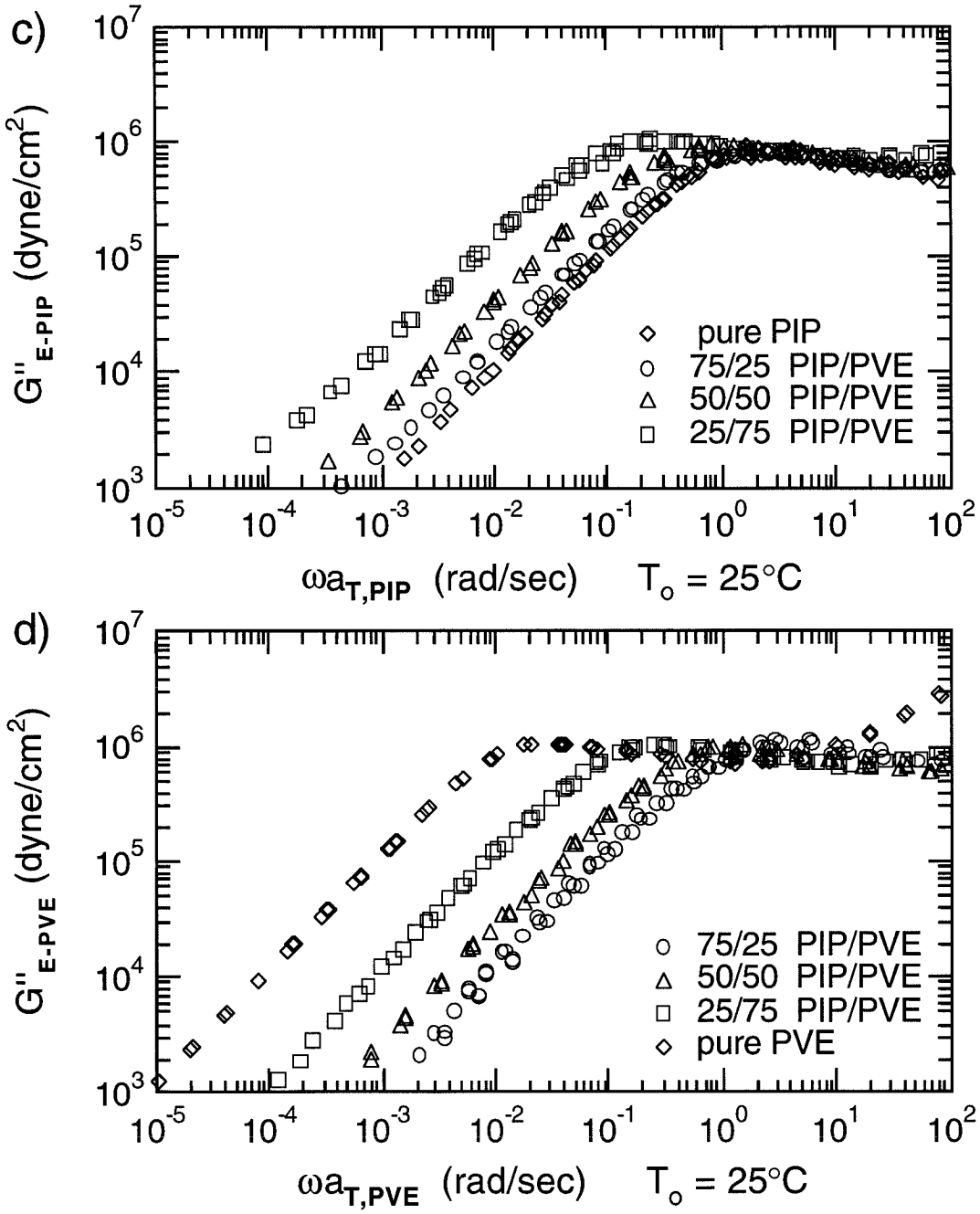

Figure 3.9: Contributions of $E - PIP$ and $E - PVE$ to the loss modulus of the blends: **c)** $E - PIP$ and **d)** $E - PVE$, with the loss modulus of pure $E - PIP$ and $E - PVE$ shown for reference.

account ($\epsilon = 0.35$) are nearly identical to those determined using the approximate analysis which did not incorporate orientational coupling ($\epsilon = 0.00$). The results obtained when the effects of orientational coupling are properly taken into account ($\epsilon = 0.35$) differ primarily in the magnitude of the component moduli (by ~20%), particularly in the terminal regime of each species, compared to those determined using the approximate analysis which did not incorporate orientational coupling ($\epsilon = 0.00$).

Compositional heterogeneity, if it were present, would be manifested in changes of the shape of the species' dynamic moduli with temperature. Even with the uncertainty in the pure component stress-optic coefficients and the precise value of ϵ, our results indicate that only subtle changes in the shape of the component $G_i^*(\omega)$ occur with blending. Thus, while we cannot exclude the effects of compositional heterogeneity, they must be extremely subtle in these blends. The differences between how the dynamics of the two components shift with temperature appears to be the dominant effect in these blends.

We now focus quantitatively on the component dynamic moduli, which show that the relaxation of PIP is slightly slower than that of PVE in each blend. This is explicitly seen in Figure 3.10, where the crossover frequencies $\omega_{x,PIP}$ and $\omega_{x,PVE}$ are plotted versus weight fraction PIP. As the concentration of the low T_g component (PIP) is reduced, the dynamics of both components shift to lower frequency. As with the effect of temperature, the dynamics of PVE are more sensitive to composition than those of PIP. The plateau moduli of the individual components are similar to

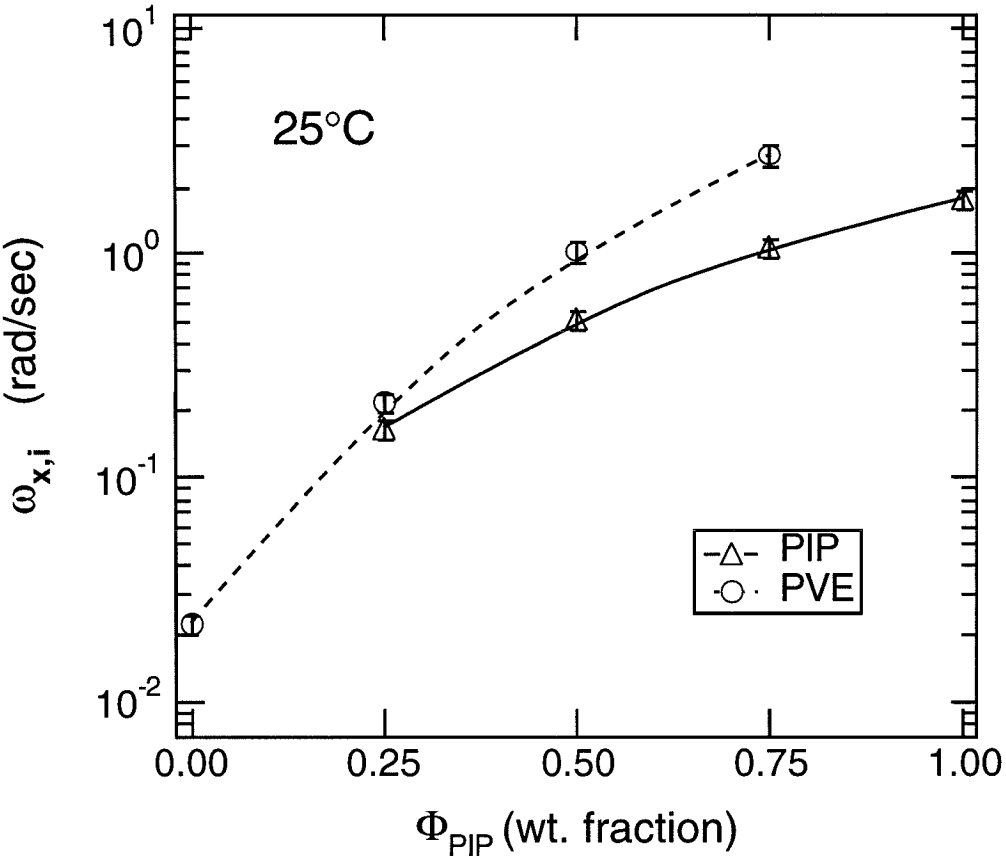

Figure 3.10: Component crossover frequencies, $\omega_{x,i}$, at 25°C, as a function of PIP content. Curves are drawn to guide the eye. The error bars indicate the range due to uncertainty in the values of the $C_i(\phi, T)$ and ϵ.

one another and vary only weakly with blend composition (Figure 3.9). Therefore, the predominant effect of changing composition is associated with the composition dependence of the friction coefficient of each species.

3.4.2 Entanglement Molecular Weight of Each Species

The values of the entanglement molecular weights of the individual components can be evaluated from their plateau moduli and literature values for the density of PIP/PVE blends [2] using

$$M_{e,i} = \frac{\rho RT}{G^o_{N,i}}. \tag{3.8}$$

To examine changes in the component $M_{e,i}$ with composition it is sufficient to examine relative values. Here we normalize $M_{e,i}(\phi)$ by the value for pure PIP, $M^o_{e,PIP}$, and take advantage of the observation that $G'(\omega_x) \propto G^o_N$, yielding

$$\frac{M_{e,i}(\phi)}{M^o_{e,PIP}} = \frac{\rho(\phi)}{\rho_{PIP}} \frac{G'_{PIP}(\omega_x)}{G'_i(\omega_x;\phi)}. \tag{3.9}$$

In this expression, only G'_i is sensitive to the values of the stress-optic coefficients and coupling coefficients used to analyze the blend data (eqn. 3.3 and 3.7).

Uncertainty in the values of $C_i(T)$ and ϵ in the blend has a small effect on the determination of the component crossover frequencies, $\omega_{x,i}$ (see error bars in Figure 3.10). In general, these uncertainties have a more significant effect on the magnitude and detailed shape of G^*_{PIP} and G^*_{PVE}, and consequently on the determination of $M_{e,i}$ (Figure 3.11). As mentioned earlier, in these equally entangled blends, however, both the shapes and magnitudes of the component moduli do not change significantly when

uncertainties of $\pm 10\%$ in the C_i's are assumed, or when values of ϵ ranging from 0.00 to 0.35 are used. Thus, uncertainty in these quantities does not alter the results dramatically.

The main feature to notice is that the component values of $M_{e,i}$ in the blend never differ by more than 30% from those of the homopolymers. Given the uncertainty in the data itself, the component $C_i(T)$ and ϵ, as well as our ability to estimate the values of $G_i'(\omega_x;\phi)$, we can only roughly bracket the values of the species' $M_{e,i}$ to the range given by the error bars in Figure 3.11. The solid line shows a linear variation between the pure component values.

3.4.3 Friction Coefficients of Each Species

The expressions for $G_i^*(\omega)$, determined using eqns. 3.3 and 3.7, are independent of any particular model for melt relaxation. If, however, we interpret the contribution of each species in light of the reptation model, we can extract their friction coefficients [43]. In the reptation model a chain in the melt is envisioned as being entangled in a network composed of the other chains, where the entanglements define a constraint tube. The long-time motion of the chain can then be imagined as snake-like, with the polymer chain sliding along the tube. It executes random-walk, curvilinear diffusion through the entanglements, on time scales over which lateral excursions are averaged out. The dynamics of the polymer chain are characterized by the constraint tube diameter, a, and the monomeric friction coefficient, ζ_o, which describes the interaction between a chain and its environment.

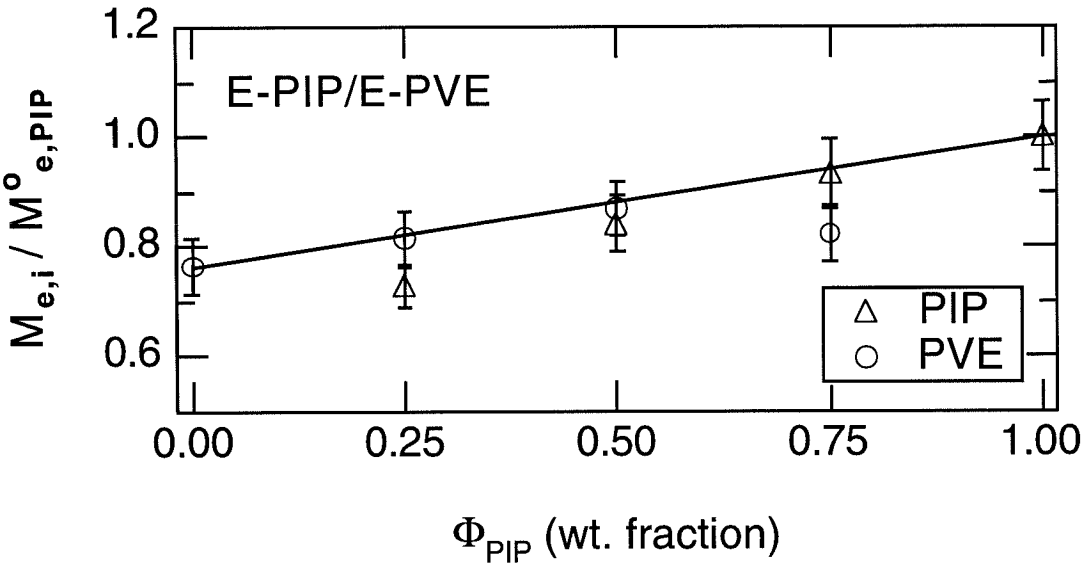

Figure 3.11: Normalized entanglement molecular weight of the homopolymers and of each component in the blend at $T = 25°C$. For comparison, the lines show a linearly weighted average of the homopolymer values at each temperature.

In the context of the reptation model, the relaxation modulus in the plateau to terminal regime is expressed as

$$G(t) = G_N^o f(t/\tau_d) \tag{3.10}$$

where G_N^o is the plateau modulus and $f(x)$ is a nearly universal relaxation function. The terminal relaxation time of the chain, τ_d, is given by

$$\tau_d = \zeta_o \left(\frac{M}{m_o}\right) \left(\frac{M}{M_e}\right)^2 \frac{a^2}{\pi^2 k_B T} \tag{3.11}$$

where $k_B T$ is the thermal energy, M is the molecular weight of the chain and m_o is the monomer molecular weight. The "tube diameter," a, characterizes the extent of lateral excursions of the chain among its neighbors, given by

$$a^2 = \frac{6 R_g^2 M_e}{M} \tag{3.12}$$

where R_g is the radius of gyration of the chain. The friction coefficient accounts for most of the temperature dependence of homopolymer dynamics. For *any* molecular model of polymer melt dynamics, $\tau_d \sim \zeta_o / T$ with a proportionality that varies weakly with ϕ and T. Therefore, the dependence of ζ_o on ϕ and T determined using eqn. 3.11 is essentially model independent.

We can evaluate the friction coefficient of each species using eqn. 3.11- 3.12, with values of $\tau_{d,i}(\phi, T)$ taken as $2/\omega_{x,i}$ [44], and values of $M_{e,i}$ calculated from the species $G_{N,i}^o$ and blend density. The $R_{g,i}$ are unaffected by blending (appropriate for $\chi \approx 0$), hence we use literature values of the species' statistical segment lengths, b_i [26], to

determine the $R_{g,i}$ for $E-PIP$ and $E-PVE$, using

$$R_{g,i}^2 = (\frac{M}{m_o})\ (\frac{b_i^2}{6}). \tag{3.13}$$

We perform a sensitivity analysis to evaluate sources of uncertainty. We calculate the friction coefficients using values of C_i spanning the range of uncertainty. For the component $M_{e,i}$ we use both $M_{e,i}(\phi, 25°\mathrm{C})$ independent of T, as well as $M_{e,i}(\phi, T)$. We also look at the variation in the values due to uncertainty in the value of ϵ. To account for the small uncertainty in the $\tau_{d,i}(\phi, T)$ due to determination of the $a_{T,i}$, we compare three criteria for superposition: overlap of G_i', G_i'', or $\omega_{x,i}$. We neglect the temperature dependence of $R_{g,i}$, as it has been shown to vary by less than 3% over the experimental range of T [26].

The $\zeta_{o,i}$ values obtained from these various calculations are shown in Figure 3.12. The symbols represent the average value determined for each friction coefficient. Error bars showing the range of values obtained are smaller than the size of the symbols. The results show that $\zeta_{o,PVE}$ is dramatically reduced by the addition of PIP to the blend, particularly at the lowest experimental temperatures (Figure 3.12b). On the other hand, $\zeta_{o,PIP}$ is much less sensitive to blend composition (Figure 3.12a). Consistent with the previously observed failure of time-temperature superposition in PIP/PVE blends, $\zeta_{o,PIP}$ and $\zeta_{o,PVE}$ in a given blend depend differently on temperature.

The observed temperature dependencies of $\zeta_{o,PIP}$ and $\zeta_{o,PVE}$ for the blends can be compared to those inferred by Roovers and Toporowski [2] for PIP/PVE blends

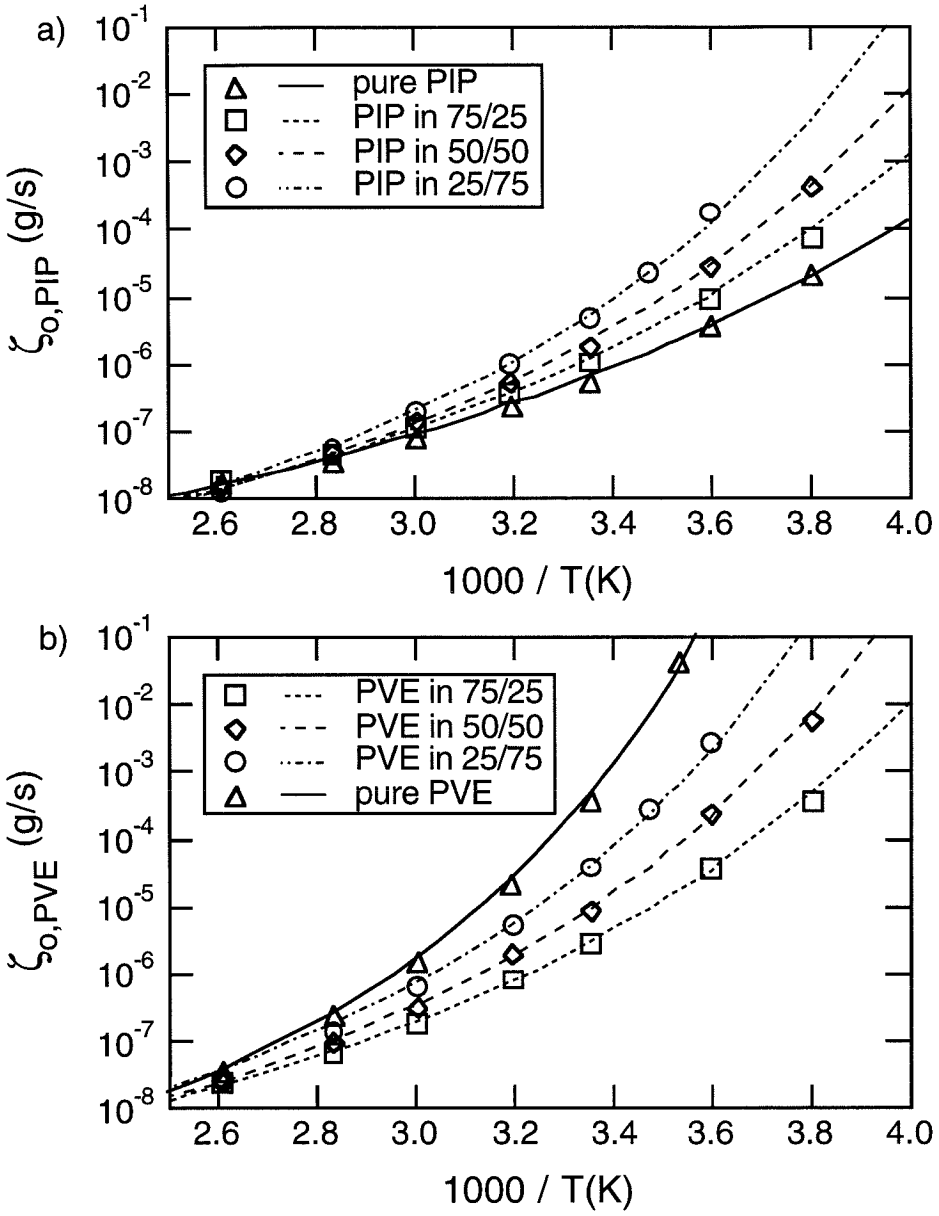

Figure 3.12: Component monomeric friction coefficients in the $E - PIP/E - PVE$ blends. **a)** PIP, **b)** PVE versus inverse absolute temperature, as a function of composition. Pure component friction coefficients are shown for reference. Curves are proportional to $a_T \cdot T$, with a_T determined from the WLF behavior established for the homopolymers and inferred for each component in PIP/PVE blends by Roovers and Toporowski [2]. See the text for discussion.

of corresponding weight fraction of PIP. The WLF dependencies they obtained for the relaxation behavior of pure PIP and PVE, as well as that of both components in the blends, are shown by curves on Figure 3.12. The vertical position is set to yield the best overall fit to the data. The values of C_1^g, C_2^g and $T_{g,i}$ they obtained for the pure components are 12.0, 52.9K and -61.0 °C for PIP and 11.4, 57.5K and 2.0 °C for PVE, respectively. The values of $C_1^g = 11.8$ and $C_2^g = 55K$, which are the average values for the pure components, are used for both components in all the blends. The $T_{g,i}(\phi)$'s for the components in the blends are taken from the average of the values given in Table VI, columns WLF^b, of their paper. For PIP $T_{g,PIP}$ = -47.0 °C, -37.5 °C and -31.0 °C, and for PVE $T_{g,PVE}$ = -40.0 °C, -27.5 °C and -17.5 °C, for $\phi_{PIP} = 0.75$, 0.5 and 0.25, respectively. Since the shift factors, $a_{T,i}$, represent the scaling of the relaxation dynamics with temperature, and the monomeric friction coefficient scales as $\tau_{d,i} \cdot T$, we compare the WLF dependencies of the two results by plotting values of $a_{T,i} \cdot T$ at each temperature. As seen from the figure, for both PIP and PVE there is good agreement between the WLF dependence inferred by Roovers and Toporowski and the present results for $\zeta_{o,i}$. From the WLF parameters, it appears that the components have different effective glass transition temperatures in the blends. Finally, it is the distinct temperature dependencies of the species' dynamics in the blend which dominates the failure of time-temperature superposition in these blends.

Previous ^{2}H-exchange NMR measurements of the effect of blending on the local segmental mobility of PIP and PVE have shown similar trends to those evident in

the friction coefficient results presented here: the mobility of the PVE component in a given blend is more sensitive to temperature and composition than the PIP component, and the segmental mobility of PVE is always lower than that of PIP in the blend, up to several orders of magnitude smaller, under identical conditions [5, 6].

3.5 Conclusions

By using blends in which the components are nearly equally entangled, we avoid the effects of polydispersity on the dynamic moduli of each species. Using both dynamic stress and birefringence measurements we determine the contributions of each species to the blend dynamic modulus. This combination of model blend and rheo-optical method allows us to examine the effect of the chemical composition of the blend on the dynamics of each species. While we cannot rule out contributions of compositional heterogeneity to thermorheological complexity in the PIP/PVE system, we find that intrinsic differences in time-temperature shifting between the two species dominate the overall failure of the superposition principle.

Blending produces minor changes in the entanglement molecular weights of PIP and PVE, and dramatic changes in their friction coefficients. The dynamics of the component with the higher glass transition temperature in the pure state (PVE) are more sensitive to blend ratio and temperature. The observation that each species retains a distinct temperature dependence of its dynamics is in qualitative accord with previous experimental studies of PIP/PVE blends [2, 5, 6]. The present approach

can be contrasted to earlier rheological approaches in which the relative position of two, often overlapping, loss peaks are monitored to determine the temperature shift of each species in a bidisperse miscible blend (Roovers and Toporowski, 1992). Stress-optical measurements facilitate quantitative determination of the friction coefficients $\zeta_i(\phi, T)$ of each component by revealing the contributions of each species to the dynamic modulus. Our results are consistent with prior studies, and better establish the precise values of the species' friction coefficients in PIP/PVE blends.

Bibliography

[1] Colby, R. H. *Polymer* **1989**, *30*, 1275.

[2] Roovers, J.; Toporowski, P. M. *Macromolecules* **1992**, *25*, 3454.

[3] Miller, J. B.; McGrath, K. J.; Roland, C. M.; Trask, C. A.; Garroway, A. N. *Macromolecules* **1990**, *23*, 4543.

[4] LeMenestrel, C.; Kenwright, A. M.; Sergot, P.; Lauprêtre, F.; Monnerie, L. *Macromolecules* **1992**, *25*, 3020.

[5] Chung, G. C.; Kornfield, J. A.; Smith, S. D. *Marcromolecules* **1994**, *27*, 964.

[6] Chung, G. C.; Kornfield, J. A.; Smith, S. D. *Marcromolecules* **1994**, *27*, 5729.

[7] Composto, R. J.; Kramer, E. J.; White, D. M. *Macromolecules* **1988**, *21*, 2580.

[8] Composto, R. J.; Kramer, E. J.; White, D. M. *Polymer* **1990**, *31*, 2320.

[9] Zawada, J. A.; Ylitalo, C. M.; Fuller, G. G.; Colby, R. H.; Long, T. E. *Macromolecules* **1992**, *25*, 2896.

[10] Zawada, J. A.; Fuller, G. G.; Colby, R. H.; Fetters, L. J.; Roovers, J.; *Macromolecules* **1994**, *27*, 6851.

[11] Zawada, J. A.; Fuller, G. G.; Colby, R. H.; Fetters, L. J.; Roovers, J.; *Macromolecules* **1994**, *27*, 6861.

[12] Zhao, Y.; Jasse, B.; Monnerie, L. *Polymer* **1989**, *30*, 1643.

[13] Roland, C. M. *Journal of Polymer Science, Polymer Physics Edition* **1988**, *26*, 839.

[14] Tsenoglou, C. *Viscoelasticity and Self-diffusion in Miscible Heteropolymer Blends. New Trends in Physics and Physical Chemistry of Polymers*; Plenum, 1989.

[15] Lau, S.; Pathak, J.; Wunderlich, B. *Macromolecules* **1982**, *15*, 1278.

[16] Zetsche, A.; Kremer, F.; Jung, W.; Schulze, H. *Polymer* **1990**, *31*, 1883.

[17] Fischer, E. W.; Zetsche, A. *ACS Polymer Preprints: Spring, San Francisco* **1992**, *78*.

[18] Ngai, K. L.; Plazek, D. J. *Macromolecules* **1990**, *23*, 4282.

[19] Kornfield, J. A.; Fuller, G. G.; Pearson D.S. *Macromolecules* **1991**, *24*, 5429.

[20] Osaki, K.; Takatori, E.; Kurata, M.; Ohnuma, H.; Kotaka, T. *Polymer* **1986**, *18*, 947.

[21] Osaki, K.; Takatori, E.; Ueda, M.; Kurata, M.; Kotaka, T.; Ohnuma, H. *Macromolecules* **1989**, *22*, 2457.

[22] Kannan, R. M.; Kornfield, J. A. *Rheologica Acta* **1992**, *31*, 535.

[23] Kannan, R. M.; Kornfield, J. A. *Journal of Rheology* **1994**, *38*, 1127.

[24] Trask, C. A.; Roland, C. M. *Macromolecules* **1989**, *22*, 256.

[25] Roland, C. M. *Macromolecules* **1987**, *20*, 2557.

[26] Tomlin, D.W.; Roland, C. M. *Macromolecules* **1992**, *25*, 2994.

[27] Roland, C. M.; Ngai, K. L. *Macromolecules* **1991**, *24*, 2261.

[28] Carella, J. M.; Graessley, W. W.; Fetters, L. J. *Macromolecules* **1984**, *17*, 2775.

[29] Gotro, J. T.; Graessley, W. W. *Macromolecules* **1984**, *17*, 2767.

[30] Ferry, J. D. *Viscoelastic Properties of Polymers*; Wiley: New York, 1980.

[31] Janeschitz-Kriegl, H. *Polymer Melt Rheology and Flow Birefringence*; Springer-Verlag: Berlin, 1983.

[32] Struglinski, M. J.; Graessley, W. W. *Macromolecules* **1985**,*18*, 2630.

[33] Wu, S. *Journal of Polymer Science, Polymer Physics Edition* **1989**, *27*, 723.

[34] Rubinstein, M.; Helfand, E.; Pearson, D. S. *Macromolecules* **1987**, *20*, 822.

[35] Doi, M.; Graessley, W. W.; Helfand, E.; Pearson, D. S. *Macromolecules* **1987**, *20*, 1900.

[36] Larson, R. G. *Constitutive Equations for Polymer Melts and Solutions*; Butterworths: Boston, 1988.

[37] Read, B. E. *Polymer* **1962**, *3*, 143.

[38] Read, B. E. *Polymer Engineering Science* **1983**, *23*, 835.

[39] Inoue, T.; Okamoto, H.; Osaki, K. *Macromolecules* **1991**, *4*, 5670.

[40] Arendt, B. H.; Kannan, R. M.; Zewail, M.; Kornfield, J. A.; Smith, S. *Rheologica Acta*, **1994**, *33*, 322; Arendt, B. H. *et al. Proceedings of the ACS, PMSE, Washington, D.C.*, **1994**,*71*, 471.

[41] Doi, M.; Pearson, D. S.; Kornfield, J. A.; Fuller, G. G. *Macromolecules*, **1989**, *22*, 1488.

[42] Ylitalo, C. M.; Zawada, J. A.; Fuller, G. G.; Abetz, V.; Stadler, R. *Polymer*, **1992**, *33*, 2949.

[43] Doi, M.; Edwards, S. F. *The Theory of Polymer Dynamics*; Oxford University Press: Oxford, 1986.

[44] Mark, J. E.; Eisenberg, A.; Graessley, W. W.; Mandelkern, L.; Koenig, J. L. *Physical Properties of Polymers. American Chemical Society*; Washington, D.C., 1984.

Chapter 4

Component Dynamics in Unequally Entangled Blends of Polyisoprene and Polyvinylethylene

4.1 Introduction

Polymer blends are systems of great importance from both a technological and scientific viewpoint. Commercial blends are typically phase separated, multicomponent systems consisting of at least two chemically distinct homopolymers of different molecular weights, and often include a third agent as a compatibilizer, such as a block or graft copolymer that is long enough to be entangled. The properties of such a system

are greatly affected by variables such as temperature, composition and processing history. In order to successfully predict the processing behavior of blends and formulate useful "blending rules," it is necessary to understand how the dynamics of each component in the blend depend on temperature and composition. The behavior of each species, i, in the blend can be characterized by certain intrinsic properties, namely the component entanglement molecular weights, $M_{e,i}(\phi)$, and monomeric friction coefficients, $\zeta_{o,i}(\phi, T)$, which depend differently on both blend composition, ϕ (volume fraction of the low-T_g component), and temperature, T. Specific interactions between the components can further complicate the blend dynamics by altering the chain conformations and interactions, as well as the phase diagram of the system. When the components have different molecular weights, polydispersity plays a role, and additional modes of relaxation, such as constraint release, affect the component dynamics.

Experimentally, it is difficult to monitor the contribution of the individual components to the bulk properties of the blends. In our previous work we used simultaneous rheological measurements of the blend dynamic moduli and polarimetric measurements of the blend birefringence to extract the dynamics of each component [1]. Miscible blends of 1,4-polyisoprene (PIP) and polyvinyethlyene (PVE) were chosen as a model system for a given mixed phase of an immiscible blend, to examine the effect of the composition and temperature on the dynamics of each species. The PIP/PVE blends are nearly ideal mixtures for which specific interactions between the two species are not present [2, 3, 4, 5, 6]. In fact, these blends remain miscible

over all molecular weights, temperatures and compositions experimentally probed. PIP/PVE are also interesting because the components have widely disparate glass transition temperatures and mobilities [1, 7, 8, 9]. For blends rich in PVE (low ϕ, defined as ϕ_{PIP}), where thermal measurements show an anomolously broad glass transition compared to the homopolymers [4, 10], the values of $\zeta_{o,PIP}(low\phi, T)$ and $\zeta_{o,PVE}(low\phi, T)$ are most disparate [1, 11, 12]. The failure of time-temperature superposition in PIP/PVE blends can be attributed to the distinct temperature dependence of each species' dynamics in the blend. Both the magnitude and temperature dependence of the component $\zeta_{o,i}$'s are different, and the dynamics of the high-T_g species (PVE) are more sensitive to temperature and composition. Thus, even this ideal blend system exhibits complex dynamic behavior.

In the previous chapter we studied PIP/PVE blends in which we chose the component molecular weights so that the two components were approximately equally entangled. Our goal was to focus on effects unique to blends of chemically distinct polymers rather than features that exist even in bidisperse blends of a single species, such as constraint release [13, 14, 15]. In our experiments we took advantage of the optical contrast inherent in these blends due to the fact that the two species have very different stress-optic coefficients. For the equally entangled blends the failure of time-temperature superposition was subtle [1, 4, 5]. However, complex *stress-optical* behavior revealed the presence of thermorheological complexity. The observed behavior could be explained by the different temperature dependencies of the dynamics of each component, as described by the species' monomeric friction coefficients

$\zeta_{o,PIP}(\phi,T)$ and $\zeta_{o,PVE}(\phi,T)$, which depend on both the bulk composition of the blend, ϕ, and the temperature, T [1, 16]. For equally entangled blends, where the relaxation spectrum resembles that of a monodisperse polymer, the modest differences between the temperature dependence of the $\zeta_{o,i}$'s causes changes in shape with temperature, thereby leading to apparent thermorheological simplicity.

Much more dramatic failure of time-temperature superposition has been observed for bidisperse PIP/PVE blends [17, 16, 8, 9]. We now focus on unequally entangled blends where the effects of polydispresity, such as constraint release, and orientational coupling make the determination of the components' dynamics more complex than in the equally entangled case, with additional modes of relaxation possible. In these blends the degree of orientational coupling can be exposed. We seek to determine the amount of orientational coupling induced in the faster-relaxing component due to the remaining orientation of the slower-relaxing matrix, which is represented by a coupling parameter, ϵ. We investigate the possible dependence of ϵ on temperature, composition and species. Where possible we will compare our results to the work of Zawada et al. [8, 9]. Finally, we want to determine whether the trends observed in the entanglement molecular weights and friction coefficients of the equally entangled blends are sufficient to describe the behavior of the components in these unequally entangled blends.

We study the dynamics of miscible blends of 1,4-polyisoprene (PIP) and polyvinylethylene (PVE), for two combinations of molecular weight, as functions of temperature and composition. In the first section we describe the properties of

the PIP/PVE model system and breifly mention the variables of interest, based on the rheo-optical technique described in Chapter 2. Next, we present the results of our dynamic stress and birefringence measurements for unequally entangled blends: ones in which PVE is the slower-relaxing species and ones in which PIP is slower-relaxing. We describe how the contribution of each component to the blend dynamic moduli and the values of the coupling coefficient, ϵ, were determined. The dependence of ϵ on temperature, composition and species are discussed. This is followed by a discussion of the results in terms of the component dynamics in the blends, from which we extract component entanglement molecular weights, $M_{e,i}$, and monomeric friction coefficients, $\zeta_{o,i}$. Finally, comparisons are made between the different relative molecular-weight blend systems.

4.2 Experimental

4.2.1 Materials

We choose as a model system blends of 1,4 polyisoprene (PIP) and polyvinylethylene (PVE), synthesized by S.D. Smith at Procter and Gamble. The misciblility of these species is well-established over the range of accessible molecular weights, temperatures and compositions [4, 6, 10]. The synthesis and characterization of the homopolymers are described elsewhere [18, 19, 16]. To determine the molecular weights and weight distributions, we performed gel-permeation chromatography in spectroscopic-grade tetrahydrofuran at 25°C, using a two column system from American Polymer

Table 4.1: Characterization of Polyisoprene (PIP) and Polyvinylethylene (PVE) Homopolymers

Sample	M_w*(kg/mol)	M_w/M_n*	$\omega_{x,i}$ (rad/s) @ 25°C	T_g(°C)**
S-PIP	110	1.05	10.9	-64.9
L-PVE	290	1.11	0.00039	-2.5
L-PIP	850	1.17	0.014	-64.0
S-PVE	80	1.09	0.022	-2.1

* From gel-permeation chromatography in tetrahydrofuran at 25°C, using PIP standards.

** From differential scanning calorimetry (DSC) heating at 10°C/min.

Standards. *PIP* standards from Polymer Laboratories were run simultaneously to calibrate the molecular weights. The glass transition temperatures of the pure components were determined on a Perkin Elmer DSC-7, using $\approx$ 25 mg samples and heating at a rate of 10°C/min. The values of the glass transition temperatures, which are very sensitive to microstucture, indicate that the *PVE* samples are >95% pendant vinyl (1,2-polybutadiene) units. We also performed room temperature ^{13}C NMR on 25% w/v $CDCl_3$ solutions of the pure components using a General Electric QE-300 spectrometer. The *PVE* microstructures are confirmed and the polyisoprene microstructures are found to contain >94% 1,4-units. The properties of our specific samples are listed in Table 4.1. The samples are designated $S-PIP$, $L-PIP$,

$S - PVE$ and $L - PVE$, where S denotes short chains and L long chains. Notice that all the polymer samples are monodisperse and long enough to be well-entangled.

The two species have very different mobilities at ambient temperatures as a consequence of the large difference between their glass transition temperatures, where $T_{g,PIP} \approx -60°\text{C}$ and $T_{g,PVE} \approx 0°\text{C}$ [10, 11, 12]. To gain selective information regarding the relaxation of each species, we take advantage of the optical contrast inherent in this system. The component stress-optic coefficients, listed in Table 4.2, are of opposite signs and differ by an order of magnitude [1]. Thus, while the two species contribute similarly to the bulk stress, their contributions to the birefringence are of opposite sign, which will allow us to detect their distinct contributions.

4.2.2 Methods

Dynamic mechanical and birefringence measurements are made using the rheo-optical instrument described in Chapter 2 and in previous studies [1, 21, 20]. Again, to expose departures from the stress-optic rule, we examine the amplitude-based stress-optic ratio SOR and the phase difference between σ_{12} and n_{12}:

$$SOR \equiv \frac{|B^*|}{|G^*|}, \tag{4.1}$$

and

$$\delta_B - \delta_G \equiv \tan^{-1}(\frac{B''}{B'}) - \tan^{-1}(\frac{G''}{G'}). \tag{4.2}$$

For miscible blends the stress-optic rule has been shown to fail [1], since the stress and birefringence are differently weighted averages of the two species' orientation (i.e.,

Table 4.2: Stress-Optic Coefficients of Polyisoprene (PIP) and Polyvinylethylene (PVE) Homopolymers*

	$C \times 10^{10}$ (cm^2/dyne)	
T(°C)	PIP	PVE
-10	1.88	-0.35
5	1.77	-0.28
15	1.73	-0.25
25	1.68	-0.23
40	1.62	-0.17
60	1.55	-0.100
80	1.47	-.048
110	1.38	+0.016
130	1.30	+0.050

* Average of values for each type of polymer. Variation of values between different samples of the same species fall within the uncertainty in the measurements.

the second moment of their segmental orientation distributions). This is particularly true if the species have C_i's of opposite sign or widely differing magnitude.

Frequencies from 0.01 to 100 rad/sec were employed, at temperatures ranging from 5 to 110°C. At high frequencies and low temperatures, oscillatory strains of 1% or less were applied. With decreasing frequency and increasing temperature, when the force signal decreased to the limit of the transducer, the strain was increased. At the highest temperatures (80, 110 and 130°C) and the lowest frequencies, strains of 50-100% were used. In all cases, it was verified that the birefringence and viscoelastic response were in the linear regime. Experiments at the lowest and highest temperatures were performed under nitrogen atmosphere. To prevent sample degradation, in addition to using the inert atmosphere, the exposed surfaces of the samples were coated with an antioxidant, 2,6-Di-tert-butyl-4-methyl-phenol (BHT).

4.3 Results

4.3.1 Homopolymer Characterization

The mechanical and optical properties of the homopolymers used in this study are given in Tables 4.1 and 4.2. The dynamic moduli of all the pure components have a single loss peak. From the positions of the loss peaks, or alternatively the cross-over frequencies, $\omega_{x,i}$, we can determine the relative relaxation rates. The cross-over frequencies at $T = 25$°C are given in Table 4.1. The homopolymers obey time temperature superposition as expected [23], and the values of their horizontal shift factors,

$a_{T,i}$, are listed in Tables 4.3 and 4.4. They agree well with previously established WLF behavior for these species [18, 19, 16]. For the PVE homopolymers no vertical shifting was required to obtain superposition. The PIP homopolymers, however, required values of $b_{T,i}$ close to unity, in accord with the literature [19]. The magnitudes of the cross-overs and plateau in the dynamic moduli differ consistently from other reported values by $\approx 27\%$ [18, 23, 19, 8, 9]. While we have been unable to account for this deviation, all our data are consistently lower by this factor; thus, it does not effect the trends in the results.

By comparing the dynamic birefringence to the dynamic modulus, it was confirmed that the stress-optic rule holds away from the dynamic glass transition for all pure components [22, 24]. Thus, the values of SOR are independent of frequency and are equal to the stress-optic coefficients given in Table 4.2. For the PIP samples the relative phase angle between the birefringence and stress, δ_B-δ_G, remains nearly zero (0 ± 0.04 rad). This is in accord with the stress-optic rule, where the stress and birefringence remain in phase. For the PVE samples the phase angle is nearly π (3.14 ± 0.04 rad), indicating that the stress and birefringence signals are 180° out of phase, i.e., that the stress-optic coefficient of PVE is *negative*. Notice that the values of C_{PVE} are an order of magnitude smaller than C_{PIP} and also of opposite sign. Furthermore, C_{PVE} varies much more strongly with temperature, over an order of magnitude and changes sign, over the range of temperature covered by our experiments. C_{PIP} varies much less so, by $\sim 25\%$ over the same range.

4.3.2 Unequally Entangled Blends

Two sets of blends were used, one in which the PVE component is faster-relaxing, denoted $L-PIP/S-PVE$, and one in which the PIP species is much faster-relaxing, denoted $S-PIP/L-PVE$. We choose the molecular weights so that the component relaxations in the blends remain well-separated for all compositions and frequencies probed. At the lowest frequencies then, below the low-frequency loss peak controlled by the slower-relaxing species, the faster-relaxing species is nearly completely relaxed and its contribution to the birefringence is due to orientation imposed by coupling to the slower-relaxing matrix. This facilitates determination of the coupling coefficient.

S-PIP/L-PVE

Dynamic Moduli:

Composite curves for the dynamic moduli of the $S-PIP/L-PVE$ blends were obtained by shifting the data at different temperatures along the frequency axis only, so as to superimpose the terminal behavior at the lowest experimental frequencies. No vertical shifting was applied. Shown in Figure 4.1 are the loss moduli for the three compositions. Failure of time-temperature superposition is much more dramatic than in the equally-entangled blends. The horizontal shift factors, a_T, for all experimental temperatures are presented in Table 4.3 for the blends and pure components.

Like binary blends of a given polymer [13, 14, 15], the low-frequency loss peak grows nonlinearly with the fraction of long chains, here ϕ_{PVE}. For the $\phi_{PIP} = 0.75$ blend only one loss peak is observed, with a low-frequency shoulder barely percepti-

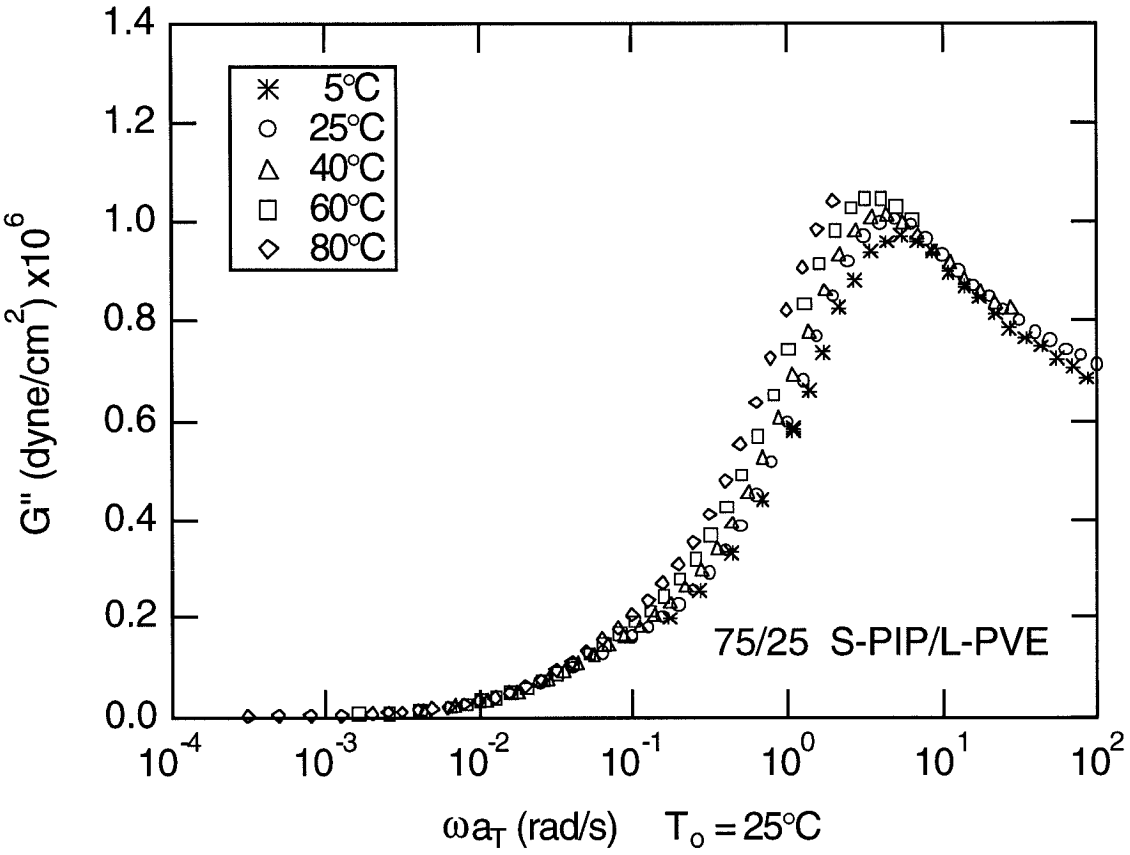

Figure 4.1: Dynamic moduli "master curves" for $S-PIP/L-PVE$ blends **a)** 75/25 w/w $S-PIP/L-PVE$. The reference temperature is $T_o = 25°$C. Note that time-temperature superposition does not hold. Only a horizontal shift was used to superimpose the data in the terminal regime.

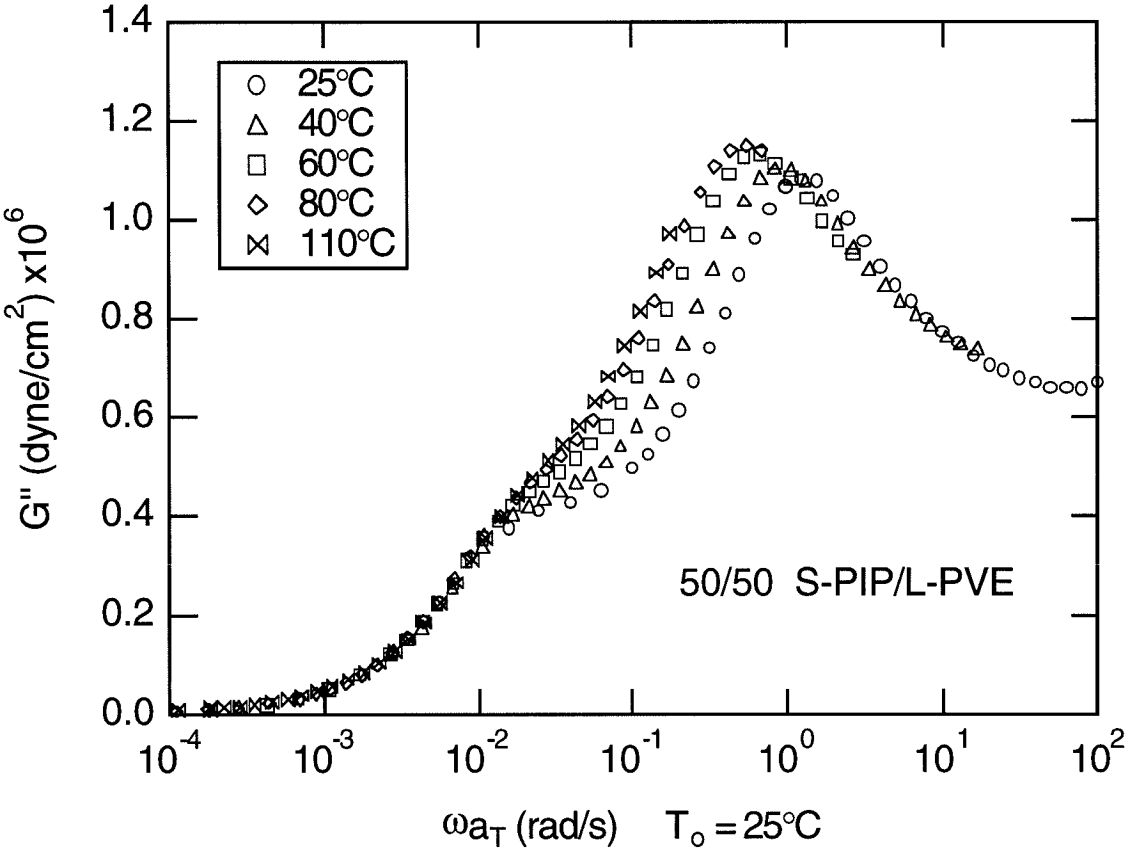

Figure 4.1: Dynamic moduli "master curves" for $S-PIP/L-PVE$ blends **b)** 50/50 w/w $S-PIP/L-PVE$. The reference temperature is $T_o = 25°C$. Note that time-temperature superposition does not hold. Only a horizontal shift was used to superimpose the data in the terminal regime.

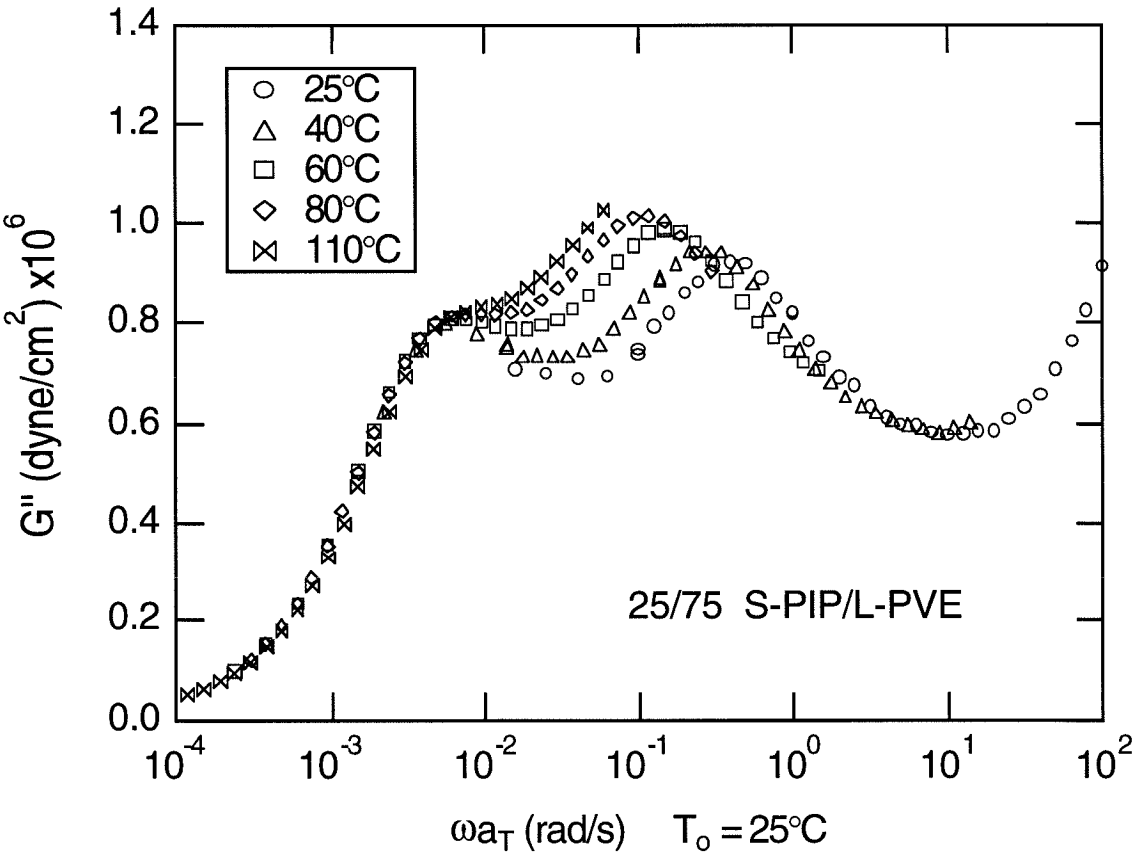

Figure 4.1: Dynamic moduli "master curves" for $S - PIP/L - PVE$ blends **c)** 25/75 w/w $S - PIP/L - PVE$. The reference temperature is $T_o = 25°C$. Note that time-temperature superposition does not hold. Only a horizontal shift was used to superimpose the data in the terminal regime.

Table 4.3: Shift Factors, a_T, of Homopolymers and S-PIP/L-PVE Blends

	Homopolymers			Blends (PIP/PVE w/w %)		
T(°C)	$b_{T,PIP}$	PIP	PVE	75/25	50/50	25/75
-10	1.08	42	-	100	-	-
5	1.03	6.5	-	11	15	-
15	1.02	2.42	18	3.2	3.5	4.5
25	1	1	1	1	1	1
40	0.98	0.35	0.055	0.28	0.17	0.14
60	0.95	0.12	0.0036	0.065	0.027	0.015
80	0.92	0.048	0.00052	0.02	0.007	0.003
110	-	-	0.00007	-	0.0018	0.0006

ble. For both the $\phi_{PIP} = 0.50$ and 0.25 blends two loss peaks are visible. Since the PVE component has a much higher molecular weight and a higher glass transition temperature, T_g, we can assign the lower-frequency loss peak to PVE. Unlike binary blends of the same polymer, the positions of both loss peaks shift to higher reduced frequency as the weight fraction of short chains (PIP) increases (moving from Figure 4.1c to b to a), though the PVE loss peak is difficult to track as it becomes a shoulder (Figure 4.1a). From the pure component loss peak positions we can see that in the $\phi_{PIP} = 0.75$ blend the relaxation of PVE must be greatly accelerated and that of PIP slightly slowed in order for only one blend loss peak to be observed. While the positions of both loss peaks shift to higher reduced frequency as the weight fraction of PIP increases, the relative shift of the PVE component loss peak from the pure component values increases dramatically, while that of PIP shifts much less so (see Figure 4.1).

We now focus on the shift of the component dynamics with temperature. Examination of how the loss peaks shift with temperature demonstrates how the relative component relaxations are changing. Unlike binary blends of the same polymer, increasing temperature shifts the high-freqeuncy loss peak to lower frequency relative to the low-frequency peak. For each blend the position of the low-frequency, PVE loss peak remains at approximately fixed reduced frequency. This makes sense since the blend dynamic moduli are superimposed with respect to the terminal, slower-relaxing tail of the spectra, which is dominated by PVE. The position of the high-frequency loss peak, however, dominated by the PIP component, shifts to lower relative re-

duced frequency as the temperature increases. A decrease in the loss peak separation and a shift of the peak to lower reduced frequency means that while the dynamics of both species in the blends accelerate with temperature, those of PVE do so more than those of PIP. This is most dramatic in the blends with higher PVE content.

Dynamic Birefringence:

The dynamic birefringence for the $S - PIP/L - PVE$ blends was measured simultaneously with the dynamic moduli, from which we calculate SOR and δ_B - δ_G. The stress-optic data are shown in Figures 4.2 and 4.3 after shifting along the frequency axis using the shift factors obtained for the dynamic moduli (Figures 4.1 and Table 4.3). Note that shifting the stress-optic data according to the corresponding mechanical shift factors does *not* lead to satisfactory time-temperature superposition.

The values of SOR for the $S - PIP/L - PVE$ blends show a distinct frequency dependence (Figure 4.2), and failure of the stress-optic rule is quite dramatic. At high frequencies the SOR reaches a plateau which is approximately the composition-weighted average of the homopolymer stress-optic coefficients (see Table 4.2) [1]. At intermediate frequencies SOR decreases, in contrast to the equally entangled blends in which the PVE component relaxes faster and SOR rises. In these $S-PIP/L-PVE$ blends the faster-relaxing species, PIP, has a large, positive stress-optic coefficient. As its positive contribution to the birefringence decays away first, SOR falls. Finally, at low frequencies SOR reaches a second plateau whose value is closer to the stress-optic coefficient of PVE, the slowest-relaxing species in the blend. The position of the inflection in SOR shifts to lower relative reduced frequency as the PIP content

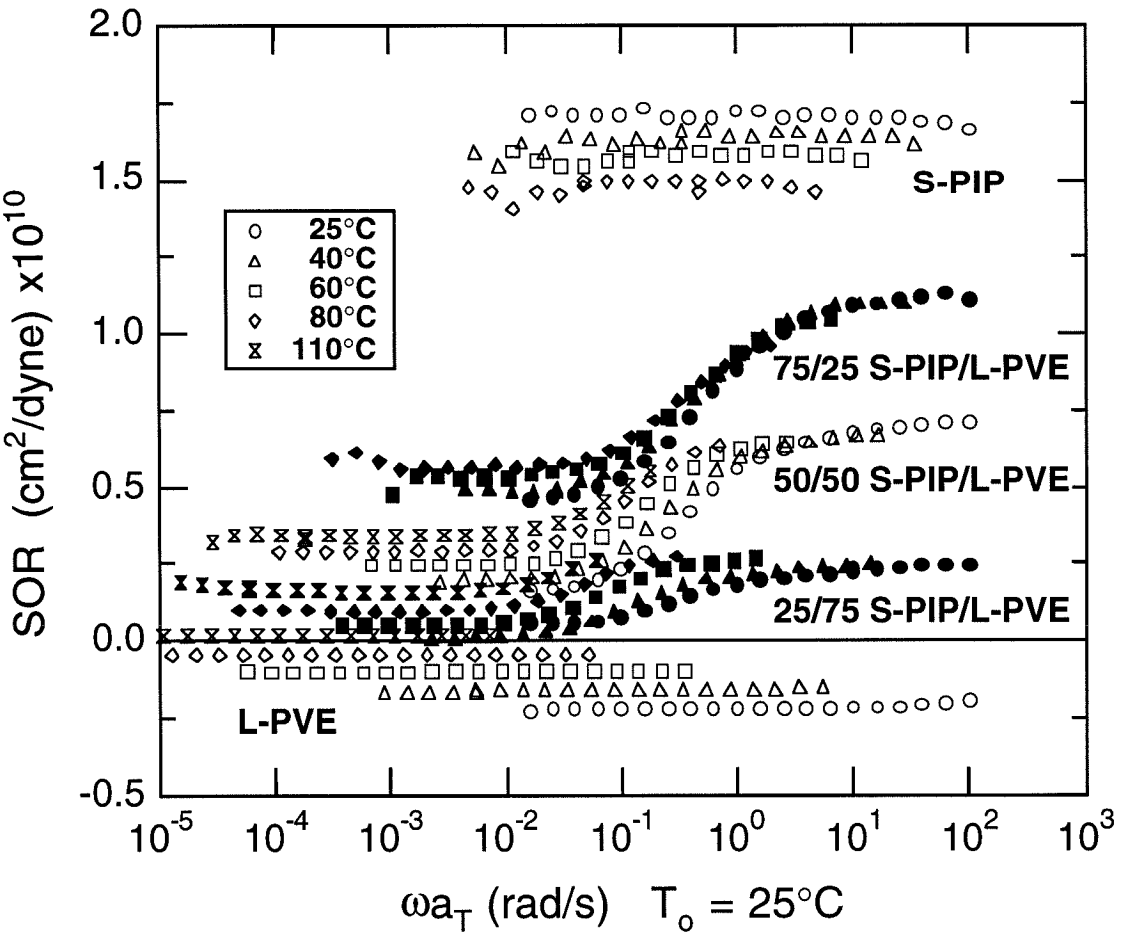

Figure 4.2: SOR of the $S-PIP/L-PVE$ blends versus the same reduced frequencies as the dynamic moduli of the respective samples. Shown for comparison are the stress-optic coefficients of the pure components.

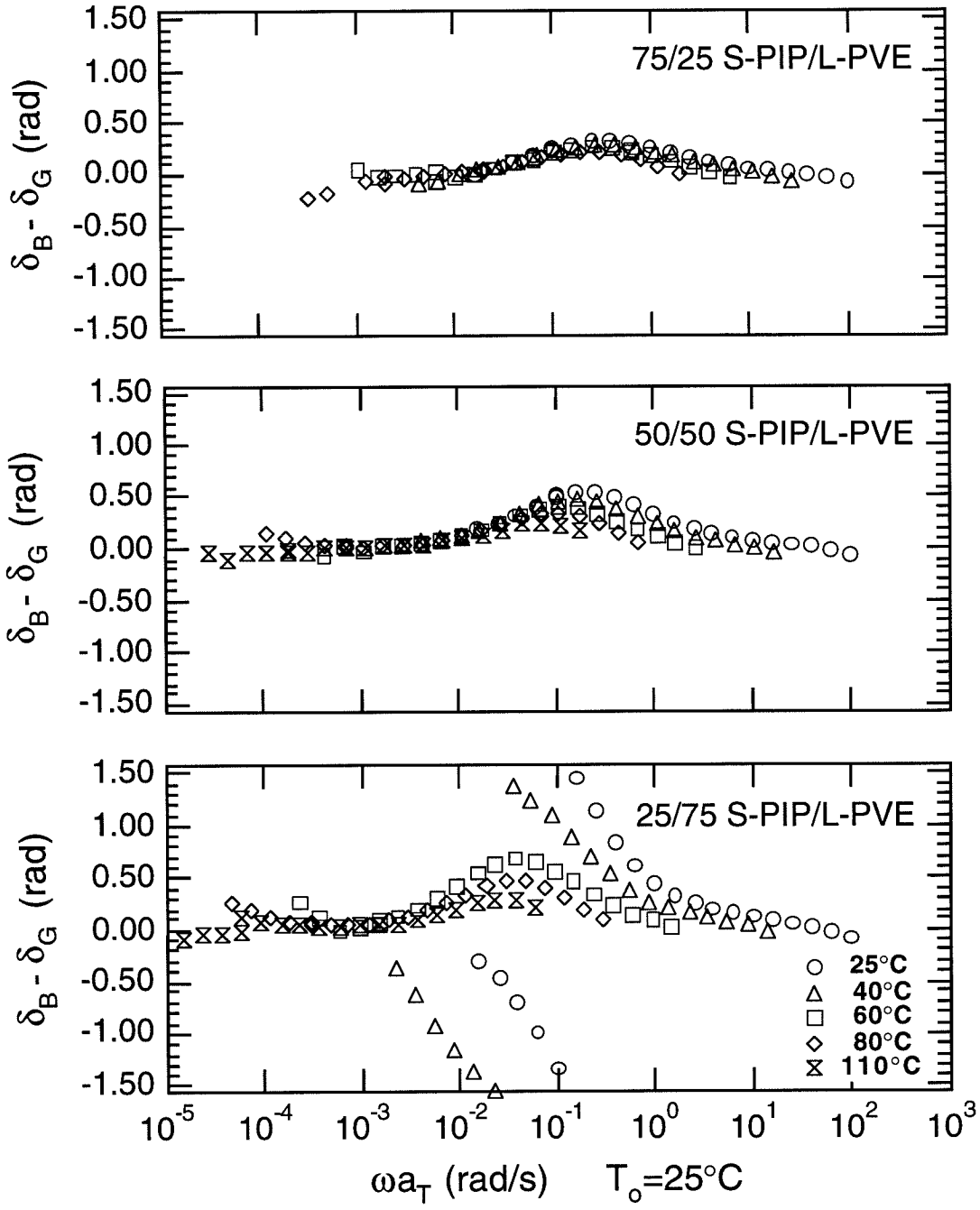

Figure 4.3: Phase difference between the dynamic birefringence and shear stress for the S-PIP/L-PVE blends.

decreases.

We now look at the temperature dependence of SOR. The characteristic reduced frequency of the upturn for all three blend compositions of the $S - PIP/L - PVE$ blends shifts to lower reduced frequency as the temperature increases. The effect is most dramatic in the blends with higher PVE content. In terms of the magnitude of SOR, for the $\phi_{PIP} = 0.75$ and 0.50 blends, at high reduced frequencies where PIP dominates the magnitude of SOR, the magnitude of the plateau decreases with temperature as does C_{PIP}. At the lowest reduced frequencies the slower-relaxing component, PVE, dominates the plateau in SOR, the magnitude of which increases with increasing temperature as does C_{PVE}. For the $\phi_{PIP} = 0.25$ blend, *both* the high- and low-frequency plateaus in SOR appear to track the behavior of C_{PVE}, increasing with temperature, as the PVE component dominates the response.

The phase difference between the dynamic birefringence and shear stress, δ_B - δ_G, is shown in Figure 4.3, where the values are kept between $\pm\ \pi/2$. Unlike the blends in which PVE relaxed first, $\delta_B - \delta_G$ these blends exhibits a hump rather than a dip, as the PIP component relaxes first. The position of the hump tracks the inflection in SOR, shifting to lower reduced frequency and increasing in height as the weight fraction of PIP decreases. Notice that for the $\phi_{PIP} = 0.25$ blend at the lowest temperature the value of the phase difference passes through $+\pi/2$ to $-\pi/2$. In this range of frequencies it is observed that values of B' are negative while those of B'' are positive, indicating that PVE is becoming dominant as ω decreases. For freqeuncies and temperatures where the PVE component is able to relax, and PIP contributes

sufficiently to the birefringence via orientational coupling, both birefringence coefficients are positive and the relative phase angle remains positive and $< \pi/2$. As a function of temperature, the hump shifts to lower reduced frequency and decreases in height as the temperature increases.

L-PIP/S-PVE

Dynamic Moduli:

Again, composite curves for the blend dynamic moduli were obtained by shifting along the frequency axis only to superimpose the data in the terminal regime. No vertical shifting was applied. The loss moduli of the $L-PIP/S-PVE$ blends are shown in Figure 4.4, and the horizontal shift factors are listed in Table 4.4 for the blends and pure components. Failure of time-temperature superposition is quite evident for all three blend compositions.

Again, the magnitude of the low-frequency loss peak increases nonlinearly with the content of long chains, now ϕ_{PIP}. For both the $\phi_{PIP} = 0.75$ and 0.50 blends, two loss peaks are visible, while the blend with $\phi_{PIP} = 0.25$ shows one loss peak with a low-frequency shoulder. In these blends the PIP component was chosen to have a slower relaxation rate in the blends than PVE, hence we can assign the higher-frequency loss peak to PVE and the lower one to PIP. Both loss peaks shift to lower reduced frequency with decreasing PIP content, though the position of the PIP loss peak is difficult to track, as it becomes a barely perceptible shoulder. As seen in the other blends, the dynamics of PVE are much more sensitive to composition than those of

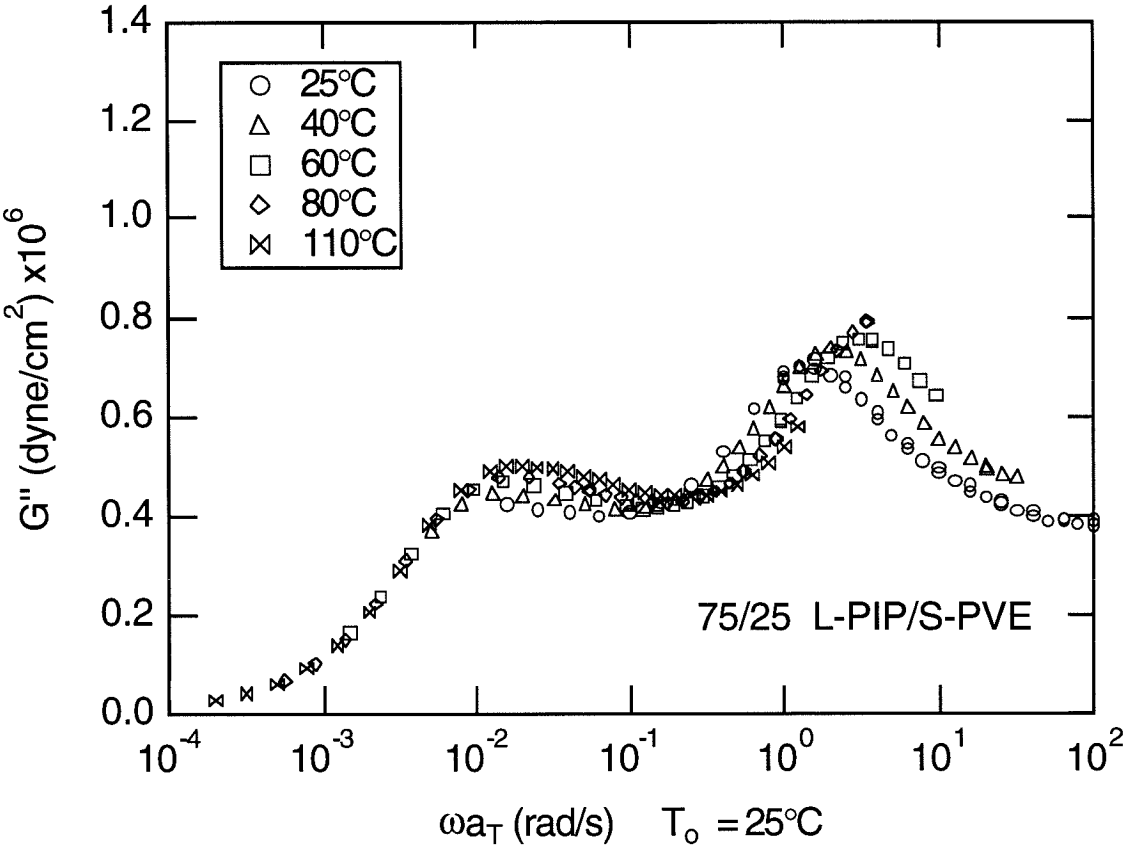

Figure 4.4: Dynamic moduli "master curves" for $L - PIP/S - PVE$ blends **a)** 75/25 w/w $L - PIP/S - PVE$. The reference temperature is $T_o = 25°C$. Note that time-temperature superposition does not hold. Only a horizontal shift was used to superimpose the data in the terminal regime.

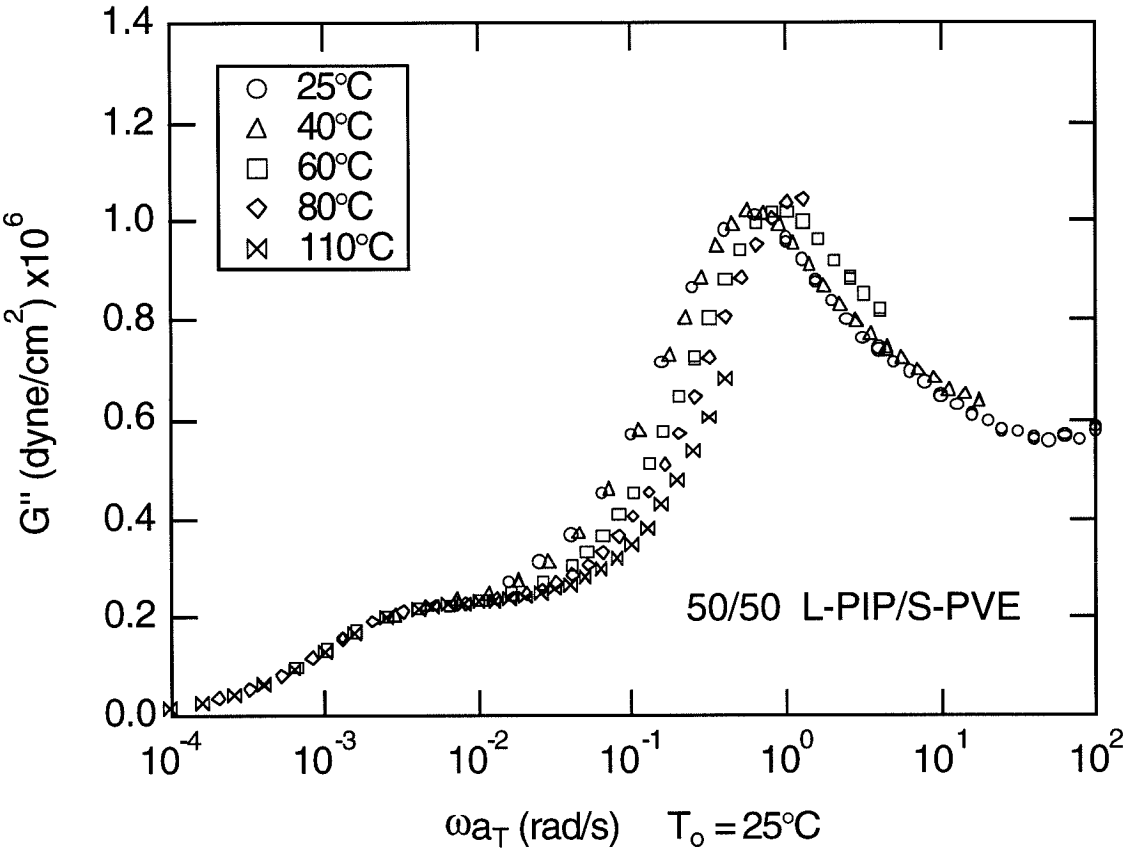

Figure 4.4: Dynamic moduli "master curves" for $L-PIP/S-PVE$ blends **b)** 50/50 w/w $L-PIP/S-PVE$. The reference temperature is $T_o = 25°$C. Note that time-temperature superposition does not hold. Only a horizontal shift was used to superimpose the data in the terminal regime.

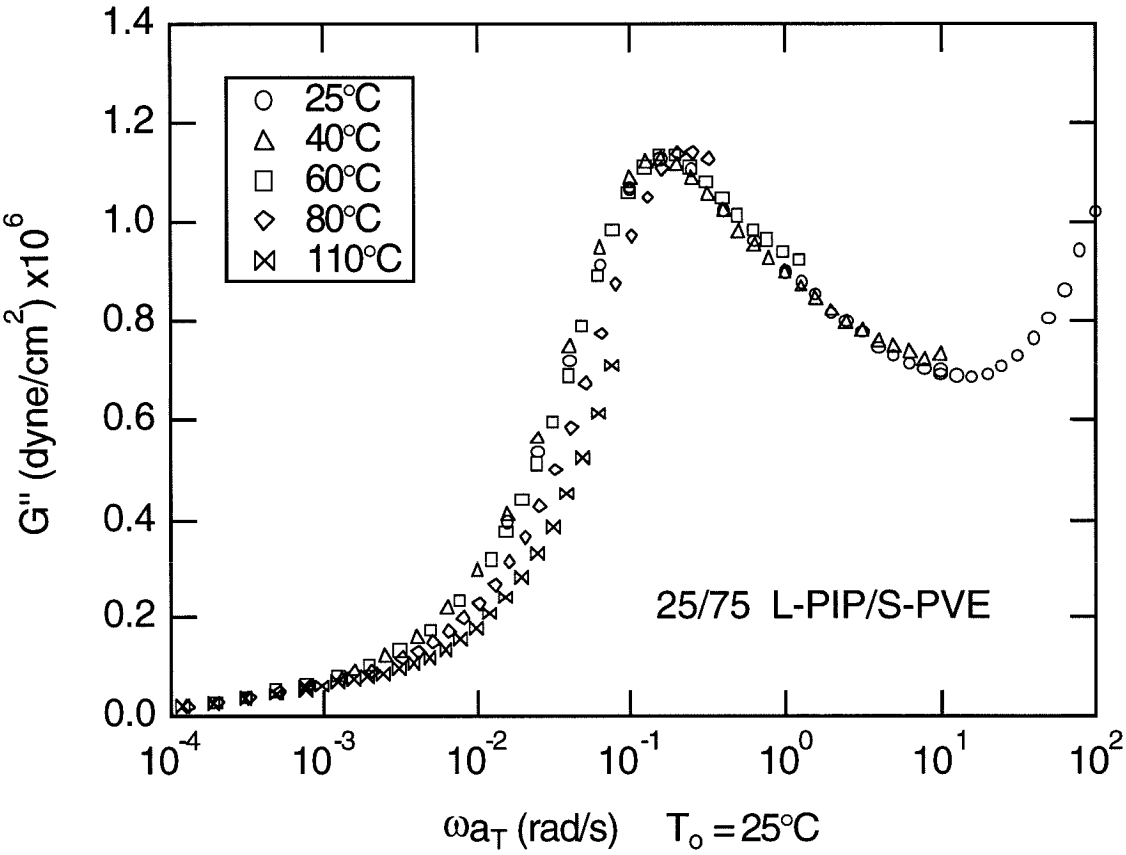

Figure 4.4: Dynamic moduli "master curves" for $L-PIP/S-PVE$ blends **c)** 25/75 w/w $L-PIP/S-PVE$. The reference temperature is $T_o = 25°C$. Note that time-temperature superposition does not hold. Only a horizontal shift was used to superimpose the data in the terminal regime.

Table 4.4: Shift Factors, a_T, of Homopolymers and L-PIP/S-PVE Blends

	Homopolymers			Blends (PIP/PVE w/w %)		
T(°C)	$b_{T,PIP}$	PIP	PVE	75/25	50/50	25/75
25	1	1	1	1	1	1
40	0.98	0.34	0.055	0.32	0.18	0.10
60	0.96	0.107	0.0035	0.095	0.041	0.0123
80	0.89	0.044	0.00046	0.035	0.013	0.00323
110	0.87	0.0163	0.000061	0.0125	0.004	0.00077
130	0.84	0.01	-	0.0085	0.0023	0.0004

PIP: while both species' dynamics accelerate with an increase in PIP content, those of PVE are affected more.

We now look at the relative shift of the components' dynamics with temperature. For all three blend compositions, the position of the low-frequency loss peak, dominated by PIP, is the basis for superposition of the dynamic moduli and hence remains at fixed reduced frequency. The position of the PVE loss peak, however, shifts to higher frequency relative to the PIP peak in all three $L-PIP/S-PVE$ blends. This is the same behavior as observed in the previous two blend systems, indicating that while the dynamics of both species accelerate with temperature, those of PVE do so more than PIP's.

Dynamic Birefringence:

The values of SOR for the $L-PIP/S-PVE$ blends shows a distinct frequency dependence similar to the behavior of the other blends, and the stress-optic rule fails quite visibly (Figure 4.5). The high-frequency plateau attains a value which is approximately the composition-weighted average of the pure component stress-optic coefficients (Table 4.2). At lower frequencies the SOR increases, reminiscent of the behavior of the equally entangled blends, as the PVE component relaxes first and its negative contribution to the birefringence decays. At the lowest frequencies the value of SOR reaches another plateau, whose value is closer to that of the slowest-relaxing component in the blends, PIP. The position of the inflection in SOR shifts to lower relative reduced frequency as the PIP content decreases.

We now examine the temperature dependence of the SOR. The values are displayed using the reduced frequencies determined from the horizontal shift factors of the dynamic moduli. Again, time-temperature superposition is not achieved. The position of the inflection in SOR shifts to higher reduced frequency with increasing temperature. This effect diminishes as the PIP concentration increases. In terms of the magnitude of SOR, for $\phi_{PIP} = 0.75$ the high-frequency plateau decreases with increasing temperature, like the stress-optic coefficient of PIP, the dominant species. Similarly, the high-frequency plateau for the $\phi_{PIP} = 0.25$ blend increases with temperature, like C_{PVE}. In the case of the $\phi_{PIP} = 0.5$ blend, the magnitude of the plateau appear unchanged over the range of temperature. At the lowest frequencies the magnitude of the plateau decreases with temperature, as does C_{PIP}. In this regime the birefringence is dominated by PIP, since it is the slower-relaxing species.

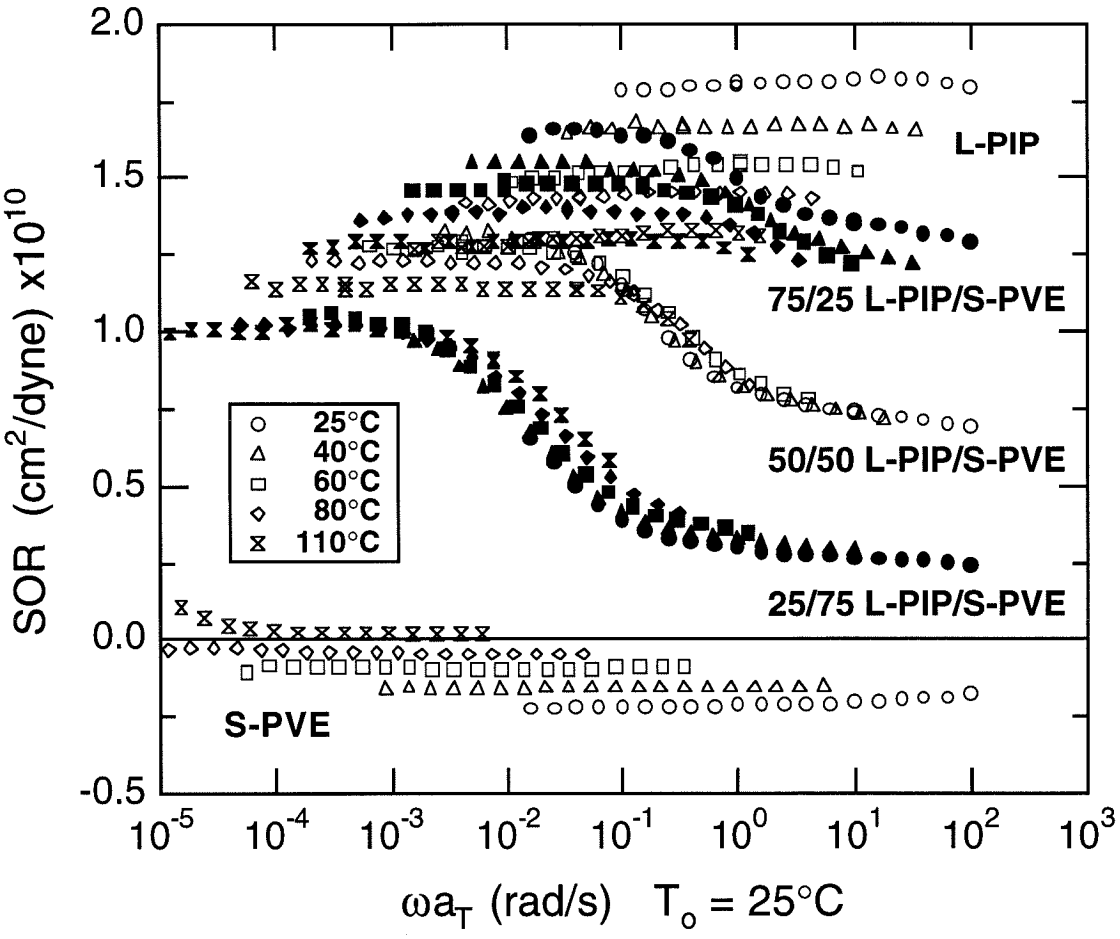

Figure 4.5: SOR of the $L-PIP/S-PVE$ blends versus the same reduced frequencies as the dynamic moduli of the respective samples. Shown for comparison are the stress-optic coefficients of the pure components.

The relative phase difference, $\delta_B - \delta_G$, is shown in Figure 4.6. As in the equally entangled system, these blends show a dip as the PVE component relaxes first. In these blends, however, the dip is deeper as the difference between the PVE and PIP relaxations is larger. The position of the dip follows that of the inflection in SOR and increases in depth as the PIP content decreases. Finally, for all three blend compositions, the position of the dip shifts to higher reduced frequency as the temperature increases.

4.3.3 Blend Plateau Moduli and High-Frequency SOR Plateau

The magnitude of the blend plateau modulus, G_N^o, is estimated from the value of the storage modulus, $G'(\omega''_{min})$, in the regime where the loss modulus reaches a minimum, above the higher-frequency loss peaks [23]. In this regime both species contribute to the blend plateau modulus. For all three blend systems the values, shown in Figure 4.7, follow an essentially linear weighting between the pure component values, as seen previously [1]. The results for the equally entangled PIP/PVE blend system of Chapter 3 are also shown for comparison. The uncertainty in the estimates are given by the error bars in the figure, and are typically 10-15% of the value.

Finally, we examine the value of the high-frequency plateau in the blend SOR. This is shown in Figure 4.8 versus weigh-fraction of PIP, at $T = 25°C$. All three blend systems follow a linear weighting of the pure component C_i's, indicating that

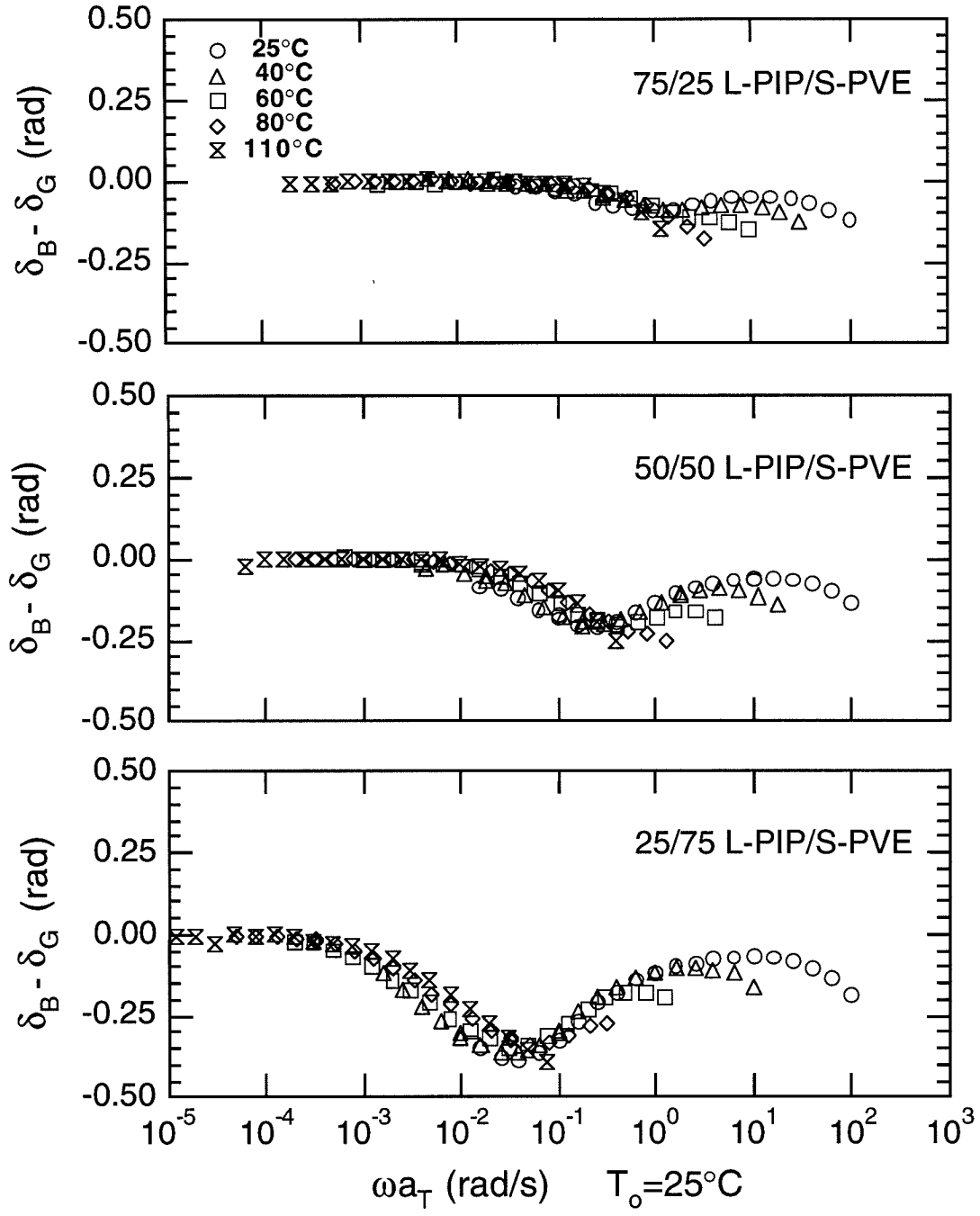

Figure 4.6: Phase difference between the dynamic birefringence and shear stress for the $L - PIP/S - PVE$ blends.

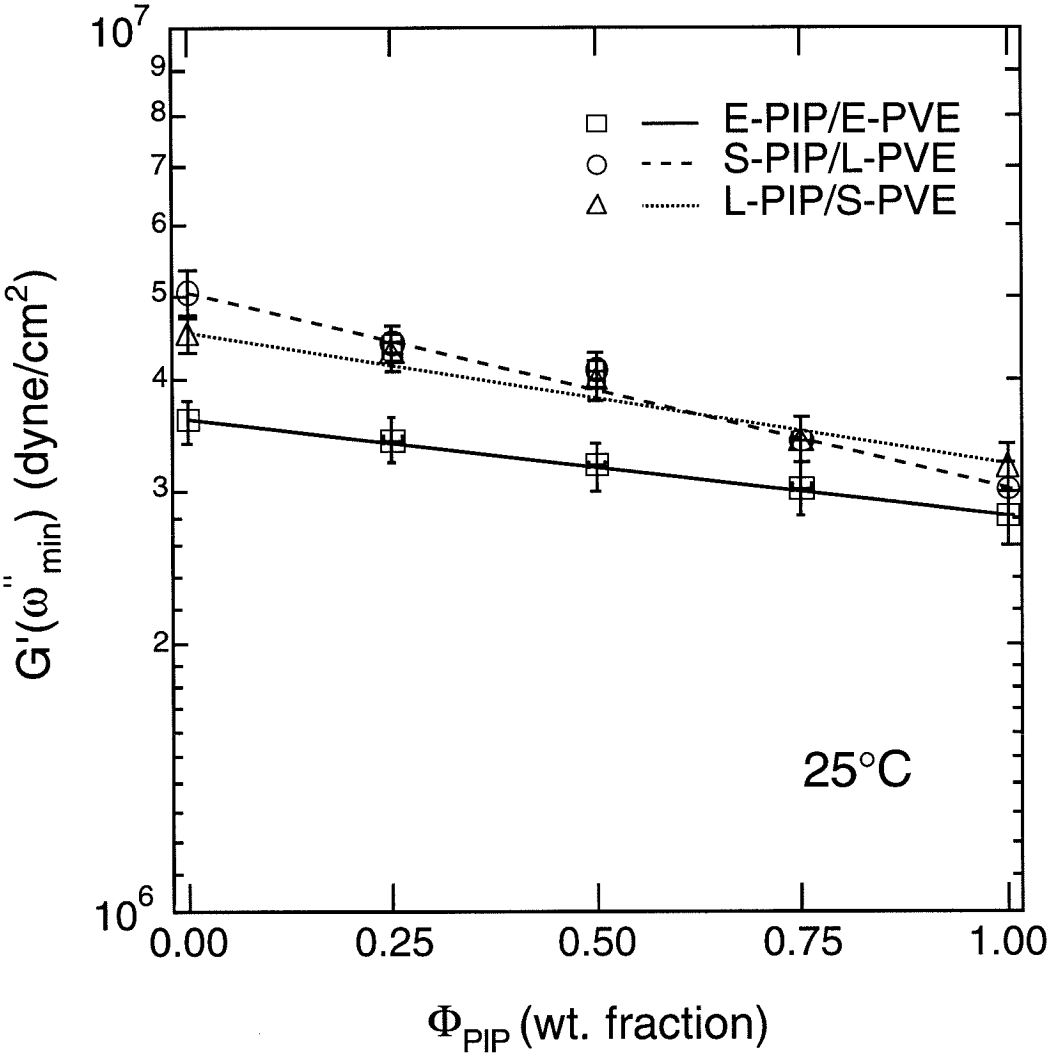

Figure 4.7: Plateau modulus for the blends and pure components versus weight percent PIP, at $T = 25°C$. The lines represents the composition-weighted average of the homopolymer values.

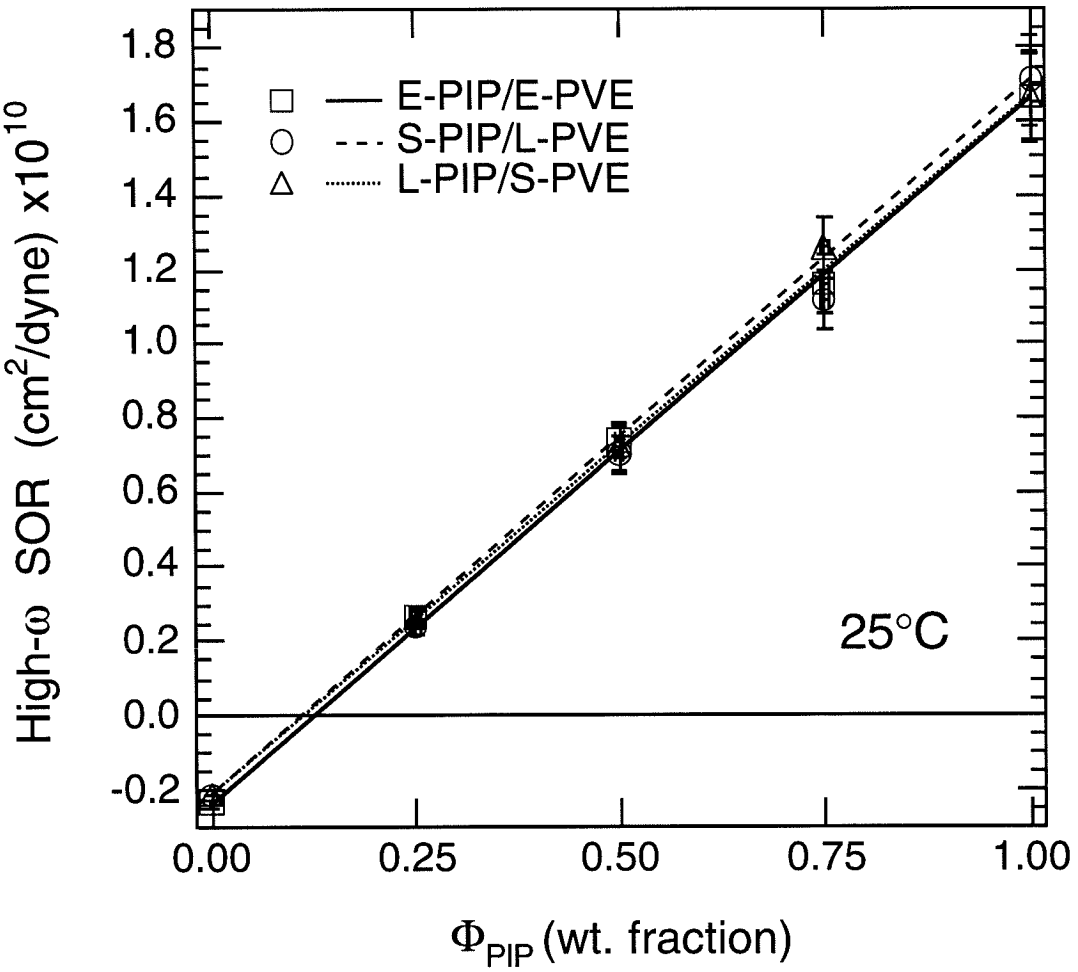

Figure 4.8: Magnitude of the high frequency plateau in SOR (high-ω SOR) for all the blends versus weight percent PIP, at $T = 25°C$. The solid line represents the composition-weighted average of the homopolymer stress-optic coefficients.

the homopolmyer stress-optic coefficients do not change significantly upon blending in the PIP/PVE system. This suggest that the stress-optic coefficients of the pure components can be applied to interpret the stress-optic behavior of the blends.

4.4 Discussion

In the previous chapter we used miscible, equally entangled blends of PIP/PVE to investigate how the component properties, namely their entanglement molecular weights and monomeric friction coefficients, are affected by blending [1]. We chose to focus on the effects of blending two chemically distinct polymers, and how the properties depend on composition and temperature, rather than on effects such as constraint release which are present even in binary blends of a single polymer species. We demonstrated that the failure of time-temperature superposition observed for the PIP/PVE system is dominated by the distinct temperature dependence of each species' dynamics in the blend [1, 16]. While blending induces only minor changes in the entanglement molecular weight of each species (less than 30% over the full range of composition), it dramatically alters the species' friction coefficients. Furthermore, the dynamics of the low-T_g component, PVE, are more sensitive to both blend composition and temperature [1].

Here, we extend our work on equally entangled, miscible PIP/PVE blends to describe the relaxation behavior of components in unequally entangled PIP/PVE blends, where polydispersity alters the shapes of the component moduli in the blend,

due to constraint release, and the effects of orientational coupling on the blend birefringence are much more obvious, as discussed below. As mentioned earlier, we chose the component molecular weights such that the species' relaxations in the blends would remain well-separated in frequency for all compositions and temperatures examined. At the lowest frequencies, below the loss peak dominated by the slower-relaxing species, the faster-relaxing species will be nearly completely relaxed; thus, its contribution to the birefringence in this regime will be almost exclusively due to orientational coupling imposed by the surrounding, slower-relaxing matrix. Extraction of the degree of coupling between the two species is thus facilitated. We investigated two sets of blends, one in which PIP is faster-relaxing and couples to an unrelaxed PVE matrix, and *vice versa*, to understand the symmetry of the coupling phenomenon as well as the effects of temperature and composition.

4.4.1 Determining the Component Moduli in the Blends

In the previous chapter on equally entangled blends, where the relaxations of the two components overlap completely, the component moduli in the blend resemble those of nearly monodisperse homopolymers. The results obtained when the effects of orientational coupling are properly taken into account, using values of the coupling coefficients from the literature [8, 9, 28] ($\epsilon = 0.35$), differed primarily in magnitude ($\sim$20%) compared to those determined using an approximate analysis which did not incorporate orientational coupling [1] ($\epsilon = 0.00$).

When the relaxations of the two components in the blend become more separated

in frequency, orientational coupling manifests itself more clearly in the stress-optic behavior. As described in Chapter 3, the primary macroscopic effect of orientational coupling on the birefringence is to increase the contribution of the faster-relaxing species in the low-frequency regime, where the faster-relaxing species is relaxed but the slower-relaxing species is still not. Thus, orientational coupling enhances the contribution of the faster-relaxing species to the low-frequency plateau in SOR. The effect on the stress-optic ratio depends on which species, PIP or PVE, is contributing an enhanced amount to the birefringence, i.e., whether its stress-optic coefficient is positive or negative.

In the blends where PVE is the slower-relaxing species and we would expect it to dominate the stress-optic response at the lowest frequencies, PIP will contribute a large positive amount to the birefringence at frequencies below its relaxation, due to orientational coupling. The magnitude of SOR in the low-frequency plateau region, then, is significantly more positive than one would expect from the contribution of PVE alone. Consequently, the coupling coefficient is fairly easily determined in these $S-PIP/L-PVE$ blends because we are measuring the contribution of the larger, positive value, proportional to C_{PIP}, to a smaller, negative quantity, proportional to C_{PVE}.

In the blends where PIP is the slower-relaxing species, orientational coupling is manifested by the effect of PVE contributing to the low-frequency values of SOR. In this case, it is more difficult to ascertain the degree of coupling because we are trying to monitor the much smaller contribution of PVE to a large, positive birefringence

dominated by PIP. Thus, small changes or uncertainties in the value of the low-frequency plateau in SOR greatly affect the amount of coupling attributed to the PVE component. This is evidenced by the larger uncertainties given in the following section for the values of the coupling coefficient determined for the $L-PIP/S-PVE$ blends.

A more realistic interpretation of the stress-optic behavior, then, must consider the effects of orientational coupling in determining the relaxation behavior of each species within the blend. As done in Chapter 3 with the equally entangled blends, we follow an approach similar to that of Zawada et al. [8, 9] to determine the underlying component moduli in the blends. Again, we use equations 3.3 and 3.7, based on simultaneously measured values for the blend dynamic moduli and birefringence coefficients and the stress-optic coefficients of the pure components. To determine the appropriate values of the orientational coupling parameter, the mechanical and optical data G^*_{blend} and B^*_{blend} are analyzed to determine the component contributions G^*_{PVE} and G^*_{PIP} for a trial value of ϵ. We vary ϵ until the dynamic moduli of the faster-relaxing component exhibit terminal regime behavior below the high frequency loss peak. Values of epsilon too large lead to unphysical, negative values of the moduli for the faster-relaxing species and decay much steeper than $G'' \sim \omega$ and $G' \sim \omega^2$, while values too small yield moduli which plateau out at low frequencies and don't acheive terminal regime behavior for the faster-relaxing component.

For the unequally-entangled PIP/PVE blends, the shape and terminal slopes of the extracted component moduli are quite sensitive to the value of epsilon used. We

found that when the relaxation times of the two species are well-separated in the blend, it is possible to estimate the values of ϵ to within $\pm$ 0.01 (Figures 4.9 and 4.10). For the $L-PIP/S-PVE$ blends, as mentioned above, it is more difficult to determine ϵ accurately, and the uncertainty is larger, at least $\pm$ 0.02 (Figure 4.10). The values of ϵ for both blend systems, shown in Figure 4.11, lie between $\approx$ 0.20 - 0.40 over the range of compositions and temperatures probed. There appears to be no systematic dependence on temperature or composition in either system [28, 8, 9]. The absence of any temperature dependence is in accord with proposed entropic origins for orientational coupling [28].

The sensitivity with which we can determine ϵ does not include the effect of uncertainty in the pure component C_i's. For the $S-PIP/L-PVE$ blends, in which PIP coupled to a slower-relaxing PVE matrix $\epsilon = 0.33 \pm 0.08$, 0.36 ± 0.07 and 0.36 ± 0.05 for $\phi_{PIP} = 0.75$, 0.5 and 0.25, respectively, given a $\pm$ 10% uncertainty in the pure component stress-optic coefficients. For the $L-PIP/S-PVE$ blends, in which PVE coupled to a slower-relaxing PIP matrix, $\epsilon = 0.23 \pm 0.14$, 0.28 ± 0.10 and 0.30 ± 0.10 for $\phi_{PIP} = 0.75$, 0.5 and 0.25, respectively, again given a $\pm$ 10% uncertainty in the pure component stress-optic coefficients (Figure 4.11). These values fall within the range previously established for various systems [28, 8, 9], and within the uncertainty in the measurements, suggesting that a single average value of ϵ is capable of describing the coupling in the PIP/PVE system.

Once the component moduli are determined at each temperature they are shifted horizontally with respect to 25°C so that the curves overlap in the terminal regime,

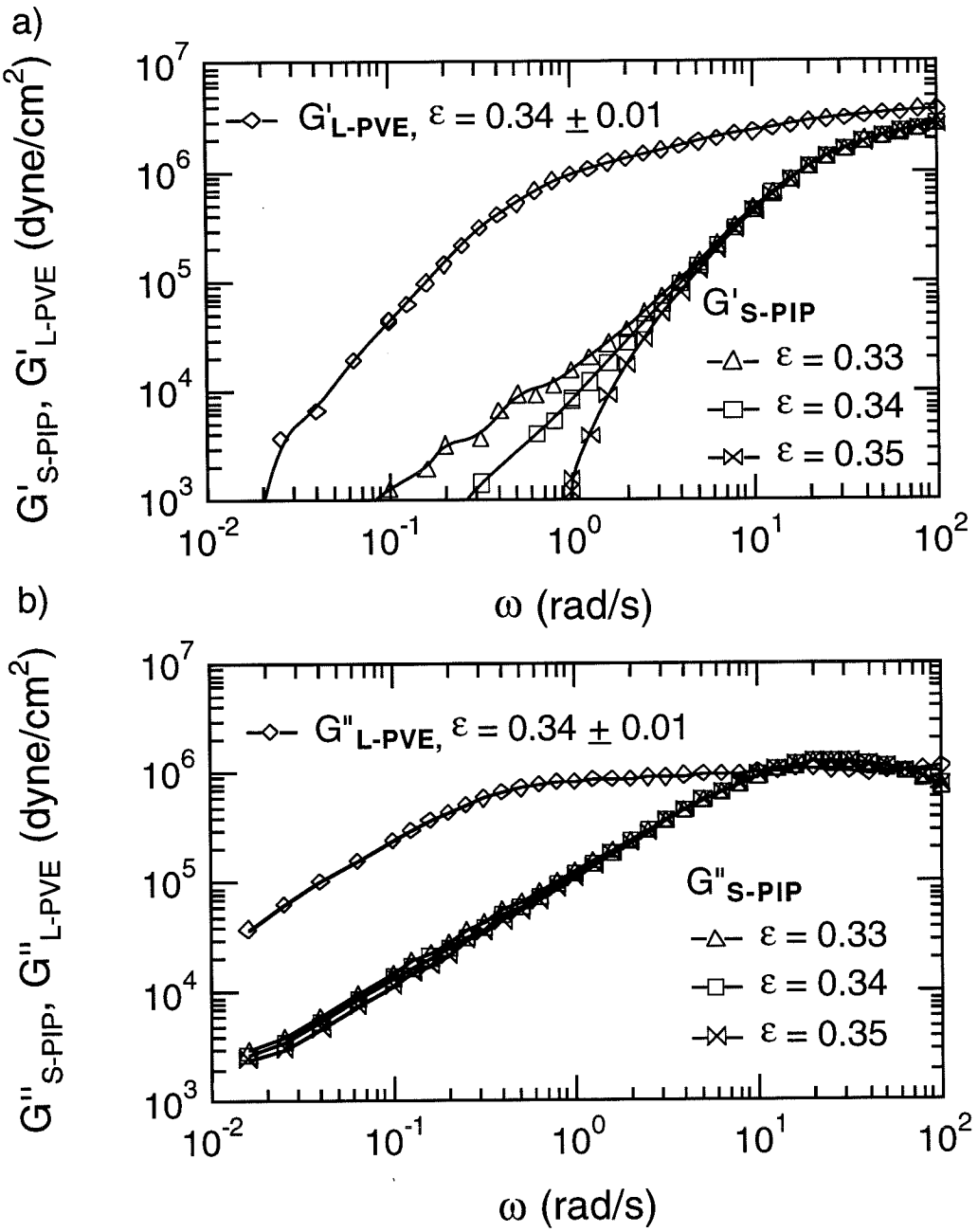

Figure 4.9: Figure detailing the determination of ϵ for a 50/50 blend of $S-PIP/L-PVE$ at 60°C, showing how it can be determined within $\pm$ 0.01 by observing the terminal behavior of the faster-relaxing species in the blend. See the text for discussion.

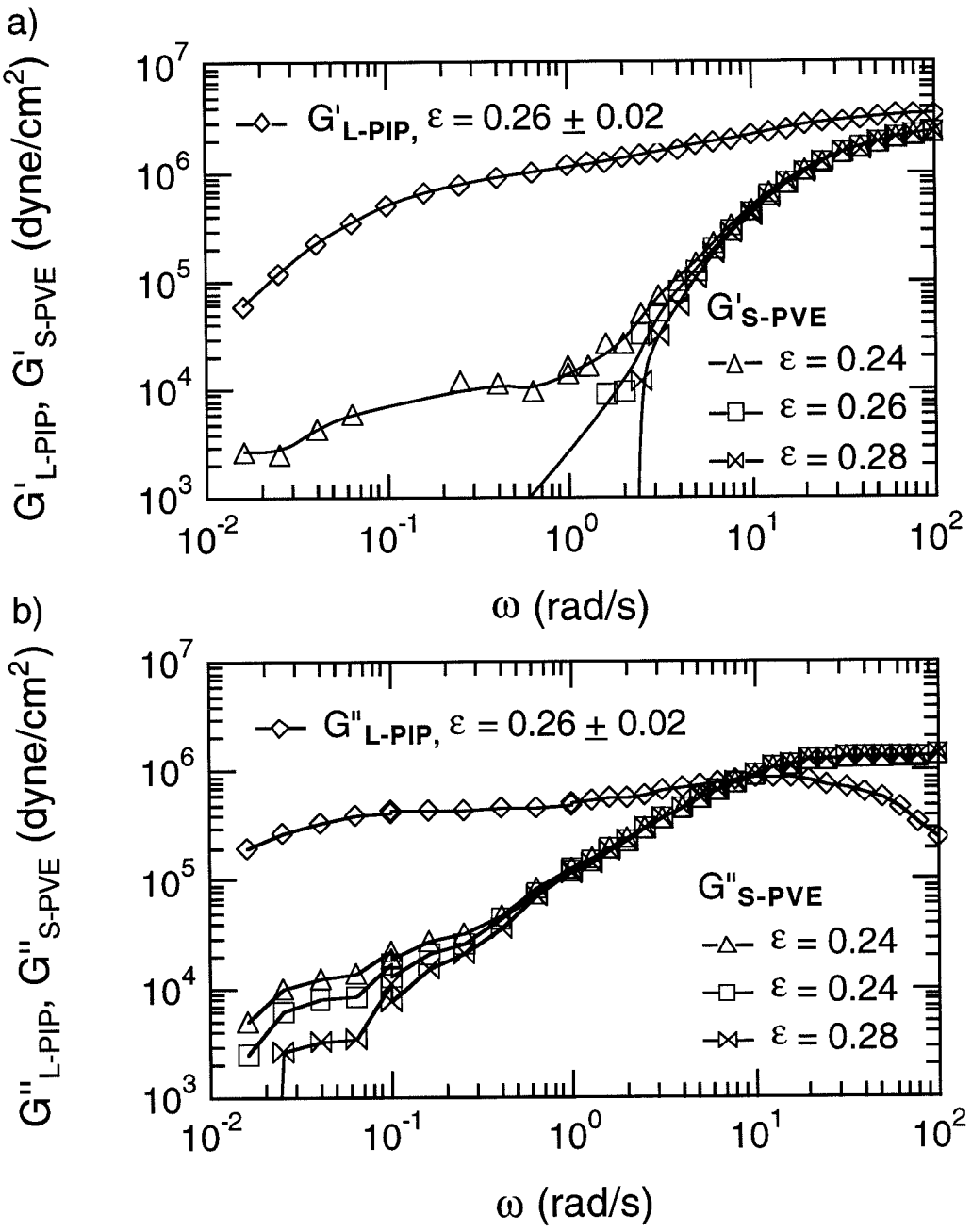

Figure 4.10: Figure detailing the determination of ϵ for a 50/50 blend of $L-PIP/S-PVE$ at 60°C, showing how it can be determined within $\pm$ 0.02 by observing the terminal behavior of the faster-relaxing species in the blend. Notice the larger uncertainty in these blends. See the text for discussion.

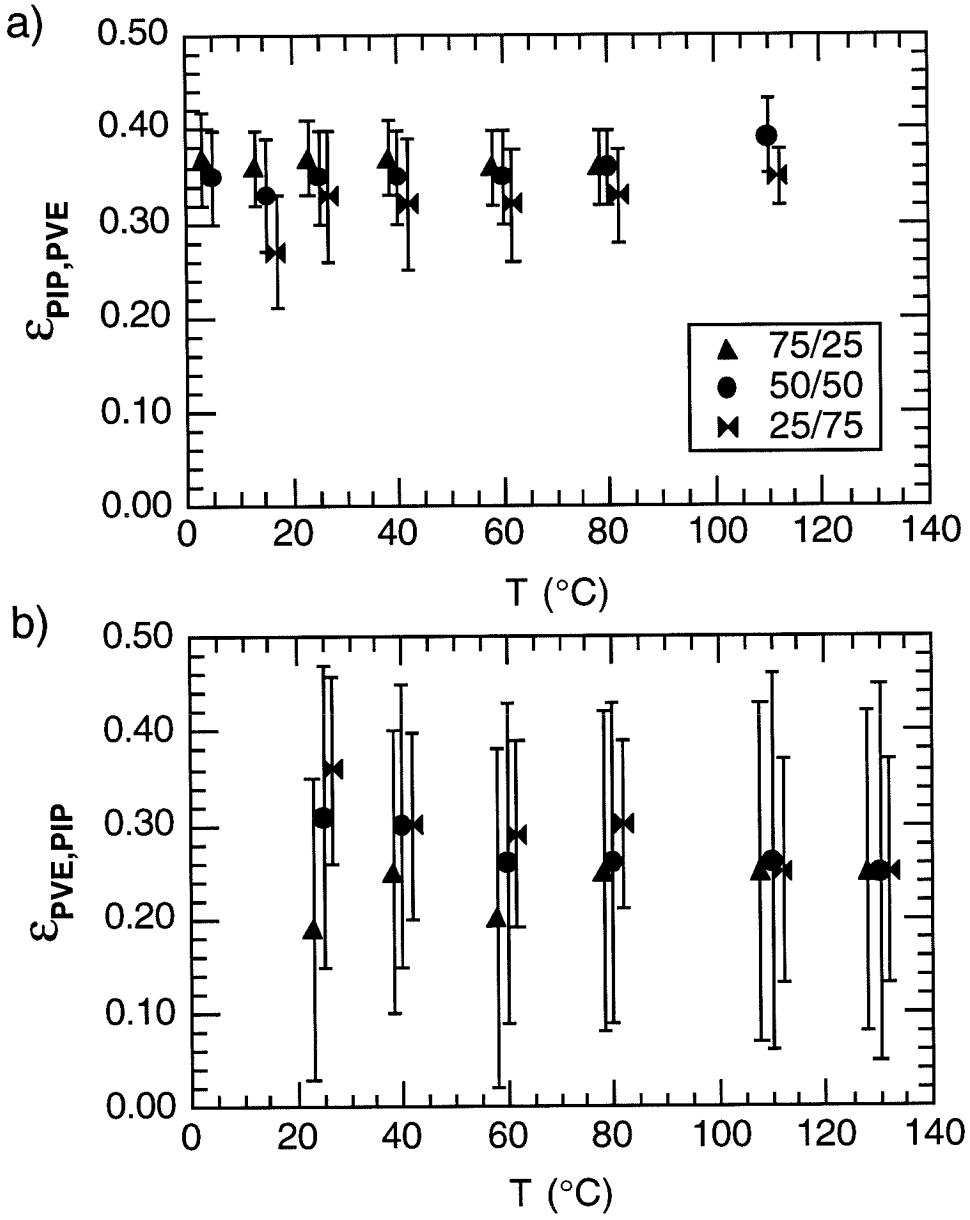

Figure 4.11: Values of the coupling coefficient determined for the **a)** $S-PIP/L-PVE$ and **b)** $L-PIP/S-PVE$ blends. Values for $\phi_{PIP}=0.75$ and 0.25 are offset horizontally from those for $\phi_{PIP}=0.5$ for clarity; the filled circles ($\phi_{PIP}=0.5$) are unshifted. Error bars indicate the uncertainty in the values, including those when a $\pm 10\%$ uncertainty in the component stress-optic coefficients is assumed.

to obtain a composite "master" curve for each component for a given blend composition. The values of the horizontal shift factors, $a_{T,i}$, for each species are given in Tables 4.5- 4.6. Again, uncertainty in the values of $C_i(T)$ and ϵ precludes a meaningful determination of vertical shift. However, horizontal shifting alone appears sufficient to superimpose the data at different temperatures in the terminal regime of each component. This is in contrast to the work of Zawada et al. [8, 9], in which large vertical shifts in the direction opposite of those established for the pure components [18, 19] were required in order to achieve superposition.

From Chapter 3, the moduli for both components in the equally entangled blends resemble those of nearly monodisperse homopolymers. As the differences between the components' relaxation times in the blend increase, the dynamic moduli of each species in the blend become more complicated, and the effects of polydispersity become evident. While the dynamic moduli of the faster-relaxing species will still resemble those of a monodisperse homopolymer, those of the slower-relaxing species possess features due to the relaxation of the faster-relaxing species. Thus, in the unequally entangled blends, time-temperature superposition holds well for the faster-relaxing species and again the dynamic moduli resemble those of a monodisperse homopolymer, as shown in Figure 4.12a and 4.13b. The dynamic moduli of the slower-relaxing species obey time-temperature superposition in the lower frequency range, below the cross-over frequency. At higher frequencies, however, above the low-frequency terminal relaxation peak in G'', the moduli exhibit additional features, as shown in Figure 4.12b and 4.13a. These features do not superimpose for all temper-

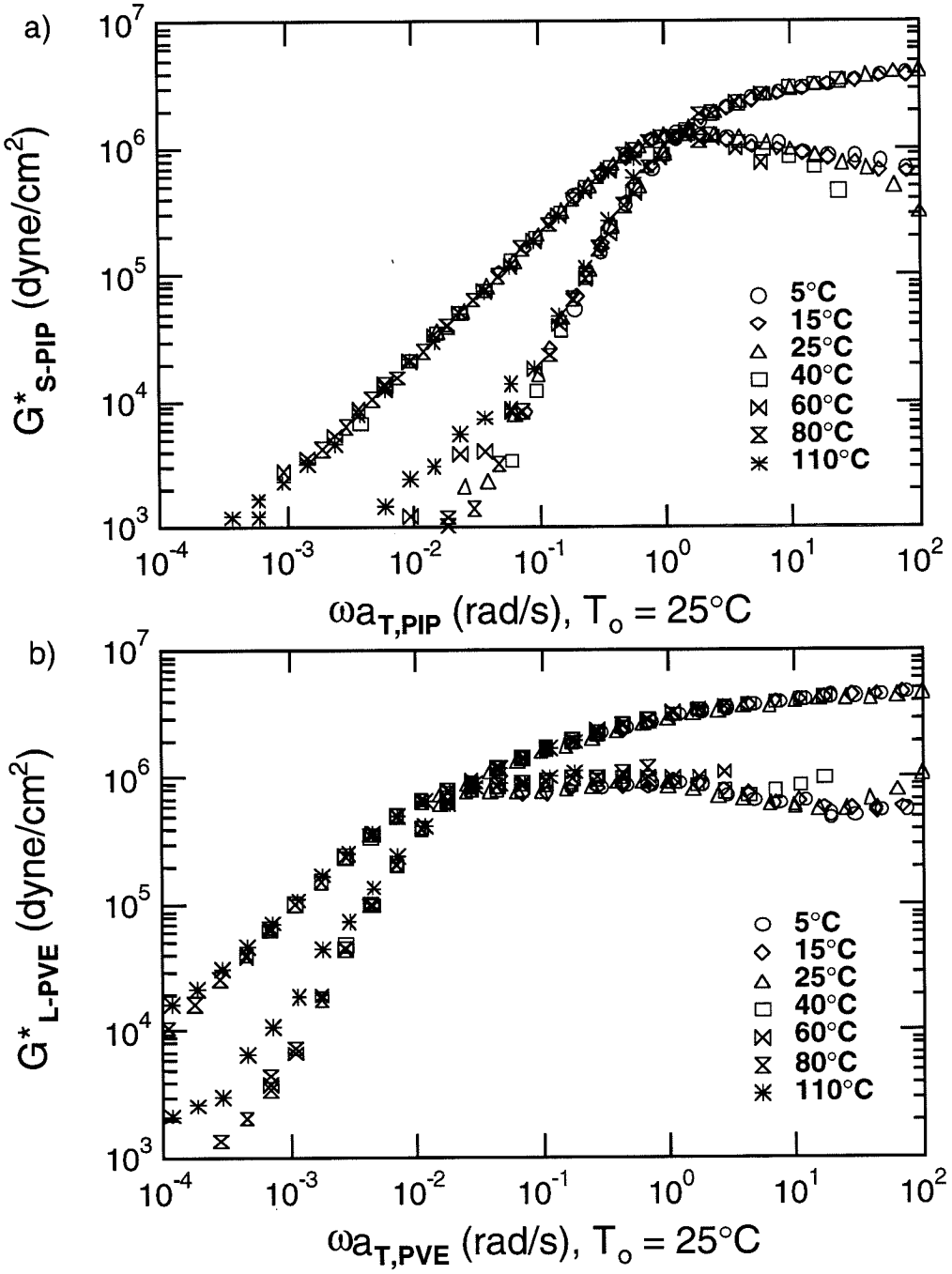

Figure 4.12: The resulting component moduli for a 50/50 blend of $S-PIP/L-PVE$. While the dynamic moduli of the PIP component resemble those of a monodisperse homopolymer, those of PVE exhibit features at higher frequencies which do not superimpose. These are related to the relaxation of the PIP component.

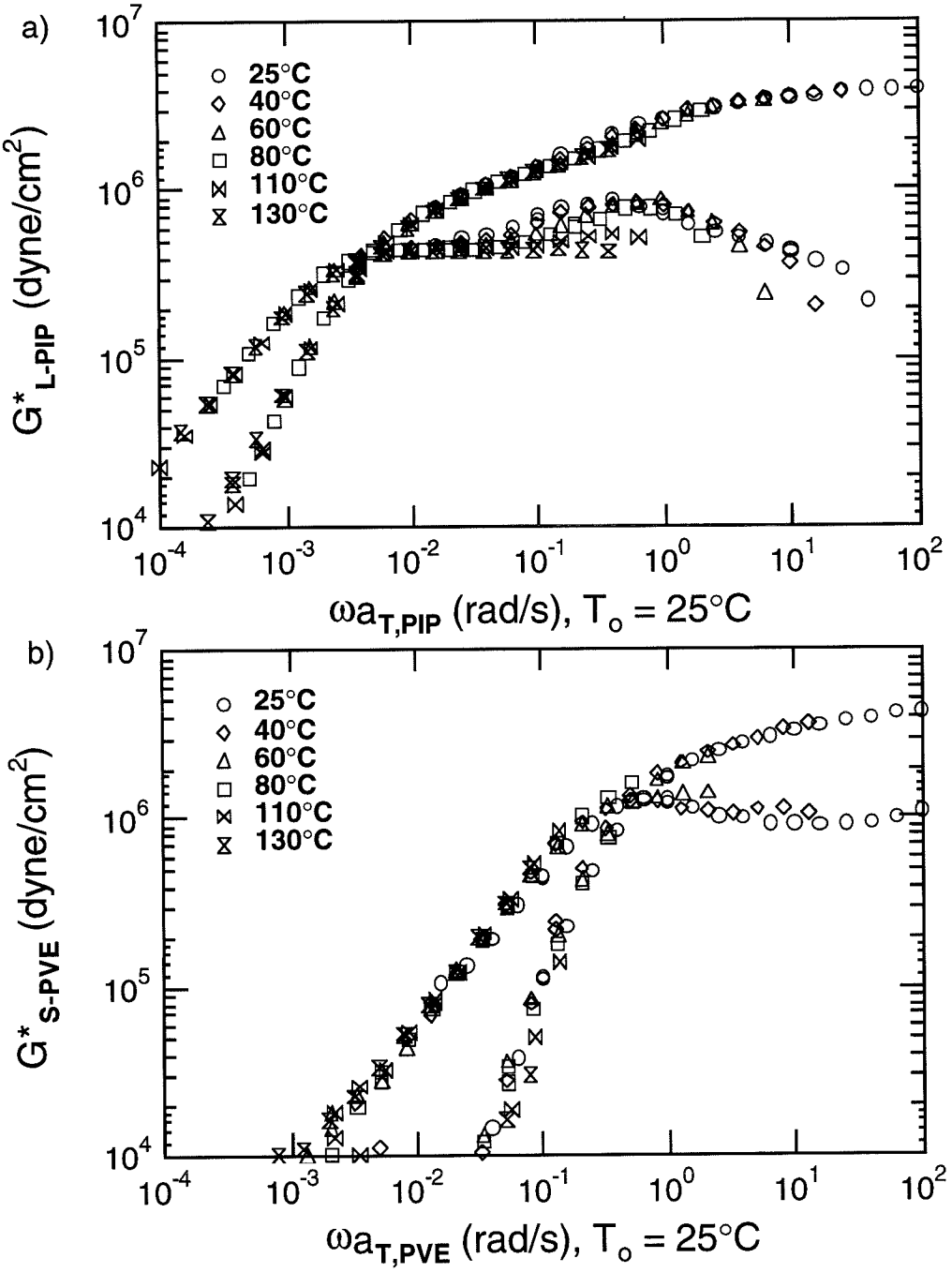

Figure 4.13: The resulting component moduli for a 50/50 blend of $L-PIP/S-PVE$. While the dynamic moduli of the PVE component resemble those of a monodisperse homopolymer, those of PIP exhibit features at higher frequencies which do not superimpose. These are related to the relaxation of the PVE component.

Table 4.5: Shift Factors, $a_{T,i}$, of Each Species in S-PIP/L-PVE Blends

	Blends (PIP/PVE w/w %)					
	75/25		50/50		25/75	
T(°C)	PIP	PVE	PIP	PVE	PIP	PVE
-10	88	105	-	-	-	-
5	10	11	12.5	19	-	-
15	3.2	3.6	3.15	4.4	4.0	8.0
25	1	1	1	1	1	1
40	0.31	0.275	0.24	0.175	0.2	0.10
60	0.09	0.06	0.055	0.0295	0.038	0.011
80	0.033	0.0185	0.019	0.0075	0.0105	0.00225
110	-	-	0.0059	0.0020	0.0026	0.00042

atures, and can be attributed to the effects of constraint release due to relaxation of the faster-relaxing component [13, 14, 15].

The lack of superposition shows that the dynamics of the faster-relaxing component do not share the same temperature dependence as those of the slower species. Similarly, the horizontal shift factors for the dynamic moduli of each component at different compositions, listed in Tables 4.5 and 4.6, are quite different as well, confirming that the dynamics of PIP and PVE in a given blend obey different temperature dependencies.

Table 4.6: Shift Factors, $a_{T,i}$, of Each Species in L-PIP/S-PVE Blends

	Blends (PIP/PVE w/w %)					
	75/25		50/50		25/75	
T(°C)	PIP	PVE	PIP	PVE	PIP	PVE
25	1	1	1	1	1	1
40	0.32	0.25	0.25	0.13	0.12	0.108
60	0.087	0.036	0.062	0.021	0.022	0.0114
80	0.033	0.011	0.019	0.0053	0.006	0.0022
110	0.012	0.0033	0.0063	0.0014	0.0019	0.0004
130	0.008	0.0019	0.0039	0.0008	0.0012	0.00018

Finally, it was previously noted that uncertainty in the values of ϵ and the pure-component stress-optic coefficients, C_i's, has a small effect on the component horizontal shift factors, and hence cross-over frequencies (relaxation times), but has a more significant effect on the detailed shape and magnitude of the component moduli (entanglement molecular weights) [1]. We now look at the component moduli in more detail to evaluate the entanglement molecular weights, $M_{e,i}$, and monomeric friction coefficients, $\zeta_{o,i}$, of each species in the unequally entangled blends. Sources of uncertainty in the various quantities will be explored, and comparisons between the blends will be made.

4.4.2 Entanglement Molecular Weight of Each Species

The entanglement molecular weights of each component, $M_{e,i}$, can be determined from their plateau moduli and the density of PIP/PVE blends given in the literature [16], using

$$M_{e,i}(T,\phi) = \frac{\rho(T,\phi)RT}{G^o_{N,i}(T,\phi)} \tag{4.3}$$

where ρ is the melt density [16], R is the universal gas constant, T is the absolute temperature and $G^o_{N,i}$ is the component plateau modulus. As in Chapter 3, to examine changes in the component $M_{e,i}$ with composition it is sufficient to compare relative values. We normalize $M_{e,i}(\phi)$ by the value for pure PIP, $M^o_{e,PIP}$, yielding

$$\frac{M_{e,i}(\phi)}{M^o_{e,PIP}} = \frac{\rho(\phi)}{\rho_{PIP}} \frac{G^o_{N,PIP}}{G^o_{N,i}(\phi)}. \tag{4.4}$$

In this expression, only $G^o_{N,i}$ is sensitive to the choice of stress-optic coefficients and coupling coefficients used to analyze the blend data.

For the faster-relaxing component, where the dynamic moduli resemble those of a monodisperse homopolymer, it is straightforward to determine the value of the plateau modulus. The plateau modulus can be estimated from the value of the storage modulus at the frequency of the minimum in the loss moduli at higher frequencies, $G^o_N = G'(\omega''_{min})$. When this is not possible, previous work has shown that when there is a single loss peak, the maximum in the loss modulus can be used as a measure of the plateau modulus, where $G^o_N = q\ G''(\omega''_{max})$ and the value of q is determined to be 3.56 for polymers with narrow molecular weight distribution [29]. For slightly broader distributions the value of q is somewhat larger, ≈ 3.9 [8, 9]. For our systems the polydispersities of the pure components lie within the range of these two experiments, bounding the value of q appropriate for us. For the faster-relaxing components in the unequally entangled blends, where the component moduli do not exhibit significant broadening from those of the pure components, such an estimate of the plateau modulus should also still be valid. In our previous work on equally entangled blends we also used the value of the moduli at the cross-over frequency, $G(\omega_x)$, to give a third estimate of the plateau modulus, under the same restrictions on the broadening of the component moduli [1]. For the slower-relaxing species, we use the first method to estimate the plateau modulus, in the high-frequency regime above the features due to relaxation of the faster-relaxing species, where both species contribute to the dynamic moduli of the slower-relaxing species.

Shown in Figure 4.14 are the entanglement molecular weights of each species as a function of composition at $T = 25°C$, for the two sets of unequally entangled blends, normalized to the value for pure PIP. As mentioned earlier, the value of the plateau modulus is sensitive to the choice of component stress-optic coefficients and value of epsilon used to determine the component moduli. The error bars in the figure are determined assuming a $\pm$ 10% uncertainty in the values of the C_i's, the range of epsilon thus determined and our ability to estimate the component plateau moduli. The lines in the figures show a linear variation between the pure component values. It is seen that we can only roughly estimate the values of the species' $M_{e,i}$. While we cannot make any detailed statements about the composition dependence of each species' $M_{e,i}$ in the different blends, we can state that the values do not vary significantly (less than $\approx 40\%$) over the range of composition. Since the entanglement molecular weights of the pure components are so similar to begin with, the effect of blending on their values is not large. As we will see in the next section, blending has a much greater effect on the relaxation dynamics of each component.

4.4.3 Friction Coefficient of Each Species

The analysis used to determine the component moduli, equations 3.3 and 3.7, does not depend on any particular model for melt relaxation. However, to examine the effect of blending on the monomeric friction coefficient of each species, we examine the component relaxations within the context of the reptation model [26], as in Chapter 3. When the component relaxation times in the blend are not reduced due to constraint

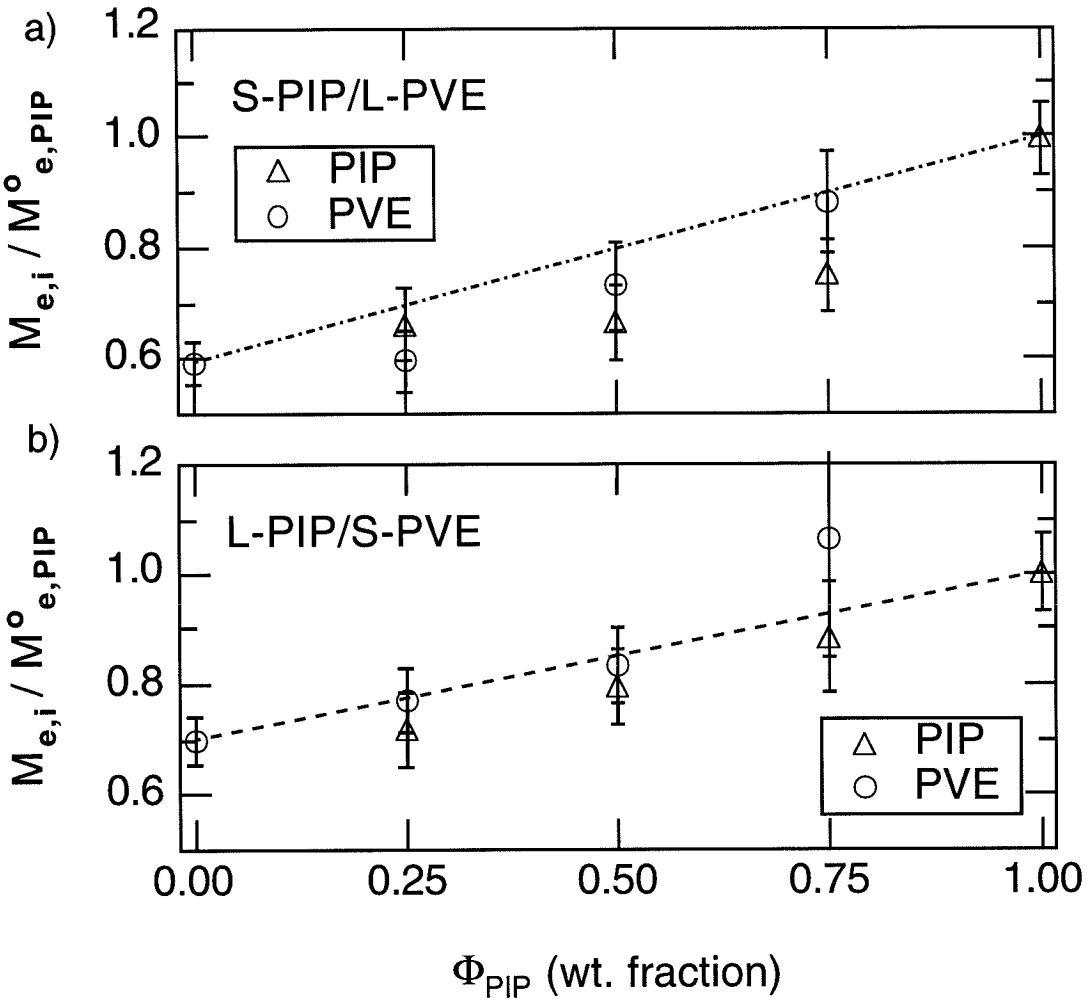

Figure 4.14: Component entanglement molecular weights in the blends **a)** $S - PIP/L - PVE$ and **b)** $L - PIP/S - PVE$ versus weight percent PIP at $T = 25°C$.

release (see comments below), the terminal relaxation time of the chain, τ_d, is given by

$$\tau_d = \zeta_o \left(\frac{M}{m_o}\right) \left(\frac{M}{M_e}\right)^2 \frac{a^2}{\pi^2 k_B T} \tag{4.5}$$

where ζ_o is the monomeric friction coefficient, $k_B T$ is the thermal energy, M_e is the entanglement molecular weight, M is the molecular weight of the chain and m_o is the monomer molecular weight. The tube diameter, a, characterizes the extent of lateral excursions of the chain among its neighbors, and is given by

$$a^2 = \frac{6 R_g^2 M_e}{M} \tag{4.6}$$

where R_g is the radius of gyration of the chain. Since the $R_{g,i}$ are unaffected by blending in our system, for which $\chi \approx 0$, we determine the value for $R_{g,i}$ using

$$R_{g,i}^2 = \left(\frac{M}{m_o}\right) \left(\frac{b_i^2}{6}\right) \tag{4.7}$$

and literature values of the species' statistical segment lengths, b_i [6].

We can evaluate the friction coefficient of each species using eqns. 4.5- 4.7. The molecular weights of the homopolymers, determined by gel-permeation chromatography, are given in Table 4.1, and the monomer molecular weights are 68 and 54 g/mol for PIP and PVE, respectively. Values for the component $M_{e,i}$ were determined in the previous section. We use the values at $T = 25°C$ since we do not have sufficient information to determine their dependence on temperature. Similarly, we neglect the temperature dependence of $R_{g,i}$ since it has been shown to vary negligibly over the experimental range [6]. To estimate the terminal relaxation time of each component,

$\tau_{d,i}(\phi, T)$, we use the inverse of its cross-over frequency, $2/\omega_{x,i}$, where $G_i'(\omega_{x,i}) = G_i''(\omega_{x,i})$ for each component i [1]. In the unequally entangled blends, we note that the relaxation times of the slower-relaxing component are not reduced in the blend due to the effects of constraint release, as deduced by comparing the rate of relaxation of the chains by reptation to the rate at which their surrounding diffuse by Rouse relaxation mechanisms [13, 14, 15, 9]. Thus the cross-over frequency of the component $G_i^*(\omega)$ should be a measure of each component's relaxation time in the blend.

The monomeric friction coefficients of each species for the range of compositions and temperatures are shown in Figures 4.15 and 4.16 on linear-logarithmic plots versus inverse temperature for the unequally entangled blends. The different symbols correspond to distinct compositions. The symbols represent the average value determined for each friction coefficient. Error bars showing the range of values obtained, given the uncertainties in the $C_i(T)$'s and ϵ, and the corresponding values determined for $M_{e,i}(\phi)$ and $\tau_{d,i}(\phi, T)$, due to uncertainties in the $a_{T,i}$, are smaller than the size of the symbols. Only for the PVE component in the $\phi_{PIP} = 0.75$ $L - PIP/S - PVE$ blend are the error bars larger than the symbols, due to the difficulty in determining the moduli of the PVE component. The values of $\zeta_{o,i}(\phi, T)$ can be compared to those for the equally entangled blends, shown in Figure 3.12 of Chapter 3.

The curves in the figures correspond to WLF fits to the data based on values from Roovers and Toporowski [16]. As noted in Chapter 3, since the shift factors, $a_{T,i}$, represent the scaling of the relaxation dynamics with temperature, and the monomeric friction coefficient scales as $\tau_{d,i} \cdot T$, we compare the WLF dependencies of the $\zeta_{o,i}$ to

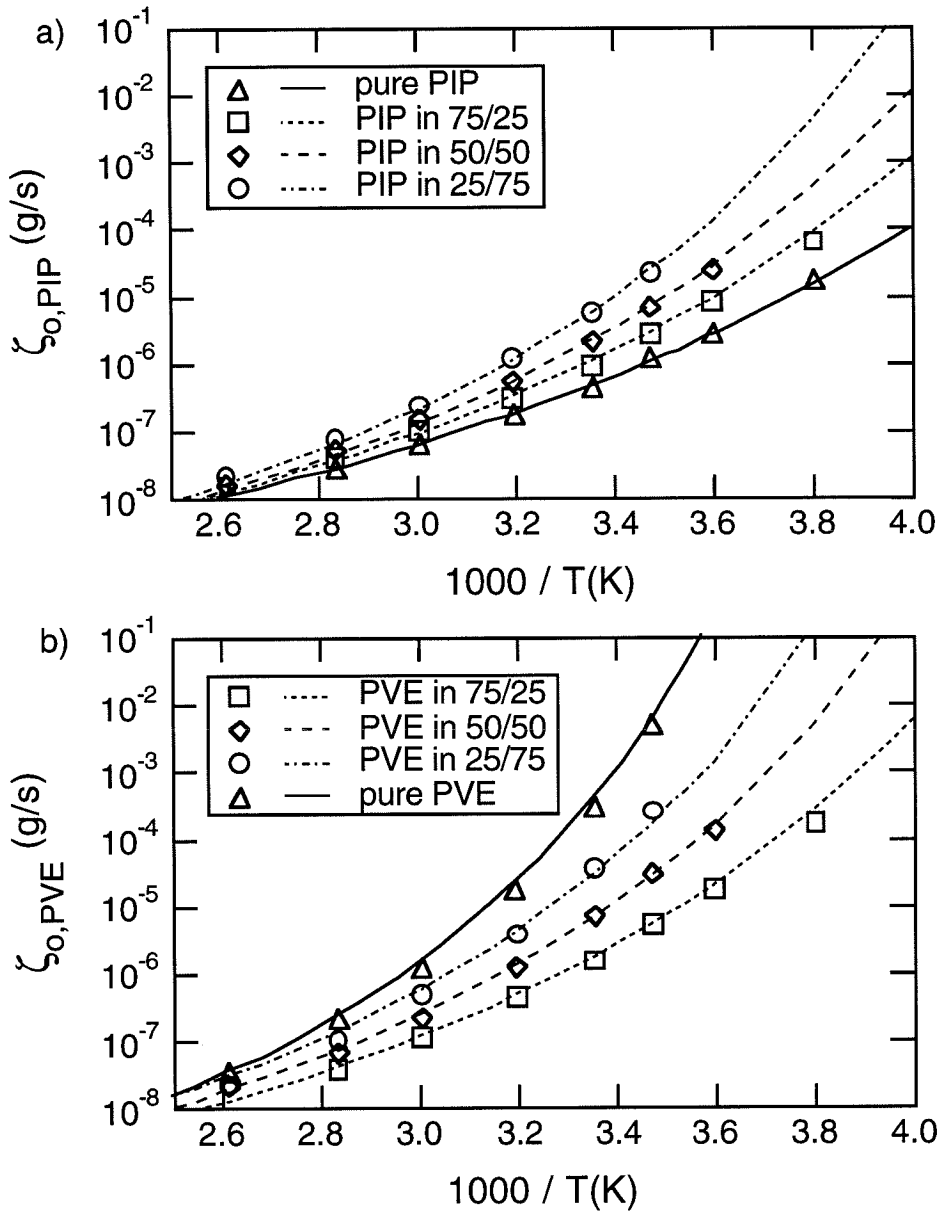

Figure 4.15: Component monomeric friction coefficients in the $S - PIP/L - PVE$ blends. a) PIP, b) PVE versus inverse absolute temperature, as a function of composition. Pure component friction coefficients are shown for reference. Curves correspond to WLF fits where $C^g_{1,i}$, $C^g_{2,i}$ and $T_{g,i}$ are taken from Roovers et al. [16]. See the text for discussion.

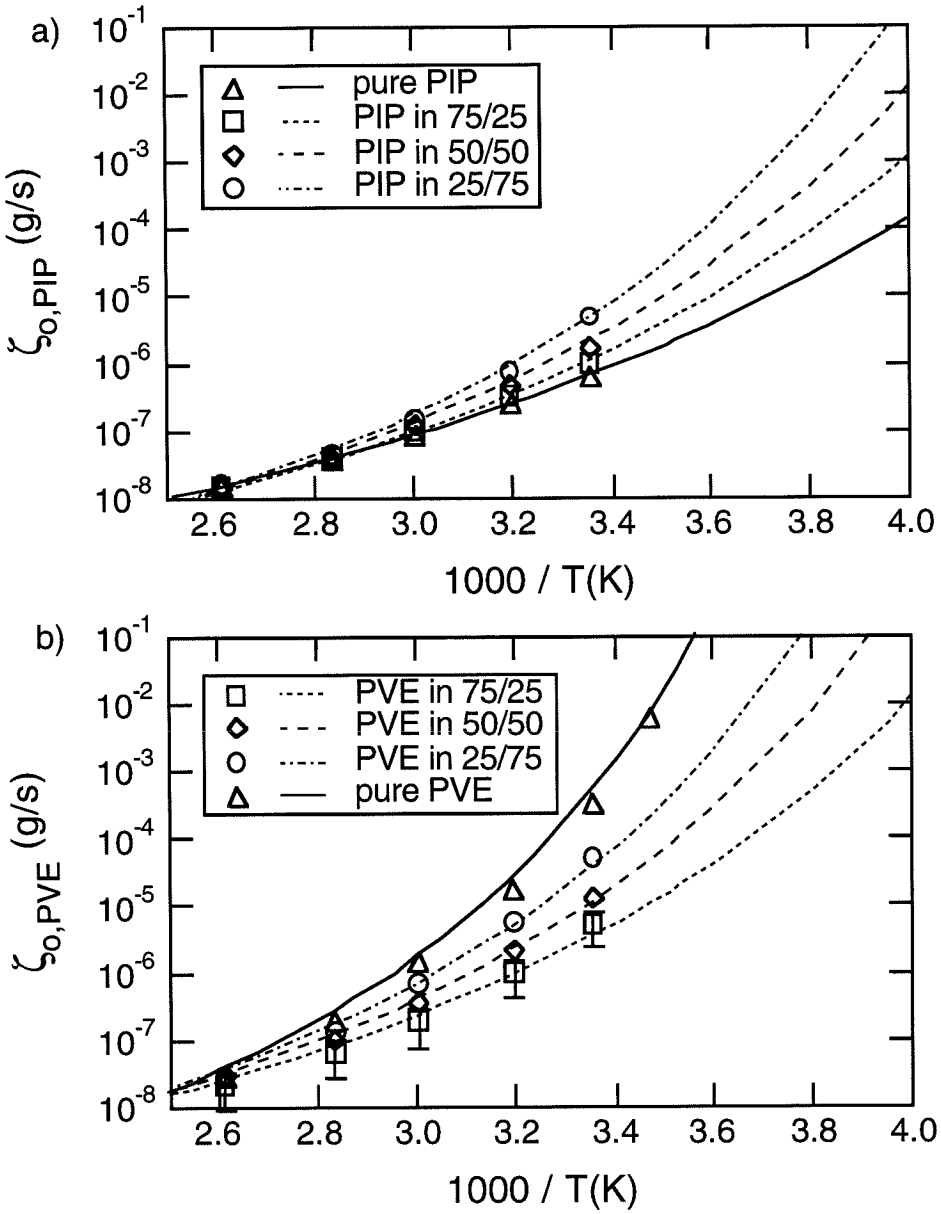

Figure 4.16: Component monomeric friction coefficients in the $L - PIP/S - PVE$ blends. **a)** PIP, **b)** PVE versus inverse absolute temperature, as a function of composition. Pure component friction coefficients are shown for reference. Curves correspond to WLF fits where $C^g_{1,i}$, $C^g_{2,i}$ and $T_{g,i}$ are taken from Roovers et al. [16]. See the text for discussion.

Table 4.7: Component WLF Paramters from Roovers and Toporowski [16]

	ϕ_{PIP}	$C^g_{1,i}$	$C^g_{2,i}$(K)	$T_{g,i}$(°C)
PIP	1	12.0	52.9	-61.0
	0.75	11.8	55	-47.0
	0.5	11.8	55	-37.5
	0.25	11.8	55	-31.0
PVE	0.75	11.8	55	-40.0
	0.5	11.8	55	-27.5
	0.25	11.8	55	-17.5
	0.0	11.4	57.5	2.0

those of the component terminal relaxation times by plotting values of $a_{T,i} \cdot T$ at each temperature. We apply only a vertical shift to the WLF curves to yield the best fit to the monomeric friction coefficient data [1]. The values of C^g_1, C^g_2 and $T_{g,i}$ used for both components, in the pure state and in the the blends, are the same as in Chapter 3 and are given in Table 4.7. Roovers and Toporowski used values of $C^g_1 = 11.8$ and $C^g_2 = 55K$, the average for the pure components, for both components in all the blends. Again, the $T_{g,i}(\phi)$'s for the components in the blends are taken from the average of the values given in Table VI, columns WLF^b, of their paper.

For both sets of blends, and both the PIP and PVE components, there is good

agreement between the WLF dependence inferred by Roovers and Toporowski and the present results for $\zeta_{o,i}$. As observed in Chapter 3, the main trends to notice are that the dynamics of the PVE component in all three blend systems depend more on composition and temperature than do those of PIP, in agreement with what we saw previously [1]. The value of $\zeta_{o,PVE}$ is dramatically reduced by the addition of PIP to the blend, particularly at the lowest experimental temperatures. $\zeta_{o,PIP}$, on the other hand, is much less sensitive to blend composition and temperature. The values of $\zeta_{o,PIP}$ and $\zeta_{o,PVE}$ depend differently on temperature, for a given blend composition, consistent with the failure of time-temperature superposition previously observed in PIP/PVE blends. The temperature dependencies and absolute magnitudes of the component monomeric friction coefficients depend only on the temperature and bulk composition; to a first approximation, the values are independent of the relative component molecular weights of the blend system (see also Figure 3.12).

4.5 Conclusions

Simultaneous analysis of the shear stress and birefringence was used to extract the relaxation of each component in miscible PIP/PVE blends, for two combinations of relative component molecular weights. The analysis of the stress-optic data incorporated the effects of orientational coupling, from which we were able to estimate the average coupling coefficient, ϵ, for the PIP/PVE system. When the species' relaxations in the blend remain well-separated over the range of temperature and compo-

sition probed, the value of ϵ can be determined leading to $\epsilon_{PIP,PVE} \approx 0.35 \pm 0.04$ and $\epsilon_{PVE,PIP} \approx 0.27 \pm 0.08$. To within experimental uncertainty it appears appropriate to use a single average value of ϵ. No perceptible dependence of ϵ on temperature or composition was observed. The values also lie within the range established for other systems [8, 9, 28]

Once the values of ϵ were determined, the component moduli in the blends were extracted as functions of temperature and blend composition, from which we calculate the component entanglement molecular weights and monomeric friction coefficients. The main trends observed in $M_{e,i}(\phi)$ and $\zeta_{o,i}(\phi, T)$ are the same as determined previously [1]. For all three blend systems, blending does not greatly affect the values of $M_{e,i}$ for either component, which change no more than $\approx 40\%$ from the pure component values over the full range of composition. It is the species' monomeric friction coefficients which are the most sensitive to blending. Again, in all the blends studied the dynamics of the high-T_g component, PVE, depend more strongly on temperature and composition. Failure of time-temperature superposition is due to the distinct temperature dependencies of $\zeta_{o,PIP}(\phi, T)$ and $\zeta_{o,PIP}(\phi, T)$, though it is both the differences between the species' friction coefficient and the relative weights of the components which determines the degree to which complex thermorheological behavior is observed.

Bibliography

[1] Arendt, B. H.; Kannan, R. M.; Zewail, M.; Kornfield, J. A.; Smith, S. *Rheologica Acta*, **1994**, *33*, 322; Arendt, B. H. *et al. Proceedings of the ACS, PMSE, Washington, D.C.*, **1994**,*71*, 471.

[2] Hasagawa, H.; Sakurai, S.; Takenaka, M.; Hashimoto, T.; Han, C. C. *Macromolecules*, **1991**, *24*, 1813.

[3] Sakurai, S.; Jinnai, H.; Hasegawa, H.; Hashimoto, T.; Han, C. C. *Macromolecules*, **1991**, *24*, 4839.

[4] Roland, C. M. *Macromolecules* **1987**, *20*, 2557.

[5] Roland, C. M. *Journal of Polymer Science, Polymer Physics Edition* **1988**, *26*, 839.

[6] Tomlin, D.W.; Roland, C. M. *Macromolecules* **1992**, *25*, 2994.

[7] Miller, J. B.; McGrath, K. J.; Roland, C. M.; Trask, C. A.; Garroway, A. N. *Macromolecules* **1990**, *23*, 4543.

[8] Zawada, J. A.; Fuller, G. G.; Colby, R. H.; Fetters, L. J.; Roovers, J.; *Macromolecules* **1994**, *27*, 6851.

[9] Zawada, J. A.; Fuller, G. G.; Colby, R. H.; Fetters, L. J.; Roovers, J.; *Macromolecules* **1994**, *27*, 6861.

[10] Trask, C. A.; Roland, C. M. *Macromolecules* **1989**, *22*, 256.

[11] Chung, G. C.; Kornfield, J. A.; Smith, S. D. *Marcromolecules* **1994**, *27*, 964.

[12] Chung, G. C.; Kornfield, J. A.; Smith, S. D. *Marcromolecules* **1994**, *27*, 5729.

[13] Doi, M.; Graessley, W. W.; Helfand, E.; Pearson, D. S. *Macromolecules* **1987**, *20*, 1900.

[14] Rubinstein, M.; Helfand, E.; Pearson, D. S. *Macromolecules* **1987**, *20*, 822.

[15] Struglinski, M. J.; Graessley, W. W. *Macromolecules* **1985**,*18*, 2630.

[16] Roovers, J.; Toporowski, P. M. *Macromolecules* **1992**, *25*, 3454.

[17] Alegria, A.; Colmenero, J.; Ngai, K. L.; Roland, C. M. *Macromolecules*, **1994**, *27*, 4486.

[18] Carella, J. M.; Graessley, W. W.; Fetters, L. J. *Macromolecules* **1984**, *17*, 2775.

[19] Gotro, J. T.; Graessley, W. W. *Macromolecules* **1984**, *17*, 2767.

[20] Kannan, R. M.; Kornfield, J. A. *Journal of Rheology* **1994**, *38*, 1127.

[21] Kannan, R. M.; Kornfield, J. A. *Macromolecules*, **1994**, *27*, 1177.

[22] Janeschitz-Kriegl, H. *Polymer Melt Rheology and Flow Birefringence*; Springer-Verlag: Berlin, 1983.

[23] Ferry, J. D. *Viscoelastic Properties of Polymers*; Wiley: New York, 1980.

[24] Read, B. E. *Polymer*, **1962**, *3*, 143.

[25] deGennes, P. G. *The Journal of Chemical Physics*, **1971**, *55*, 572.

[26] Doi, M.; Edwards, S. F. *The Theory of Polymer Dynamics*; Oxford University Press: Oxford, 1986.

[27] Doi, M.; Pearson, D. S.; Kornfield, J. A.; Fuller, G. G. *Macromolecules*, **1989**, *22*, 1488.

[28] Ylitalo, C. M.; Zawada, J. A.; Fuller, G. G.; Abetz, V.; Stadler, R. *Polymer*, **1992**, *33*, 2949.

[29] Raju, R. V.; Menezes, E. V.; Martin, G.; Graessley, W. W. *Macromolecules*, **1981**, *14*, 1668.

Chapter 5

Dynamics of Disordered Diblocks of Polyisoprene and Polyvinylethylene

5.1 Introduction

Commercial polymer blends are typically phase separated multicomponent systems consisting of at least two homopolymers and a compatibilizing block copolymer that is long enough to be entangled. Toward the goal of predicting the processing behavior of blends, we have used miscible blends as model systems to examine the effect of the composition and temperature on the dynamics of each species in a given mixed phase [1, 2]. To probe the dynamic behavior of block copolymer chains that are diffusing through a given blend phase as they would to reach the interfacial regions between

blend phases, to act as compatibilizers, we examine disordered block copolymers. In particular, we focus on disordered, entangled diblock copolymer (BCP) melts, investigating the effect of composition and temperature on the dynamics of BCPs when they are homogeneously mixed.

In bidisperse blends of 1,4-polyisoprene (PIP) and polyvinylethylene (PVE), a nearly ideal mixture with widely disparate component glass transition temperatures, time-temperature superposition has been shown to fail dramatically [3, 4]. The presence of thermorheological complexity has been attributed to the different temperature dependences of the relaxation of each component, described by the monomeric friction coefficients $\zeta_{o,PIP}(\phi, T)$ and $\zeta_{o,PVE}(\phi, T)$. The friction coefficients of the two species are found to depend differently on both blend composition, ϕ (volume fraction of PIP), and temperature, T. For blends rich in PVE, where an anomolously broad glass transition is observed in thermal measurements, the values of $\zeta_{o,PIP}(\phi, T)$ and $\zeta_{o,PVE}(\phi, T)$ are most disparate and it is in these blends that the largest departures from thermorheological simplicity are observed.

Paradoxically, rheological studies of diblock copolymers of $PIP - PVE$ over a wide range of compositions show no such failure of time-temperature superposition [5]. The dynamic moduli of these model block copolymers resemble those of monodisperse homopolymers, displaying only one loss peak. However, consistent with the results obtained for blends, these disordered diblock copolymers have an anomalously broad glass transition compared to the homopolymers [5, 6]. The DSC traces of the diblock copolymers and blends of the same overall composition are similar, implying that the

distribution of local segmental mobilities in the block copolymer and blend are similar. These observations motivate using the same rheo-optical methods that allowed us to extract the dynamics of each species in blends where the components had completely overlapping relaxations. This technique should then be well-suited to observe the relative relaxations of each block of the block copolymers.

In blends of PIP and PVE with molecular weights chosen so that the two components have comparable terminal relaxation times in the blend, i.e., the two components are approximately equally entangled, the failure of time-temperature superposition is extremely subtle [1, 7, 8]. Thus when the relaxation spectrum resembles that of a monodisperse polymer, the modest difference between the temperature dependencies of the component friction coefficients leads to small changes in the shape of the frequency dependence of the dynamic moduli with temperature, thereby leading to thermorheological in equally entangled blends.

These observations suggest how to resolve the apparent paradox in the block copolymer data. To interpret the BCP relaxation dynamics, then, it is desirable to draw upon the blend results, namely $\zeta_{o,PIP}(\phi, T)$ and $\zeta_{o,PVE}(\phi, T)$. These can be applied to describe the segments of each block of the BCPs: i) Since the BCPs are disordered, the majority of chain segments are in a blend-like environment; and ii) since the present diblocks have long, well-entangled blocks, most of the segments of each block are not influenced by end effects due to either the chain end or the block junction. Thus each block should have the same friction coefficient as the corresponding homopolymer chain in a blend with identical overall composition. If the blend

results are indeed applicable, they suggest that failure of time-temperature superposition will be negligible for the high-ϕ_{PIP} BCP, where the $\zeta_{o,PIP}$ (high ϕ_{PIP}, T) $\approx$ $\zeta_{o,PVE}$ (high ϕ_{PIP}, T), but noticable for the low-ϕ_{PIP} BCP, where $\zeta_{o,PIP} < \zeta_{o,PVE}$, and the disparity increases with decreasing T. Thus failure of time-temperature superposition is expected in disordered $PIP - PVE$ diblocks, particularly in samples rich in PVE. However, based on the results for equally entangled blends, the effect may not be nearly as dramatic as in blends in which the component relaxations are well-separated.

We seek to understand why such thermorheological complexity is not observed in diblock copolymers and to reconcile this behavior with the established dynamics of miscible PIP/PVE blends. To do so, we follow the method of Osaki [9, 10], using the observed stress-optic behavior to infer the contribution of each block to the relaxation dynamics of the whole chain. We study the dynamics of disordered diblock copolymers of PIP and PVE as a function of temperature for two compositions (ϕ_{PIP} = 0.25 and 0.75). In the second section we describe the polymers chosen as our model system and briefly describe the quantities of interest obtained from the rheo-optical instrument of Chapter 2. Next, we present the results of our dynamic stress and birefringence measurements. This is followed by a preliminary interpretation based on the Doi-Edwards reptation model for mechanically uniform, entangled, linear polymers. Finally, the dynamics of each block of the disordered diblock copolymers and those of each species in miscible blends of similar bulk composition are compared.

Table 5.1: Polyisoprene–Polyvinylethylene Diblock Copolymers from J. Roovers

Sample	75-25 $PIP-PVE$ $\phi_{PIP}=0.76$	25-75 $PIP-PVE$ $\phi_{PIP}=0.25$
M_w (kg/mol)*	366	242
M_w/M_n*	1.08	1.06
$N_{e,PIP}$	49	11
$N_{e,PVE}$	24	49
% Vinyl (PVE)*	94	98
T_g(°C)*	-57	-25

* From Roovers and Wang, J. Non-Cryst. Solids, 1994

5.2 Experimental

5.2.1 Materials

We choose as a model system diblock copolymers of 1,4-polyisoprene (PIP) and polyvinylethylene (PVE), synthesized by J. Roovers at N.R.C. Canada. The miscibility of PIP and PVE is well-established [7, 11, 6], hence these diblock copolymers remain in the disordered state under all experimental conditions. The synthesis and characterization of the diblock copolymers are described elsewhere [5]; their properties are listed in Table 5.1.

The molecular weights of the diblock copolymers are sufficiently long that the shortest block is well-entangled (the number of entanglements per block, $N_e \geq 11$). The two pure species have very different mobilities at ambient temperatures, as a consequence of the large difference between their glass transition temperatures [7, 8, 6] ($T_{g,PIP} \approx -60°C$ and $T_{g,PVE} \approx 0°C$). To gain selective information regarding the relaxation of each block, we use the optical contrast inherent in this system. The component stress-optic coefficients (Table 5.2) are of opposite signs and differ by an order of magnitude [1].

5.2.2 Methods

Simultaneous dynamic mechanical and birefringence measurements are made using the rheo-optical instrument described in Chapter 2. As in the previous chapters, we define the amplitude-based stress-optic ratio SOR and the phase difference between σ_{12} and n_{12} in order to characterize departures from the stress-optic rule:

$$SOR \equiv \frac{|B^*|}{|G^*|}, \tag{5.1}$$

and

$$\delta_B - \delta_G \equiv \tan^{-1}(\frac{B''}{B'}) - \tan^{-1}(\frac{G''}{G'}). \tag{5.2}$$

Again, for homopolymer melts these are both independent of frequency, with SOR being the stress-optic coefficient, C_i, of homopolymer i and δ_B - δ_G remains ≈ 0 for PIP, and $\approx \pi$ for PVE, characteristic of the stress-optic rule. For disordered diblock copolymers the stress-optic rule is expected to fail [9, 10] since the stress

Table 5.2: Stress-Optic Coefficients of Polyisoprene (PIP) and Polyvinylethylene (PVE) Homopolymers

	$C \times 10^{10}$ (cm^2/dyne)	
T(°C)	PIP	PVE
0	1.83	-0.30
10	1.78	-0.26
20	1.73	-0.225
30	1.69	-0.19
40	1.65	-0.16
50	1.61	-0.13
60	1.57	-0.105
80	1.51	-0.048
110	1.42	+0.0097

and birefringence will be differently weighted averages of the orientation of the segments comprising each block (i.e., the second moment of their segmental orientation distributions). This is particularly true if the blocks have stress-optic coefficients of opposite sign or widely differing magnitude, as in our system. Thus, to extract the contribution of the species of each block to the overall properties, we will characterize departures from the stress-optic rule. To do so, we observe the amplitude-based stress-optic ratio SOR (eqn 5.1) and the phase difference between the shear stress and birefringence, $\delta_B - \delta_G$ (eqn 5.2).

Frequencies from 0.01 to 100 rad/sec were employed, at temperatures ranging from 0 to 110°C. At high frequencies and low temperatures, oscillatory strains of 1% or less were applied. With decreasing frequency and increasing temperature, when the force signal decreased to the limit of the transducer, the strain was increased. At the highest temperatures and the lowest frequencies, strains of 50-100% were used. In all cases, it was verified that the viscoelastic response was in the linear regime. Experiments at the lowest and highest temperatures were performed under nitrogen atmosphere to prevent sample degradation.

5.3 Results

5.3.1 Block Copolymers: Dynamic Moduli

The BCP dynamic moduli resemble those of entangled, nearly monodisperse homopolymer melts, showing only one loss peak (Figure 5.1), in accord with previous

results on entangled, disordered diblock copolymers far from the ordering transition [14, 15, 16, 5]. Only data at a few representative temperatures are shown. Master curves were obtained by shifting the data along the frequency axis only, so as to superimpose the terminal behavior at low frequencies. The horizontal shift factors, a_T, for all temperatures are presented in Table 5.3, along with those of the pure homopolymers for comparison. If time-temperature superposition fails for these BCP's, it does so quite subtlely and is not observable within the sensitivity of the experiments.

These results reproduce the dynamic moduli previously reported on this system by Roovers and Wang [5]. (The magnitude of the cross-over in the dynamic moduli differ consistently from their reported values, as well as those of others for the pure components [17, 18, 4] by $\approx 27\%$. While we have been unable to account for this deviation, all our data are consistently lower by this factor.)

5.3.2 Block Copolymers: Dynamic Birefringence

The dynamic birefringence was measured simultaneously with the dynamic moduli. The stress-optic data are shown in Figures 5.2, 5.3 and 5.4 after shifting along the frequency axis using the shift factors obtained for the dynamic moduli (Figure 5.1 and Table 5.3). Excellent superposition of B' and B'' are acheived for the case of $\phi_{PIP} = 0.75$ block copolymer using the mechanical shift factors, as shown in Figures 5.2a-b. However, shifting the complex birefringence for the $\phi_{PIP} = 0.25$ block copolymer according to the mechanical shift factors does not lead to time-temperature superposition (Figures 5.2c-d). In fact, no set of shift factors yields

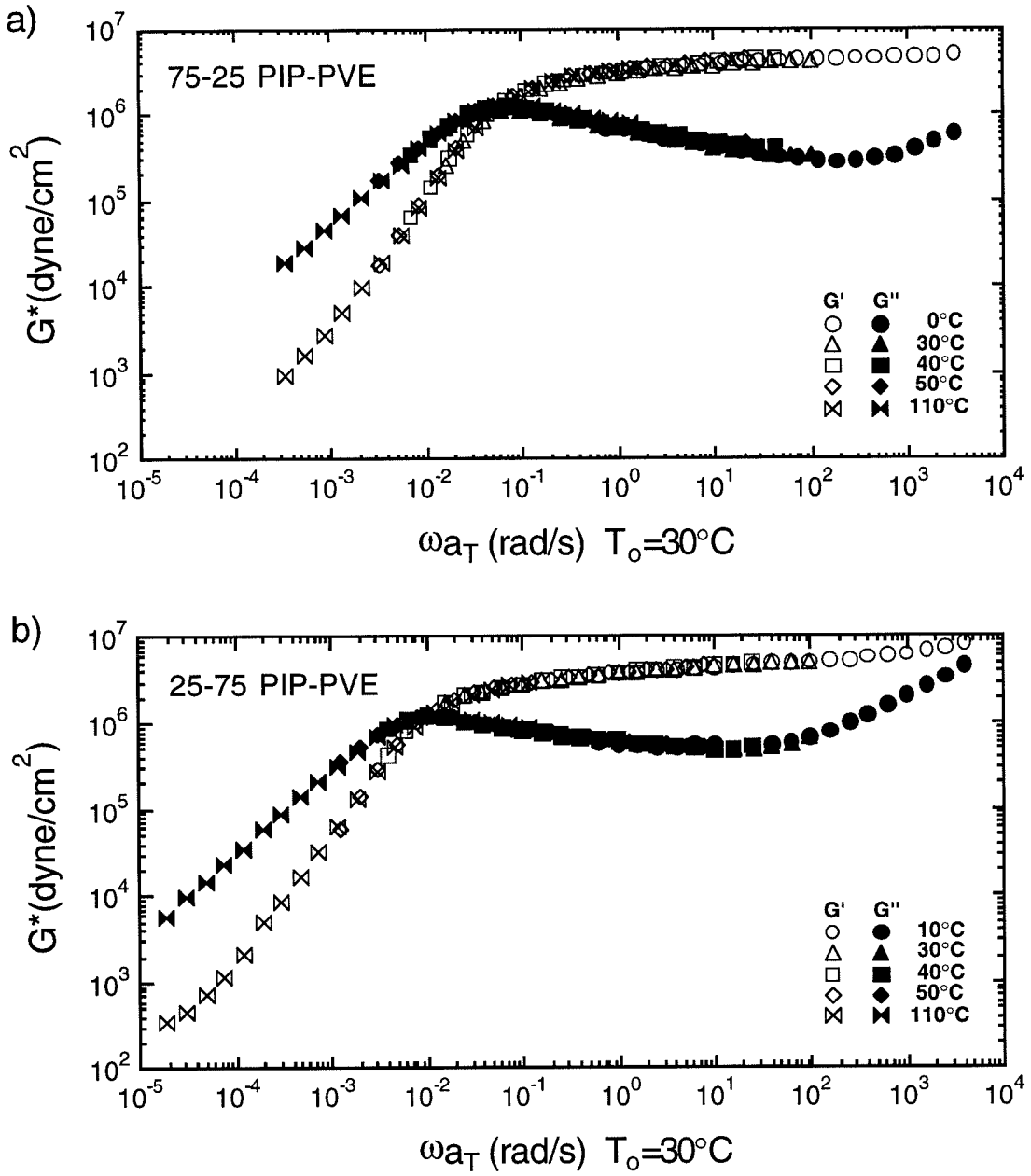

Figure 5.1: Dynamic moduli master curves for the **a)** $\phi_{PIP} = 0.75$ and **b)** $\phi_{PIP} = 0.25$ block copolymers. The reference temperature is $T_o = 30°C$. Note that time-temperature superposition appears to hold for both samples. Only a few representative temperatures are shown (see Table 5.3).

Table 5.3: Shift Factors, a_T, of Homopolymers and Block Copolymers

	Homopolymers		Block Copolymers ($PIP - PVE$ w-w %)	
T(°C)	PIP	PVE	75-25	25-75
0	16	14000	30	-
10	5.3	300	8.5	40
15	3.3	18	4.0	14
20	2.2	12	2.9	5
30	1	1	1	1
40	0.51	0.15	0.44	0.25
50	0.29	0.033	0.21	0.080
60	0.17	0.0095	0.115	0.030
70	0.11	0.0035	0.065	0.0128
80	0.072	0.0014	0.040	0.0062
95	0.043	0.00045	0.022	0.0025
110	0.027	0.00022	0.0135	0.0012

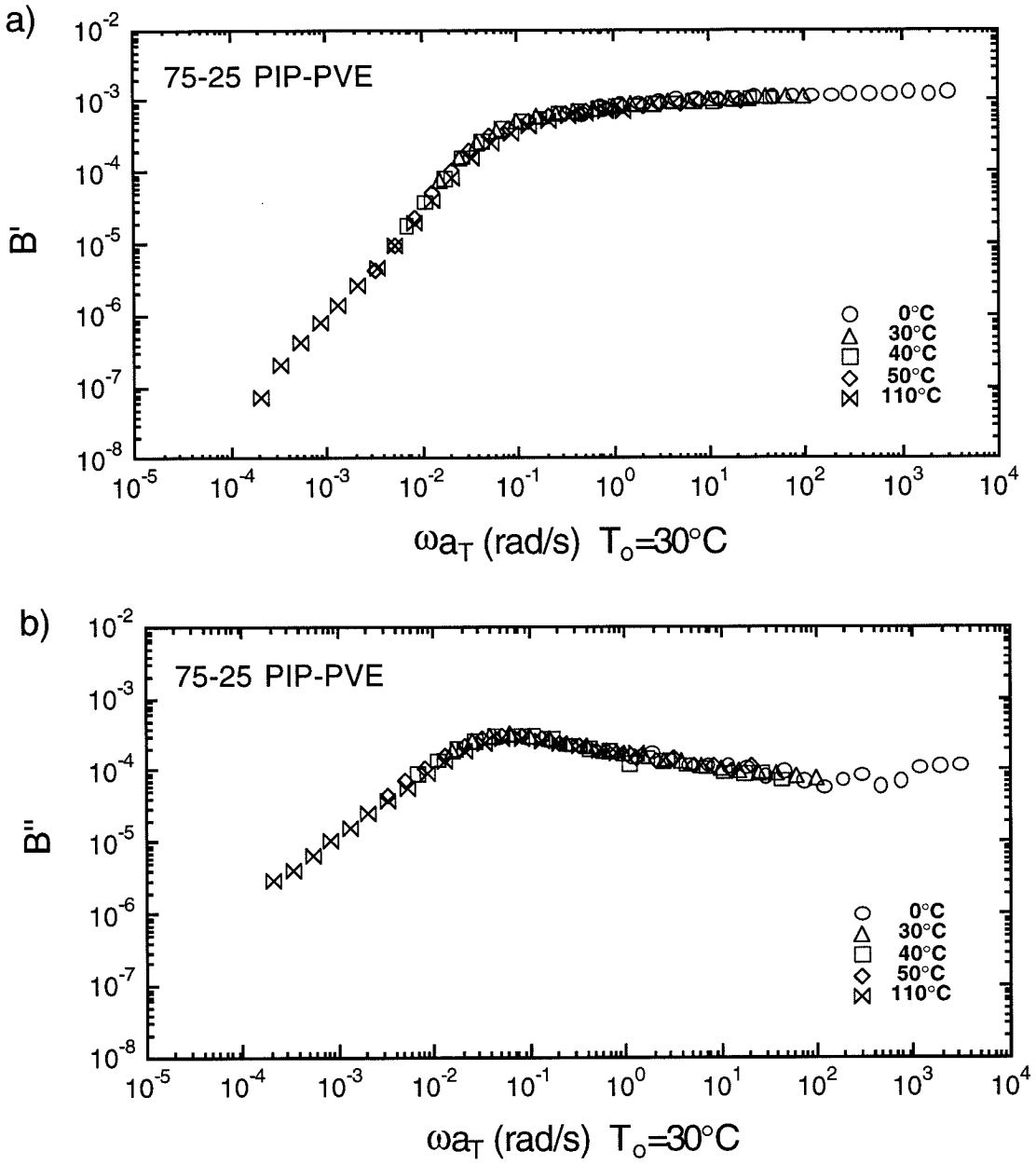

Figure 5.2: Complex birefringence coefficient "master curves" for the $\phi_{PIP} = 0.75$ block copolymer: **a)** B' and **b)** B''. The reference temperature is $T_o = 30°C$ and the horizontal shift factors are those used for the mechanical dynamic moduli (Table 5.3). Notice that the birefringence data superimpose.

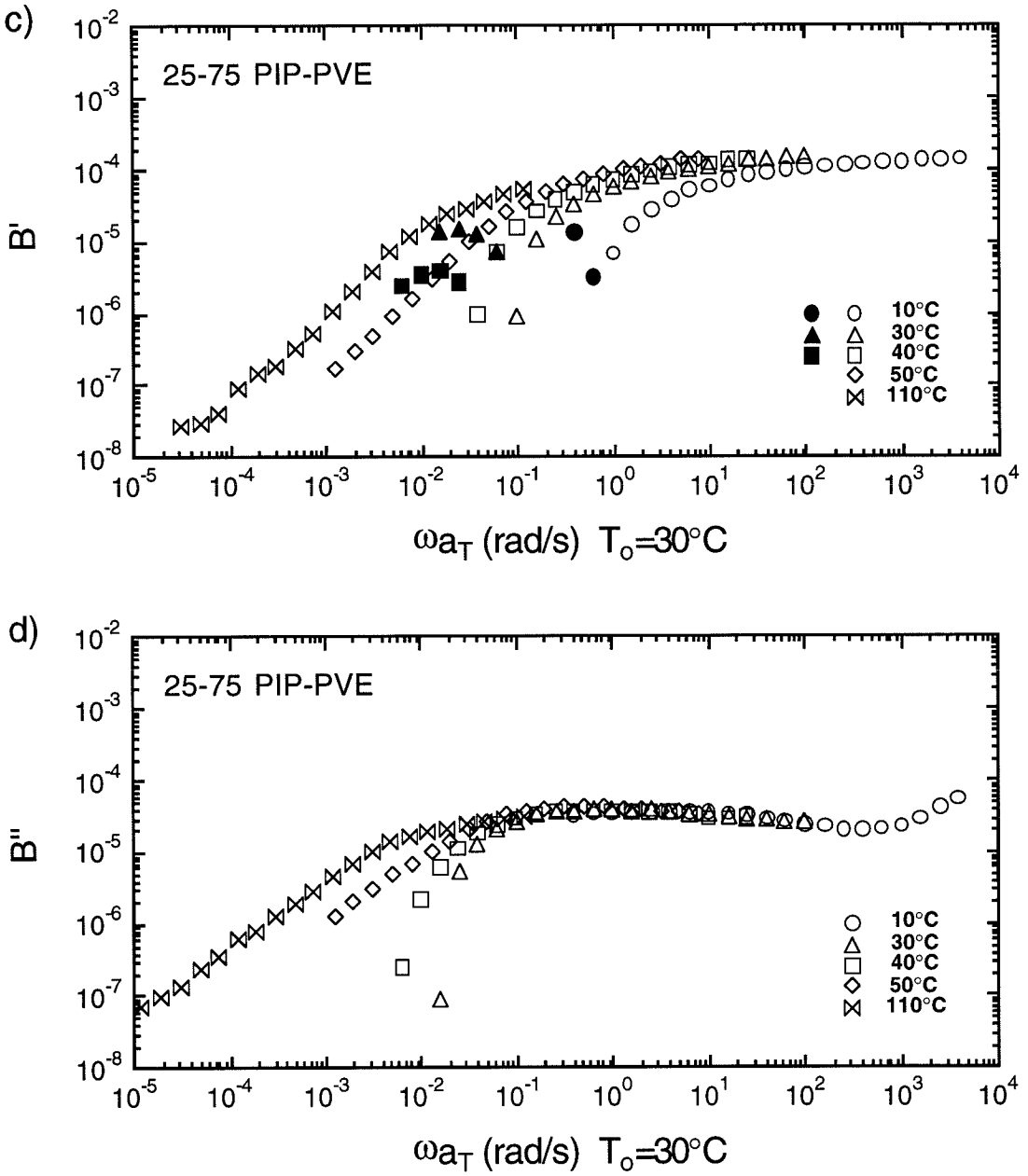

Figure 5.2: Complex birefringence coefficient "master curves" for the $\phi_{PIP} = 0.25$ block copolymer: **c)** B' and **d)** B''. The reference temperature is $T_o = 30°C$ and the horizontal shift factors are those used for the mechanical dynamic moduli (Table 5.3). Notice that the mechanical a_T do not result in superpositioning of B' and B''. Filled symbols in **c)** correspond to values of B' which are negative.

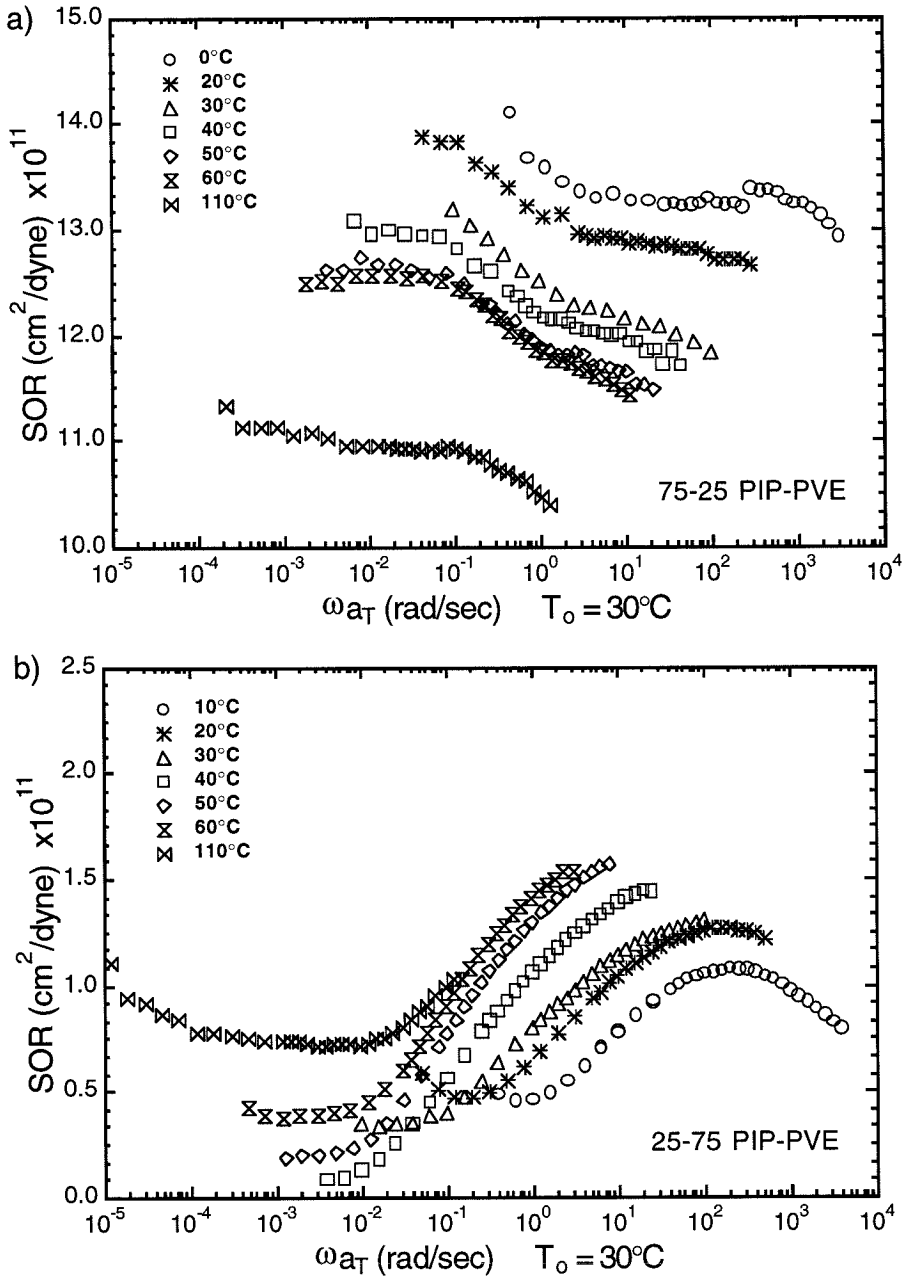

Figure 5.3: *SOR* of the block copolymers versus the same reduced frequencies as the dynamic moduli of the respective samples (Table 5.3). The expanded vertical scale shows the inflection region of each *SOR*. Note that while for the $\phi_{PIP} = 0.75$ BCP, **a**), the inflection remains at a fixed reduced frequency, that of the $\phi_{PIP} = 0.25$ BCP, **b**), does not.

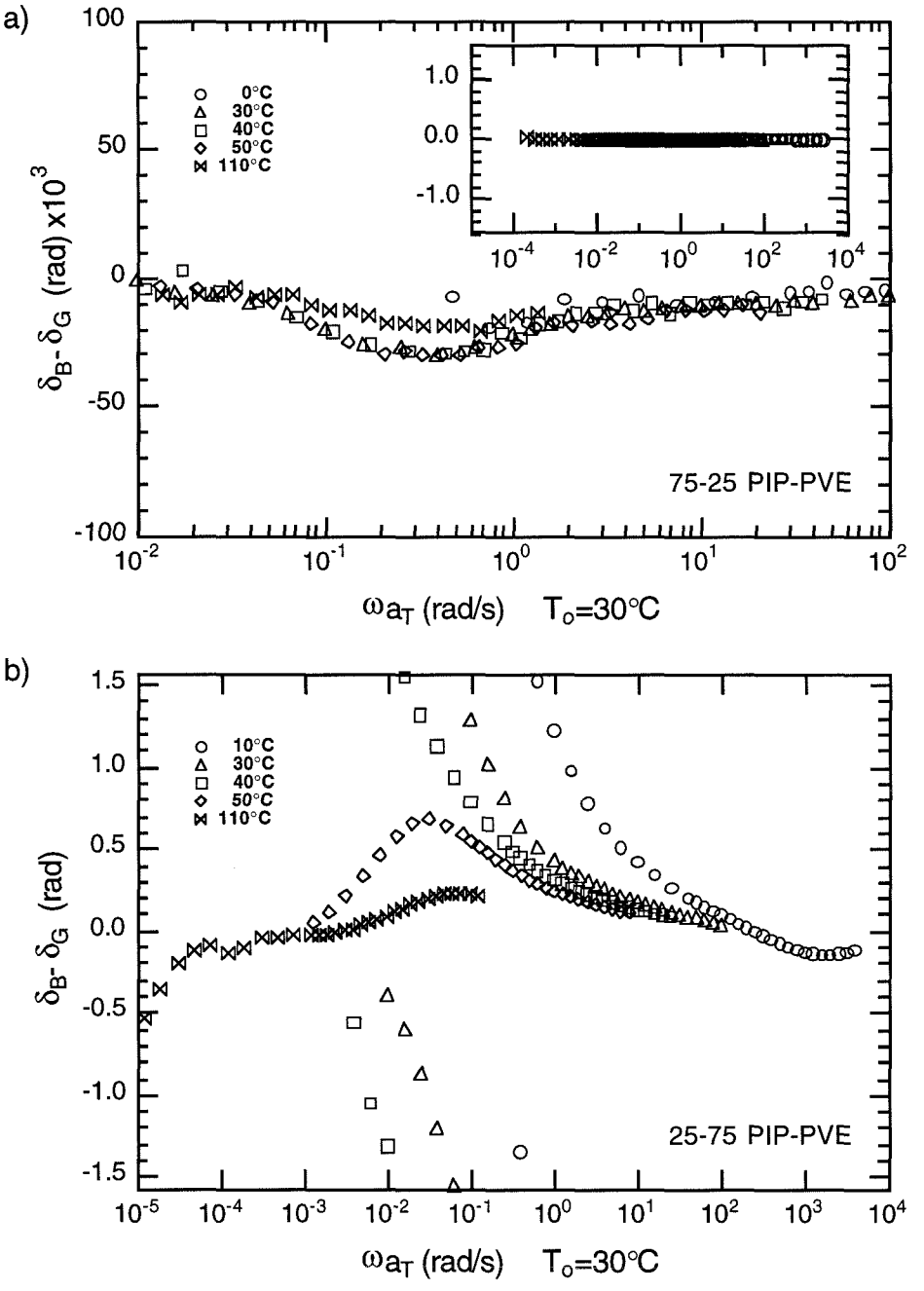

Figure 5.4: Phase difference between the dynamic birefringence and shear stress versus the same reduced frequencies as the dynamic moduli of the respective samples (Table 5.3). The position of the dip for the $\phi_{PIP} = 0.75$ BCP, **a)**, remains at a fixed reduced frequency for all temperatures. However, the peak position for the $\phi_{PIP} = 0.25$ BCP, **b)** shifts to higher reduced frequency as the temperature increases.

superposition. This reveals changes in the shape of the relaxation profile of the chain with temperature – as is expected based on failure of time-temperature superposition of blends rich in PVE. This idea will be explored further in the Discussion.

The SOR of both block copolymers show distinct frequency dependencies (Figure 5.3): the stress-optic rule fails quite dramatically. At high frequencies the BCP SOR reaches a plateau that is approximately the composition-weighted average of the homopolymer stress-optic coefficients (see Table 5.2), very similar to the behavior of blends of the corresponding homopolymers [1, 2]. With decreasing frequency the SOR changes: it rises when the shorter block has a negative stress-optic coefficient ($\phi_{PIP} = 0.75$, Figure 5.3a) and falls when the shorter block has a positive stress-optic coefficient ($\phi_{PIP} = 0.25$, Figure 5.3b). The characteristic reduced frequency of the upturn appears to remain fixed for the $\phi_{PIP} = 0.75$ block copolymer (Figure 5.3a). However, for the block copolymer with $\phi_{PIP} = 0.25$, the characteristic frequency at which the SOR decreases shifts to lower reduced frequency as the temperature increases (Figure 5.3b). Again, as in Figures 5.2c-d, the mechanically determined shift factors do not superimpose the optical data for $\phi_{PIP} = 0.25$. At low frequencies the BCP SOR reaches a second plateau whose value is closer to the stress-optic coefficient of the species which comprises the slowest relaxing section of the chain, i.e., the central portion [19, 9, 10, 20, 21]. The temperature dependence of the magnitude of SOR reflects the temperature dependence of the stress-optic coefficient for the dominant species, decreasing with increasing temperature for the $\phi_{PIP} = 0.75$ BCP and increasing with increasing temperature for the $\phi_{PIP} = 0.25$ block copolymer.

The phase difference between the dynamic birefringence and shear stress, δ_B - δ_G, is shown in Figure 5.4. Values are kept between $\pm$ $\pi/2$. For the BCP with ϕ_{PIP} = 0.75 BCP the values are nearly zero, independent of frequency, with a slight dip occurring at the frequency at which the upturn in SOR is observed in Figure 5.3. Both the position and the depth of the minimum appear to be independent of temperature. The ϕ_{PIP} = 0.25 sample exhibits a dramatically different trend (Figure 5.4). At low temperatures, i.e., from 10 to 40°C, the phase difference moves from 0, passing through $+\pi/2$ to $-\pi/2$. This occurs when values of B' become negative. At temperatures greater than 60°C, a distinct peak is observed and the magnitude of this peak appears to diminish with increasing temperature. These features will be discussed in the next section.

5.4 Discussion

Most of the salient features of the complex stress-optical behavior can be explained in terms of relaxation of optically non-uniform chains, i.e., chains for which the segments of the two blocks have different anisotropic polarizabilities. Experimentally, it has been observed that for a chain of uniform friction and entanglement molecular weight, the portions of the chain near the ends relax faster than the portions comprising the central part of the chain [19, 9, 10, 20, 21].

For the ϕ_{PIP} = 0.75 block copolymer the upturn in SOR is indicative of the relaxation of the chain ends. In particular, as the two ends relax, the negative contribution

of the PVE block to the birefringence decays. (Figure 5.5). Consequently, SOR increases toward that of PIP, which dominates the slower-relaxing central portion of the chain. Conversely, for the $\phi_{PIP} = 0.25$ BCP, relaxation of the ends reduces the positive contribution of the PIP block, which is manifested by a decrease in SOR as the chain center (PVE) contributes proportionally more to SOR. We now consider the temperature dependence of SOR. If the relaxation dynamics of the whole BCP chain shifted in the same way with temperature, one would expect the horizontal shift factors determined from $G^*(\omega)$ to also superimpose $B^*(\omega)$ and consequently $SOR(\omega)$. While this may be the case for $\phi_{PIP} = 0.75$ (Figure 5.3), it is definitely not the case for $\phi_{PIP} = 0.25$. In particular, the mechanical terminal relaxation time appears to speed up more strongly with increasing temperature than does the inflection in SOR; that is, the inflection in SOR moves to *lower* reduced frequency as the temperature increases. This indicates that the dynamics of the PIP segments do not shift as much with temperature as those of the PVE segments, which form the basis for low-frequency superpositioning.

For the $\phi_{PIP} = 0.75$ BCP, SOR is nearly constant and $\delta_B \approx \delta_G$, which is equivalent to the close resemblance between G' and B', and G'' and B'' (Figures 5.1a and 5.2a-b). Both birefringence coefficients remain positive, with the birefringence dominated by the large, positive stress-optic coefficient of PIP. The dip in δ_B - δ_G corresponds to the relaxation of the PVE segments, which are at one chain end, as suggested by the thought experiment in Chapter 3 for the hypothetical blend [1]. This can be seen by considering the mechanical and optic contributions to the relative

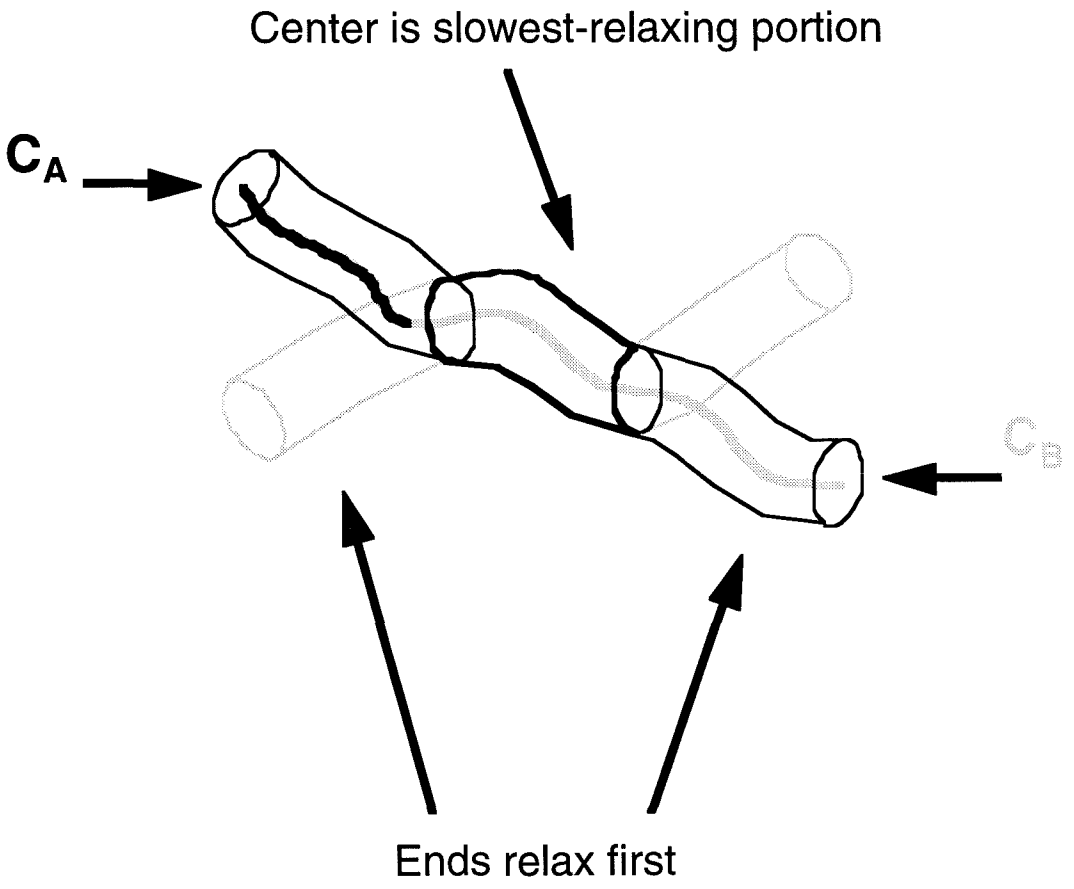

Figure 5.5: Schematic figure demonstrating how the main features observed in the stress-optic data can be qualitatively explained by visualizing the relaxation of a chain with blocks having distinct stress-optic coefficients.

phase difference individually. From equation 5.2 it can be seen that if the ratio of B''/B' decreases relative to G''/G', then δ_B decreases relative to δ_G. The relative phase difference is approximately zero at higher frequencies, where the components of the stress remain in nearly constant proportion to those of the birefringence. At intermediate frequencies, the chain ends begin to relax and the *negative* contribution of the PVE segments to the birefringence decays. δ_B - δ_G then moves to negative values as B' becomes more positive (and B'' less positive) than expected compared to G' (and G''). Eventually, the PIP segments comprising the center portion of the chain begin to relax, and B'' then becomes more positive as well. Thus, in the terminal regime, where the central segments of PIP dominate the stress-optic response, the value of δ_B - δ_G returns to ≈ 0. Since there is not a significant change in the relative contrast in relaxation rates between the two blocks over the range of temperatures probed, the position of the dip in δ_B - δ_G remains at fixed frequency and approximately constant depth.

For the $\phi_{PIP} = 0.25$ diblock, the relative phase angle shows significantly different behavior. This can be rationalized by noticing in Figures 5.1b and 5.2c-d that for intermediate frequencies the shape of G' does not resemble B', and G'' does not resemble B''. At higher frequencies, the components of the stress and birefringence are nearly proportional and δ_B - $\delta_G \approx 0$. It then increases to large positive values, passing through $+\pi/2$ through to $-\pi/2$ near where the values of the in-phase birefringence coefficient, B', become negative. At intermediate frequencies the chain ends begin to relax, and the large, *positive* contribution of the PIP segments to the birefringence

decays. δ_B - δ_G moves to large, positive values as B' becomes less positive (and B'' more positive) than expected compared to G' (and G''). Eventually, the PVE segments comprising the center portion of the chain begin to relax, and B'' then becomes less positive as well. Thus, in the terminal regime, where the central segments of PVE dominate the stress-optic response, the value of δ_B - δ_G returns to ≈ 0. As the temperature increases, both the contrast between the friction coefficients of the species comprising the two blocks decreases and the value of C_{PVE} becomes less negative relative to C_{PIP}. We are no longer able to probe the region where δ_B - δ_G passes through $+\pi/2$. At high enough temperatures, both B' and B'' remain positive and δ_B - $\delta_G < \pi/2$. As the temperature increases, the peak shifts to higher relative frequency and decreases in height, indicating the change in relative relaxation rates of the two blocks.

To provide a more quantitative interpretation, the following section compares the stress-optical behavior of the BCP's to the reptation model [22, 23]. For the reptation model, it is possible to incorporate optical contrast between the blocks; however, it is not yet known how to extend the model to a mechanically non-uniform chain ($M_{e,A} \neq M_{e,B}$ and/or $\zeta_{o,A} \neq \zeta_{o,B}$). The condition of mechanical uniformity is a reasonable approximation for the $\phi_{PIP} = 0.75$ case, where results on PIP/PVE blends [1, 2, 4, 12, 13] show $\zeta_{o,PVE}/\zeta_{o,PIP}$ ranges from 1.3 to 3.7 over the present temperature range and $M_{e,PVE}/M_{e,PIP} \approx 0.6$. However, the restriction of the reptation model to mechanically uniform chains proves inadequate for the $\phi_{PIP} = 0.25$ case, where $\zeta_{o,PVE}/\zeta_{o,PIP}$ ranges from 1.4 - 15.0 over the same temperatures.

5.4.1 Comparison to Reptation Model Predictions

The reptation model [19] parameterizes both the intramolecular structure of a chain as well as its interaction with the surrounding melt, via the tube diameter, a, and the monomeric friction coefficient, ζ_o. It is capable of describing macroscopic quantities, in particular the plateau modulus, G_N^o, and the molecular weight dependence of the disengagement time, τ_d. The value of the plateau modulus is characteristic of M_e, the entanglement molecular weight, which is related to the tube diameter a. The disengagement time corresponds to the longest relaxation mode of the chain and characterizes the time over which distortions of the chain relax. It is related to the friction coefficient governing the local interaction of a chain with its environment as well as the intrinsic "stiffness" of the chain.

We compare the dynamic stress-optic data to the predictions of the reptation model, which is limited to the case of mechanical uniformity [24, 9, 10]. The stress-optical quantities are given by the expressions

$$G'(\omega) = \sum_{odd\ p=1}^{\infty} \frac{1}{p^2} \frac{\omega^2\tau_p^2}{1+\omega^2\tau_p^2} \qquad G''(\omega) = \sum_{odd\ p=1}^{\infty} \frac{1}{p^2} \frac{\omega\tau_p}{1+\omega^2\tau_p^2} \tag{5.3}$$

$$B'(\omega) = \sum_{odd\ p=1}^{\infty} C_p \frac{1}{p^2} \frac{\omega^2\tau_p^2}{1+\omega^2\tau_p^2} \qquad B''(\omega) = \sum_{odd\ p=1}^{\infty} C_p \frac{1}{p^2} \frac{\omega\tau_p}{1+\omega^2\tau_p^2} \tag{5.4}$$

The optical weighting factors, C_p, are given by

$$C_p = \frac{1}{2} \{(q_A + q_B) + (q_B - q_A)\ cos(\pi\ p\ f_A)\}, \tag{5.5}$$

where q_i are the species' anisotropic polarizabilities (proportional to their stress-optic coefficients), p (odd, see eqns. 5.3 and 5.4) is the mode number ($p = 1$ corresponds

to the longest relaxation time of the chain, the reptation time, τ_d) and f_A is the fractional length of block A [24]. The relaxation times, τ_p, are related to the longest relaxation time by $\tau_p = \tau_d/p^2$. Equations for SOR and δ_B - δ_G are given in the Methods section.

The qualitative features of the observed SOR and δ_B - δ_G are captured by the dynamics of a reptating, mechanically uniform diblock ($\zeta_{o,A} = \zeta_{o,B}$ and $M_{e,A} = M_{e,B}$) in which the two blocks have different stress-optic coefficients. In this case we neglect the possible difference between the entanglement molecular weights of the two blocks, which is a good approximation for the PIP/PVE system [17, 18, 4]. The relative block lengths are set to correspond to those of the two diblock copolymers, and we take the terminal relaxation time, τ_d, of each chain to equal $2/\omega_x$, the crossover frequency of the dynamic moduli (Figure 5.1) [1]. Calculated values of the stress-optical properties are plotted versus $\log(\omega\tau_d)$ for each chain, which superimposes the calculated mechanical data at different temperatures for a given chain. Thus, direct comparisons can be made with our experimental data (Figures 5.3- 5.4), which are plotted with respect to the reduced frequencies required to superimpose the mechanical data of Figure 5.1.

The optical properties, q_i, of each block are set to correspond to the homopolymer values of $C_{PIP}(T)$ and $C_{PVE}(T)$ (Table 5.2). In the absence of internal field effects or of changes in local chain configuration upon blending, each segment will contribute to the birefringence in the BCP in proportion to its contribution to the stress, with the constant of proportionality being the stress-optic coefficient C_i of the pure species

i [1]. Furthermore, the PIP-PVE blends and BCPs we focus on here are miscible, but with very weak interactions, so that changes in local chain statistics due to blending are negligible [7, 11, 6]. The consequences of connectivity of the two blocks on the segmental distribution should also be negligible except for the small fraction of segments near the junction, since each block is long.

We first consider cases where no orientational coupling is present. The reptation model prediction of $SOR(\omega;T)$ (Figure 5.6) captures the inflection observed in the experimental SOR (Figure 5.3). The temperature dependencies of $C_{PIP}(T)$ and $C_{PVE}(T)$ are primarily responsible for the vertical shift of the observed SOR with T. For both BCPs the model correctly predicts the general *shapes* of the relative phase differences, δ_B - δ_G (Figure 5.7). Experimentally, the reduced frequency at which the upward inflection occurs in SOR and the dip occurs in $\delta_B - \delta_G$ for the $\phi_{PIP} = 0.75$ diblock does not change with temperature (Figures 5.3a and 5.4a), in accord with the model. In contrast, the experimental data show that the reduced frequency of the inflection in SOR for the $\phi_{PIP} = 0.25$ diblock moves to lower frequency as temperature increases (Figure 5.3b). This is in distinct disagreement with the predictions of the mechanically-uniform reptation model. In addition, for the $\phi_{PIP} = 0.25$ BCP the magnitude and frequency dependence of $\delta_B - \delta_G$ are in particular disagreement with experiment. These discrepencies persist even when the effects of orientational coupling [19, 24] are included, using the values of ϵ determined from our previous blend paper [2, 12, 13]. Orientational coupling reduces the magnitude of the departure from the stress optic rule (smaller step in SOR and smaller peak/valley in

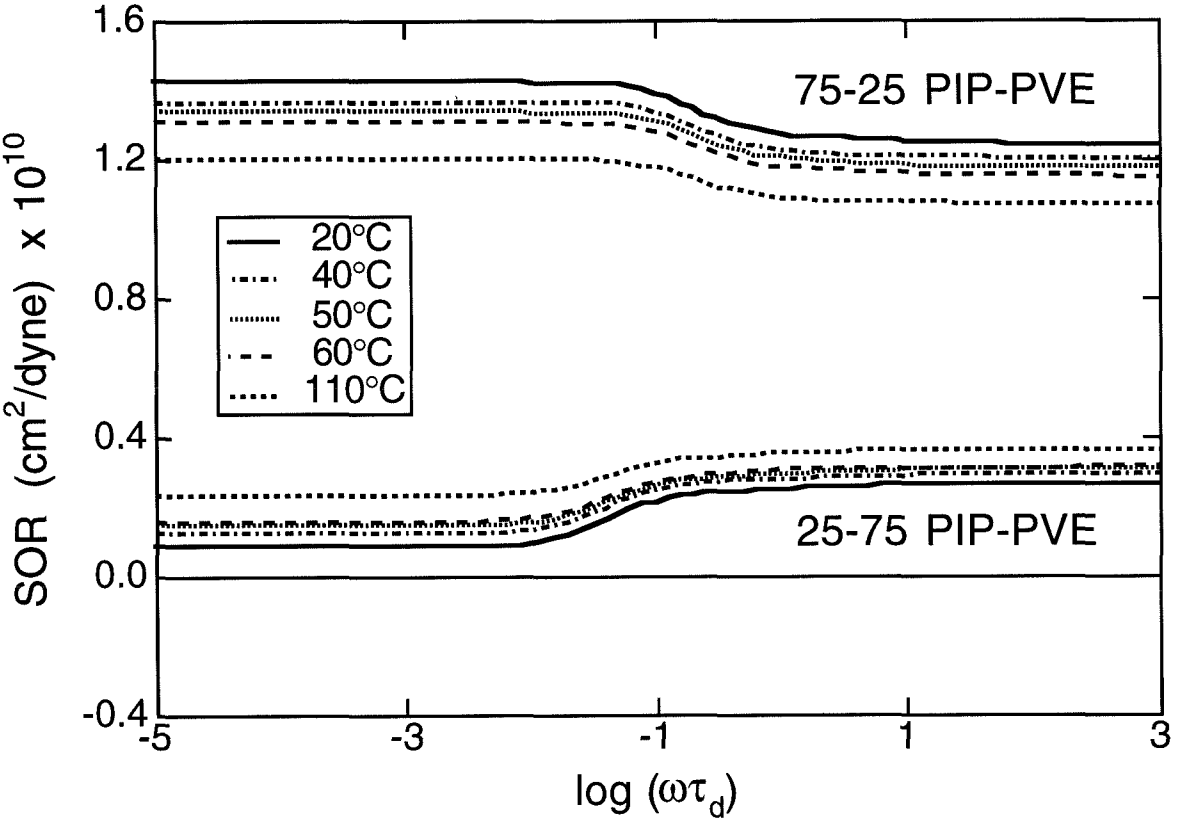

Figure 5.6: Calculated BCP *SOR* based on the reptation model, under the assumption of chains of uniform friction coefficient and statistical segment length (mechanical uniformity). The stress-optic coefficients of the homopolymer species are used at each temperature to determine the optical properties of the chain. See the text for discussion.

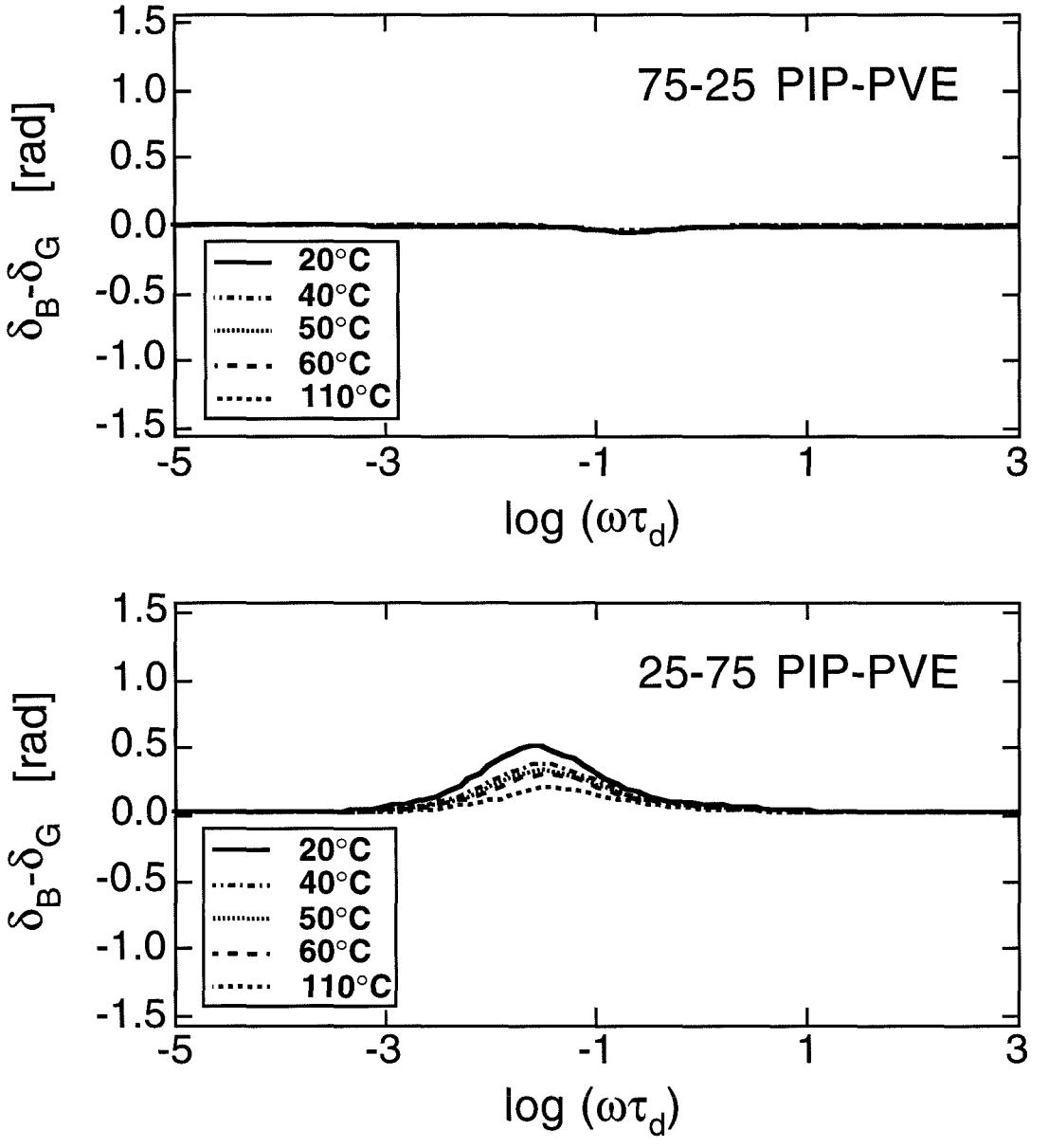

Figure 5.7: Calculated phase difference between dynamic birefringence and stress for a mechanically-uniform reptation model. See the text for discussion.

$\delta_B - \delta_G$, but does not shift the frequency dependence of SOR vs. $\delta_B - \delta_G$ (Figures 5.8 and 5.9).

We now draw upon our knowledge of the dynamics of PIP/PVE blends to explain why the model is capable of reproducing the essential features observed experimentally for the $\phi_{PIP} = 0.75$ BCP but fails to capture the behavior of the $\phi_{PIP} = 0.25$ BCP. Previous work on miscible PIP/PVE blends has shown that the failure of time-temperature superposition observed for this system can be attributed to the distinct temperature dependence of each species' dynamics in the blend [25, 26, 1, 2, 4, 12, 13]. While blending induces only minor changes in the entanglement molecular weight of each species, $M_{e,i}$, it dramatically alters the species' friction coefficients, $\zeta_{o,i}$, and the dynamics of the low-T_g component, PVE, are more sensitive to both blend composition and temperature [1]. Here, we extend the work on miscible PIP/PVE blends to describe the relaxation behavior of $PIP - PVE$ block copolymers.

On scales from a Rouse segment up to $M_{e,i}$ a given segment in the middle of a block cannot distinguish between the block copolymer and corresponding blend environment. Therefore, we can take the friction coefficient of the respective species in each block of the block copolymer to be the same as that in the miscible blend of corresponding composition $\zeta_{o,i}(\phi, T)$.

For the $\phi_{PIP} = 0.75$ BCP the mechanically uniform reptation model successfully reproduces the reduced-frequency and temperature dependence of the stress-optic data. Based on the assumptions of the model, this indicates that the relative rate of relaxation of the PVE end with respect to the slowest relaxing portion of the chain

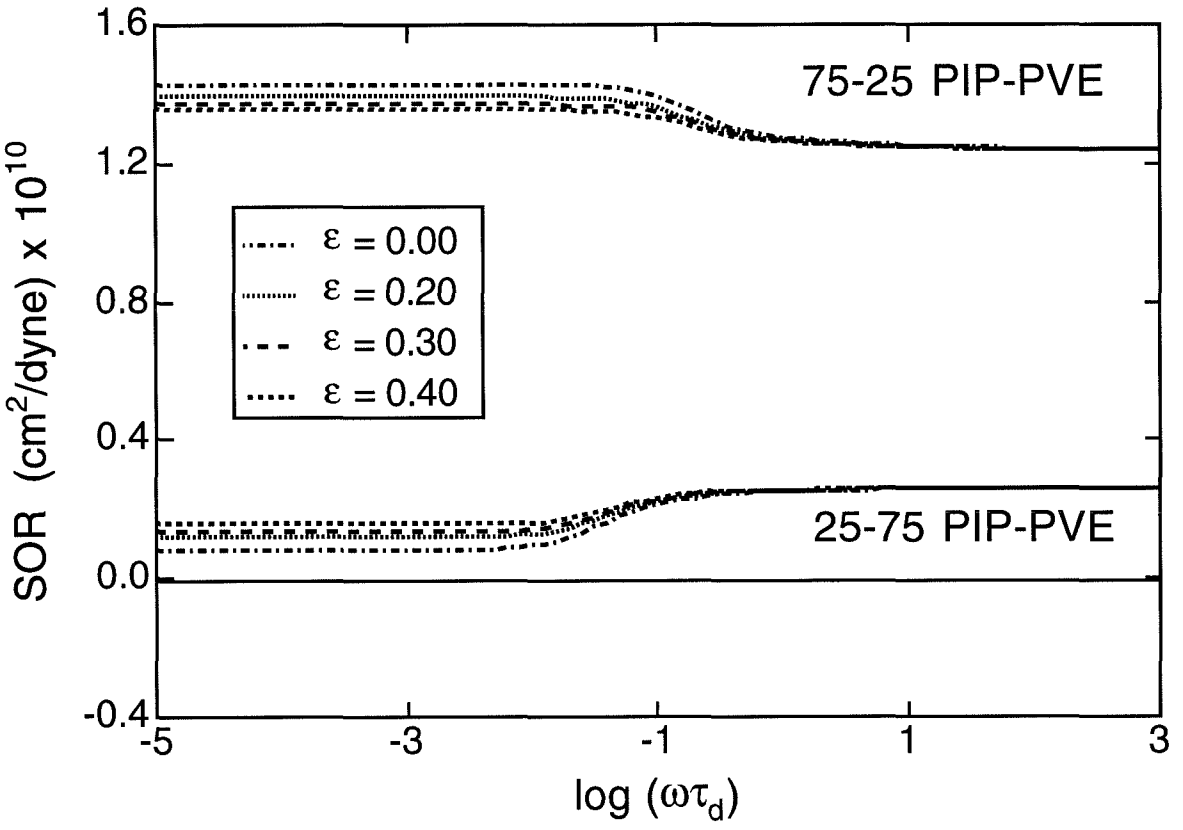

Figure 5.8: Calculated BCP *SOR* based on the mechanically uniform reptation model at 20°C. The coupling coefficient, ϵ, is varied from 0 to 0.40. Results at other temperatures show similar behavior.

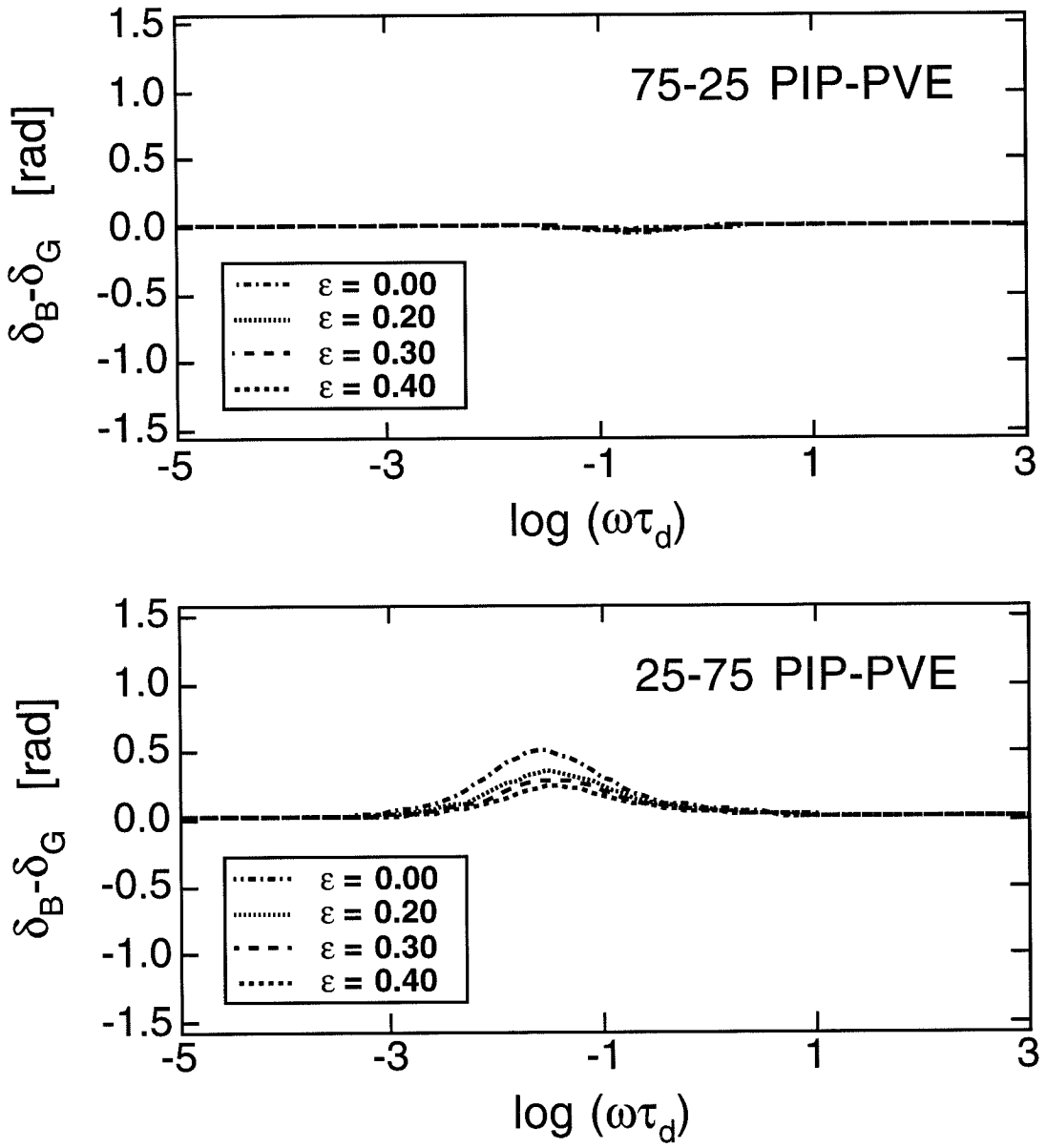

Figure 5.9: Calculated phase difference between dynamic birefringence and stress for a mechanically-uniform reptation model at 20°C. The coupling coefficient, ϵ, is varied from 0 to 0.40. Results at other temperatures show similar behavior.

Table 5.4: Friction Coefficients of Polyisoprene and Polyvinylethylene in Blends [1, 2]

Composition	$\phi_{PIP} = 0.75$		$\phi_{PIP} = 0.25$	
T (°C)	$\zeta_{o,PIP}$ (g/s)	$\zeta_{o,PVE}$ (g/s)	$\zeta_{o,PIP}$ (g/s)	$\zeta_{o,PVE}$ (g/s)
-10	6.5×10^{-5}	2.4×10^{-4}	-	-
5	7.9×10^{-6}	2.5×10^{-5}	1.8×10^{-4}	2.7×10^{-3}
15	2.4×10^{-6}	7.0×10^{-6}	2.5×10^{-5}	2.7×10^{-4}
25	9.6×10^{-7}	2.4×10^{-6}	5.3×10^{-6}	4.1×10^{-5}
40	3.3×10^{-7}	6.9×10^{-7}	1.0×10^{-6}	5.0×10^{-6}
60	1.0×10^{-7}	1.6×10^{-7}	2.1×10^{-7}	6.1×10^{-7}
80	4.0×10^{-8}	5.5×10^{-8}	6.7×10^{-8}	1.2×10^{-7}
110	1.8×10^{-8}	2.4×10^{-8}	1.9×10^{-8}	2.7×10^{-8}

(the PIP center), which was used as the basis for determining the shift factors, is not changing. This, in turn, means that the overall shape of the chain's relaxation spectrum is not changing with temperature - like a uniform-friction chain (Figures 5.6 and 5.7). This behavior is in reasonable accord with the established friction coefficients of PIP and PVE in a $\phi_{PIP} = 0.75$ environment, where the two friction coefficients are similar at all temperatures, and their relative magnitudes change little ($1.3 \leq [\zeta_{o,PVE}/\zeta_{o,PIP}] \leq 3.7$) over the temperature range probed (110°C to -10°C) (Figure 5.10 and Table 5.4).

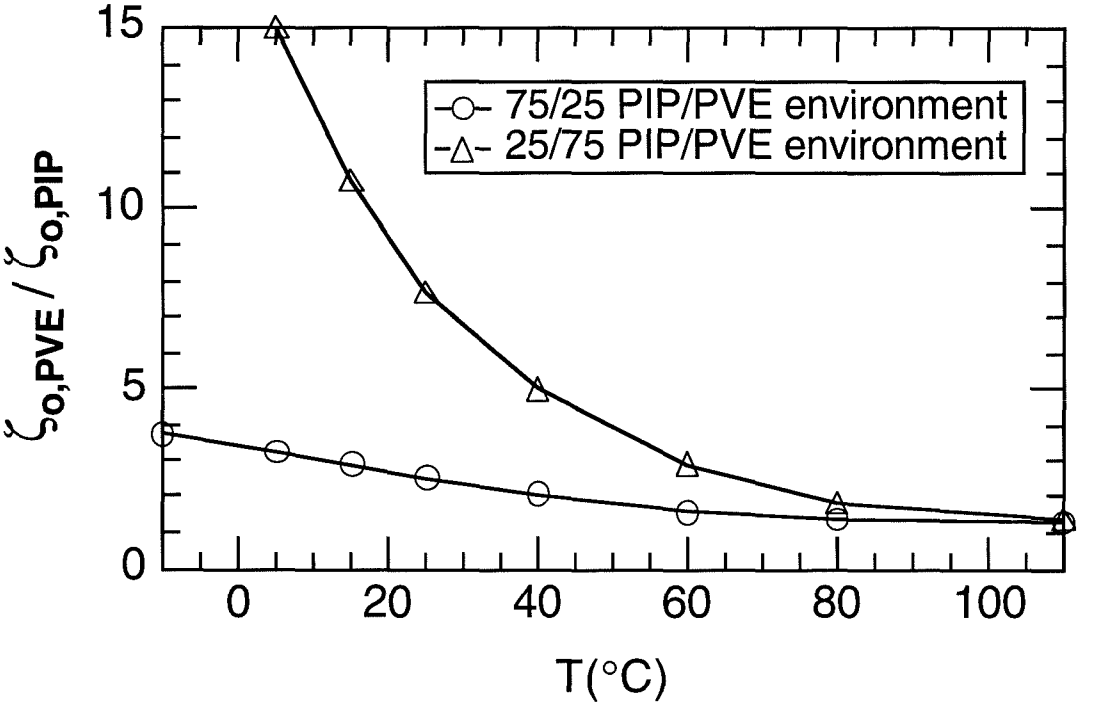

Figure 5.10: Ratio of the monomeric friction coefficients of PIP and PVE, based on the blend results, in environments of 75/25 and 25/75 PIP/PVE, corresponding to the compositions of the BCPs. Notice that the contrast in friction coefficient for 25/75 PIP/PVE changes much more with temperature.

For the $\phi_{PIP} = 0.25$ BCP the shift of the inflection in SOR with temperature can be understood in terms of the relative rates of relaxation of the two blocks. Since the shift factor is based on the slowest relaxation modes, the reduced frequency scale is appropriate for the center of the chain, which consists of PVE in this diblock. The movement of the inflection to lower frequency indicates a *decrease* in the relative rate of relaxation of the PIP block compared to the middle of the chain. This is consistent with the established temperature dependence of the friction coefficients of PIP and PVE in a $\phi_{PIP} = 0.25$ environment, which shows that the dynamics of PVE speed up more strongly than those of PIP with temperature (Table 5.4). The observable decrease in the relative rate of relaxation of the PIP block arises because the contrast in monomeric friction is large at ambient temperature ($\zeta_{o,PVE}/\zeta_{o,PIP} = 15.0$ at 5°C), and decreases significantly with increasing temperature ($\zeta_{o,PVE}/\zeta_{o,PIP} = 1.4$ at 110°C), reflecting a decrease in the relative rate of relaxation of PIP with respect to PVE (Figure 5.10).

The inability of the reptation model to capture the magnitude of the relative phase difference, δ_B - δ_G, is not due to any scaling prefactors neglected in the calculation of the dynamic moduli or birefringence coefficients, since only ratios of these quantities determine the relative phase difference. Such disagreement is a consequence of the model assumptions, namely uniform friction along the chain.

5.5 Conclusions

Coordinated analysis of the shear stress and birefringence in dynamic shear is used to monitor the relaxation of each block in a disordered diblock copolymer. Qualitatively, the frequency dependence of the complex stress-optic behavior can be explained in terms of the relaxation of chains with blocks having distinct stress-optic coefficients, with the center portion of the BCP dominating at low frequencies. Quantitatively, comparison to predictions of the reptation model reveal that in a diblock in which the friction coefficients of the distinct blocks are similar, the chain relaxes like a chain having uniform friction, as is the case for the $\phi_{PIP} = 0.75$ diblock. On the other hand, if there is a significant contrast between the friction coefficients of the two blocks, combined with a change in this contrast with temperature, then departure from the uniform-friction relaxation dynamics can be significant. This is observed when the diblock is rich in the high-T_g component (PVE).

Failure of time-temperature superposition for the mechanical moduli is not noticable for these BCPs because the relaxation spectrum is always nearly that of a monodisperse homopolymer. However, the lack of superposition of SOR using the mechanically determined shift factors shows that failure of time-temperature superposition is, in fact, present. It is more noticeable in the BCP rich in the low-T_g component (PVE), as it was in the corresponding miscible blend. Thus, the apparent time-temperature superposition paradox has been resolved.

Bibliography

[1] Arendt, B. H.; Kannan, R. M.; Zewail, M.; Kornfield, J. A.; Smith, S. *Rheologica Acta*, **1994**, *33*, 322; Arendt, B. H. *et al. Proceedings of the ACS, PMSE, Washington, D.C.*, **1994**,*71*, 471.

[2] Arendt, B. H.; Krishnamoorti, R.; Kornfield, J. A.; Smith, S. D. *Manuscript in preparation.*

[3] Alegria, A.; Colmenero, J.; Ngai, K. L.; Roland, C. M. *Macromolecules*, **1994**, *27*, 4486.

[4] Roovers, J.; Toporowski, P. M. *Macromolecules* **1992**, *25*, 3454.

[5] Roovers, J.; Wang, F. *J. Non-Cryst. Solids*, **1994**, *172-4*, 698.

[6] Trask, C. A.; Roland, C. M. *Macromolecules* **1989**, *22*, 256.

[7] Roland, C. M. *Macromolecules* **1987**, *20*, 2557.

[8] Roland, C. M. *Journal of Polymer Science, Polymer Physics Edition* **1988**, *26*, 839.

[9] Osaki, K.; Takatori, E.; Kurata, M.; Ohnuma, H.; Kotaka, T. *Polymer* **1986**, *18*, 947.

[10] Osaki, K.; Takatori, E.; Ueda, M.; Kurata, M.; Kotaka, T.; Ohnuma, H. *Macromolecules* **1989**, *22*, 2457.

[11] Tomlin, D.W.; Roland, C. M. *Macromolecules* **1992**, *25*, 2994.

[12] Zawada, J. A.; Fuller, G. G.; Colby, R. H.; Fetters, L. J.; Roovers, J.; *Macromolecules* **1994**, *27*, 6851.

[13] Zawada, J. A.; Fuller, G. G.; Colby, R. H.; Fetters, L. J.; Roovers, J.; *Macromolecules* **1994**, *27*, 6861.

[14] Bates, F. S.; Rosedale, J. H.; Fredrickson, G. H. *The Journal of Chemical Physics*, **1990**, *92*, 6255.

[15] Kim, J. K.; Han, C. D. *Macromolecules*, **1992**, *25*, 271.

[16] Rosedale, J. H.; Bates, F. S. *Macromolecules*, **1990**, *23*, 2329.

[17] Carella, J. M.; Graessley, W. W.; Fetters, L. J. *Macromolecules* **1984**, *17*, 2775.

[18] Gotro, J. T.; Graessley, W. W. *Macromolecules* **1984**, *17*, 2767.

[19] Doi, M.; Edwards, S. F. *The Theory of Polymer Dynamics*; Oxford University Press: Oxford, 1986.

[20] Tassin, J. F.; Monnerie, L.; Fetters, L. J. *Macromolecules*, **1988**, *21*, 2404.

[21] Ylitalo, C. M.; Fuller, G. G.; Abetz, V.; Stadler, R.; Pearson, D. S. *Rheologica Acta*, **1990**, *29*, 543.

[22] deGennes, P. G. *The Journal of Chemical Physics*, **1971**, *55*, 572.

[23] Doi, M.; Pearson, D. S.; Kornfield, J. A.; Fuller, G. G. *Macromolecules*, **1989**, *22*, 1488.

[24] Lodge, T. P.; Amelar-Lodge, S. *Rheologica Acta* , **1992**, *31*, 32.

[25] Chung, G. C.; Kornfield, J. A.; Smith, S. D. *Marcromolecules* **1994**, *27*, 964.

[26] Chung, G. C.; Kornfield, J. A.; Smith, S. D. *Marcromolecules* **1994**, *27*, 5729.